http://waikato.researchgateway.ac.nz/

Research Commons at the University of Waikato

Copyright Statement:

The digital copy of this thesis is protected by the Copyright Act 1994 (New Zealand).

The thesis may be consulted by you, provided you comply with the provisions of the Act and the following conditions of use:

- Any use you make of these documents or images must be for research or private study purposes only, and you may not make them available to any other person.
- Authors control the copyright of their thesis. You will recognise the author's right to be identified as the author of the thesis, and due acknowledgement will be made to the author where appropriate.
- You will obtain the author's permission before publishing any material from the thesis.

Dynamic Electroporation Modelling

A thesis presented for the degree of

Doctor of Philosophy

in Electronic Engineering

University of Waikato

by

Sadhana Ravi Talele

THE UNIVERSITY OF
WAIKATO
Te Whare Wānanga o Waikato

2009

Abstract

In this thesis, modelling and simulation of the effects of electric fields on a single spherical cell are undertaken. Of interest is the effect that different electric field waveforms have on the induced transmembrane potential of the cell and by consequence the electropermeabilization of the cell membrane in terms of pore density or the fraction of the cell area that the pores occupy. Conventional biotechnology processes of electroporation make use of unipolar electric field pulses, which are known to generate undesirable conditions such as asymmetrical electropermeabilization. These electrical protocols also contribute to lower efficiencies in electroporation based applications (in terms of uptake of molecules in the cell) by being sensitive to cell radii.

Until recently, theoretical models of electroporation have lagged behind the experimental research. In order to optimize the efficiency of electroporation, it is important to consider as many biological and physical aspects as possible and it is a necessity that a variety of electric pulse parameters be tested. Thus a comprehensive model which can predict electropermeabilization as a result of any form of applied electric field and other important electroporation parameters is necessary. None of the existing theoretical modelling studies present simulations of dynamic electroporation modelling as a cell response to bipolar electric field wave-shapes. Developing such a model is the aim of this thesis.

In this thesis two numerical models are developed. These models consider electroporation as a dynamic process and include the non-linear dynamic effects of membrane electropermeabilization. The first model assumes all pores are identical and small (0.76 nm radius) and is capable of simulating transmembrane potential and pore density temporally and spatially, given any form of applied electric field and other important electroporation system parameters such as external medium, membrane, and cytoplasm complex dielectric properties. The piece-wise step response model presented here is used to simulate

cell response to several different applied electric field wave-shape pulses.

Additional results from the first model demonstrate how the efficiency of electroporation related applications can be significantly improved by appropriately adjusting the parameters of the applied electric field and the extracellular conductivity. Emphasis is given on the normalization of the degree of electroporation (in terms of pore density) for two cell radii (7.5 μm and 15 μm).

Although, these results gave a fair indication of the extent of electroporation in terms of pore density, the approximation that all pores have the same size, and do not change with time, may not be appropriate. There is a need to model electroporation so as to reflect the growth or shrinkage of pores with time, as well as efficiently handle arbitrary waveshapes of electric fields. The additional information about pore radius evolution gives a more realistic picture of the extent of electroporation, especially if one is to model for longer time (longer than 1 μs) or if an application necessarily required existence of larger pores (radius lager than 1 nm) rather than just the total pore area. Pore radius and pore numbers affect the transmembrane potential, which in turn affects pore density and pore radius. Literature includes information on spatial and temporal aspects of pore radius evolution. However, the electric fields used in these models were limited to unipolar DC pulses and details of temporal and spatial evolution of transmembrane potential and pore radius have not been reported.

The second model developed in this thesis simulates spatial and temporal aspects of pore radius as an effect of any given form of applied electric field (including unipolar or bipolar), and other important electroporation system parameters. The transmembrane potential and pore radii as function of time and angular position about the cell membrane are presented. The results show that pore radii tend to be more normalized when an AC (bipolar) field is used when compared to a DC (unipolar) field (pore radii ranging from 1 nm to 8 nm for DC protocol compared with 1 nm to 3.4 nm for AC protocol when the pulse amplitude used in both cases is such as to give a similar fractional pore area at the end of 2 μs).

Additional simulation results from this model are used to compare the extent of electroporation in response to sinusoidal AC (bipolar) electric field pulses of two different frequencies in a range of extracellular conductivity for two different cell radii (7.5 μm and 15 μm). It is observed that a higher frequency (1 MHz) bipolar sinusoidal applied electric field pulse reduces the relat-

ive difference in fractional pore area for the two cell sizes compared to a lower frequency (100 kHz) pulse. Nevertheless for the high frequency, a significantly higher amplitude is required to create the same level of average fractional pore area. Asymmetry of fractional pore area between the two hemispheres of the cell is observed for both field protocols.

Acknowledgements

The completion of this thesis would not have been possible without the help and support of great many people, and to them I am very grateful.

First and foremost I am extremely grateful for the good fortune of having Paul Gaynor as my supervisor, especially continuing to be my supervisor even after he changed jobs. Those discussions with him during the initial year of the PhD were extremely helpful. I am thankful to Michael Cree for being my first supervisor after Paul changed university. I thank both my supervisors for their guidance, encouragement and correction they have given me during the course of my project. Working with them individually and as a team has been an honour and a privilege. Apart from the professional guidance, they always proved to be inspirational whenever I felt I needed it the most. I also thank Michael and Paul for the many hours they put in reading and correcting drafts of this thesis and the publications related this research work.

The help provided by the rest of the staff and students in the Department of Engineering at the University of Waikato is much appreciated.

Thanks to my children Kushal and Dipika. You have been very patient. Last, but definitely not the least, my sincere thanks to my husband Ravi, for his support and cooperation during my postgraduate years. I sincerely believe that if Ravi had not been by my side, the chances of me accomplishing what I have would have been severely affected. Thanks to my late parents for their encouragement.

To all others who have contributed but whose names I fail to mention here, thank you very much.

Glossary

Terminology	
Cancerous tumour	an abnormal growth
Cell membrane	the semi-permeable phospho-lipid bilayer that surrounds the constituents of all cells
Cytoplasm	all constituents of a cell excluding the cell membrane and the genetic material
Cell tissue	structurally connecting cells
Dynamic model	model incorporating effects of pore formation on the cell parameters
Electrochemotherapy	treatment of disease by chemical agents in conjunction with electropermeabilization
Electroporation (Electropermeabilization)	process where high amplitude electric field pulses are used to alter the permeability of cell membrane by pore formation
Electrogenetransfection	application of electroporation for transfer of DNA into cells to affect some form of gene therapy
Electrofusion	membrane fusion in close-contact adjacent cells achieved by applying electric field pulses
Electroinsertion	application of electroporation for insertion of molecules into the cell membrane
Hybridoma	a hybrid cell produced by the fusion of an antibody with a tumour cell
in vitro	experiments performed on biological cells in an isolated solution of growing cells
in vivo	experiments performed on whole biological systems
Lysis	death of a cell by breaking of the cellular membrane

Membrane permeability	transparency of membranes to material transport
Transdermal drug delivery	application of high-voltage pulses to the skin to induce ionic and molecular transport across the skin

Abbreviations

BLM	bilayer lipid membrane
ECT	electrochemotherapy
EF	electrofusion
EI	electroinsertion
EGT	electrogenetransfection
FPA	fractional pore area
ODE	ordinary differential equation
PDE	partial differential equation
SE	Smoluchowski equation
TDD	transdermal drug delivery

Mathematical notations

Symbol (Unit)	Description
a (μm)	cell radius
a_p (Fm^{-2})	constant for calculating energy drop across membrane in Chapter 2
A (m^2)	cell surface area
A_p (m^2)	total area occupied by the pores at any given time
b	pore creation constant
C_m (Fm^{-2})	specific membrane capacitance
D_f ($\mathrm{m}^{-2}s^{-1}$)	diffusion coefficient for pore radius
$E(t)$ (Vm^{-1})	time-varying electric field
$\varepsilon_{\mathrm{in}}$ (Fm^{-1})	intracellular permittivity
ε_m (Fm^{-1})	membrane permittivity
$\varepsilon_{\mathrm{ex}}$ (Fm^{-1})	extracellular permittivity
$\bar{\varepsilon}$ (Fm^{-1})	complex permittivity
F (Cmol^{-1})	Faraday's constant
$F_{\max}$ (NV^{-2})	max electric force for $V_m = 1$ V
F_p (NV^{-2})	electric force acting on the pore
g_m (Sm^{-2})	specific membrane conductance
g_p (Sm^{-2})	specific conductance due to electroporation
h (nm)	membrane thickness
i_{lge} (A)	current through the electropores larger than 1 nm
i_{sml} (A)	diffusion current through a single small electropore
J_{ion} (Am^{-2})	ionic current density
J_{sml} (Am^{-2})	current density through small pores
J_{lge} (Am^{-2})	total current density through large electropores
J_m (Am^{-2})	total current density at the cell membrane
n	relative entrance length of pores

N (m^{-2})	pore density
N_o (m^{-2})	equilibrium pore density when $V_m = 0$ mV
Φ_{in} (V)	internal potential
Φ_{ex} (V)	external potential
Q	number of large pores
r_q (m)	radius of the q^{th} pore
R_p (Ω)	pore resistance
R_{in} (Ω)	series input resistance
R ($\mathrm{JK}^{-1}\mathrm{mol}^{-1}$)	universal gas constant
r_d (nm)	radius at global maximum
r_h (m)	constant used in calculating electric force
r_m (nm)	minimum energy radius at V_m=0
r_* (nm)	minimum radius of hydrophilic pores
r_t (m)	constant used in calculating electric force
σ_{in} (Sm^{-1})	intracellular conductivity
σ_m (Sm^{-1})	membrane conductivity
σ_m^p (Sm^{-1})	conductivity of electroporated membrane
σ_{ex} (Sm^{-1})	extracellular conductivity
σ_{ps} (Sm^{-1})	conductivity of aqueous solution in pores
ψ ($\mathrm{m}^{-2}\mathrm{s}^{-1}$)	creation rate coefficient
θ (radian)	polar angle
τ_{mw} (s)	the membrane relaxation time constant
T (K)	absolute temperature
V_{ep} (mV)	characteristic voltage of electroporation
V_m (V)	transmembrane potential
v_m (V)	nondimensional transmembrane potential
V_{rest} (mV)	membrane rest potential
w_d (kT)	energy at global maximun
w_{ed} (Jm^{-1})	edge energy
w_m (kT)	energy at local maximun
w_* (kT)	energy at local maximun
w_o (constant)	energy barrier within pore
w_{st} (J)	steric repulsion energy
w_{stc} ($\mathrm{J}^{1/4}m$)	steric repulsion energy constant
ξ_0 (Jm^{-2})	tension of the bilayer without pores

ξ' (Jm^{-2})	tension of hydrocarbon-water interface

Preface

Electroporation is an application in biotechnology and is used in a number of medical treatments, however, the process of electroporation is still not completely understood. The development of theoretical models of electroporation has lagged behind experimental research.This thesis is a comprehensive report of the work I have completed in theoretical dynamic modelling of electroportaion. The aim of the research presented here is to develop numerical models that allow the simulations of dynamic electroporation of a single spherical cell when exposed to bipolar electric field wave-shapes.

The thesis proceeds as follows: Chapter 1 provides a brief background to cell biology necessary for understanding of what follows in the thesis. This leads into a brief explanations of applications of electroporation.

Electroporation/Electropermeabilization is the use of high magnitude electric field pulses to alter the permeability of a cell membrane. This change in permeability is achieved by using an electric field pulse to induce microscopic 'pores' in the cell membrane. These pores are commonly called 'electropores,' which is why the process is commonly referred to as *electroporation*. Chapter 2 lays the foundations for electroporation modelling. Terms, concepts and mathematical formulae relevant to electroporation are reviewed.

Chapter 3 presents the first part of the research. A novel method of modelling electroporation that simulates cell response to applied arbitrary electric field wave-shape pulses is developed. Results of transmembrane potential simulations to 100 kHz and 1 MHz bipolar sinusoidal field pulse at four different amplitudes (below the threshhold for electroporation) are presented to confirm the model. Simulations of cell response to a unipolar square field, bipolar square field, bipolar sinusoidal field, bipolar rectangular field (rectangular pulse train), and a bipolar triangular field are presented.

Chapter 4 presents additional simulation results using the model developed in Chapter 3. These results concentrate on how the efficiency of electroporation

related applications can be significantly improved by appropriately adjusting the parameters of the applied electric field and the extracellular conductivity. Emphasis is given on the normalization of the degree of electroporation for a range of cell radii.

Chapter 5 presents the second numerical model for electroporation. This model simulates spatial and temporal aspects of pore radius as an effect of any given form of applied electric field (including unipolar or bipolar), and other important electroporation system parameters of single spherical cell electroporation. Results of transmembrane potential simulations to 100 kHz and 1 MHz bipolar sinusoidal field pulse at two different amplitudes (below the threshhold for electroporation) are presented to confirm the model. The transmembrane potential and pore radius at various polar angular positions about the cell membrane and as a function of time are presented.

Additional simulation results from this model are used to compare the extent of electroporation in response to sinusoidal AC (bipolar) electric field pulses of two different frequencies in a range of extracellular conductivity for two different cell radii.

At the onset of this thesis in 2003, electroporation modelling was planned to be investigated to be able to simulate dynamic electroporation results (transmembrane potential and pore density) as a function of variety of applied electric field waveforms including bipolar electric fields, on a single spherical cell. The effect of frequency of the bipolar electric field and extracellular conductivity was to be tested, with an intention to suggest ways to get high electroporation efficiency. This has been achieved in Chapter 3 and 4. It was then thought necessary that in order to allow entry of large size molecules (like DNA) into electroporated cells, a model should simulate pore radii evolution spatially and temporally as a function of any given form of applied electric field (including unipolar or bipolar fields). This has been achieved in Chapter 5.

The thesis as a whole is concluded in Chapter 6. The main results are briefly summarized and future work is proposed.

Publications

The following publications were prepared during the course of this research:

Talele, S. and P. Gaynor. Nonlinear time domain model of electropermeabilization: Response of a single cell to an arbitrary applied electric field.

Journal of Electrostatics, **65**, pp. 775–784 (2007).

Talele, S. and P. Gaynor. Non-linear time domain model of electropermeabilization: Effect of extracellular conductivity and applied electric field parameters. *Journal of Electrostatics*, **66**, pp. 328–334 (2008).

Talele, S., P. Gaynor, J. van Ekeran, and M. J. Cree. Modelling membrane pore dynamics during electroporation of a single spherical cell with bipolar field pulses for use in biotechnological applications. *In preparation.*

Presentations

The following papers were presented orally during the course of this research:

Talele, S. High electric fields - electroporation and electrofusion. In: *SciCon 2006: Celebrating Science Innovation.* New Zealand (2006).

Talele, S. and P. Gaynor. Nonlinear time domain model of electropermeabilization: Response of a single cell to an arbitrary applied electric field. In: *Proceedings of the International Conference on Bioinformatics-2006*, pp. 306–306. New Delhi, India (2006).

Talele, S., P. Gaynor, J. van Ekeran, and M. J. Cree. Modelling membrane pore dynamics during electroporation of a single spherical cell with bipolar field pulses for use in biotechnological applications. In: *Proceedings of the International Conference on Engineering Technology*, pp. 499–508. Penerbit Universiti, Kuala Lumpur, Malaysia (2007).

Talele, S., P. Gaynor, J. van Ekeran, and M. J. Cree. Modelling membrane pore dynamics during electroporation of single spherical cell for multipulse electric field protocols. In: *Proceedings of the International Conference on Modelling and Simulation*, pp. 1163–1168. Allied publishers, Coimbatore, India (2007).

Talele, S., P. Gaynor, J. van Ekeran, and M. J. Cree. Modelling single cell electroporation with bipolar pulse: Simulating dependence of electroporated fractional pore area on the bipolar field frequency. In: *Presented in International Joint Conferences on Computer, Information, and Systems Sciences, and Engineering*, Sponsored by the University of Bridgeport, co-sponsored by the IEEE Computer Society, Communications Society and Education Society, USA (2008).

Contents

List of Figures

List of Tables

Chapter 1

Biology Background

This chapter gives a brief overview of basic biological terminology and theory needed for understanding this thesis. The interested reader can find further information in the text by Curtis and Barnes (1983). The chapter concludes with an introduction for the biological phenomenon of electroporation. The theoretical electromagnetic description of electroporation is fundamental to this thesis, and an in-depth development is saved for a separate chapter namely Chapter 2.

1.1 The Cell

Most of the content of this thesis deals with electromagnetic characteristics of biological cells and the effect of electric field on them. One of the fundamental statements of biology (Curtis and Barnes, 1983) is that all living organisms are composed of cells. The cell is thermodynamically an open system that is in constant exchange with its environment. Each cell is self contained and self maintaining: it is able to take in nutrients and convert the nutrients into something else that may be helpful in multiplication, expansion, power, or defence.

Each cell is made of a set of common components. A particular type of cell is determined by the details and combinations of these components. The common component of every cell is the cell membrane and the genetic material.

The cell membrane is a physical barrier which separates the cell interior and its environment, regulates what moves in and out, and maintains the electric potential between the cell exterior and cell interior.

The organisation of the genetic material of the cell determines two different types of cell: the prokaryotic and the eukaryotic cell. Prokaryotic cells are usually singletons, the primary example being bacteria. In contrast eukaryotic cells are usually found in multicellular organisms like plants and animals. Prokaryotes (meaning before nucleus) concentrate most of their genetic material to a loosely defined region called the nucleoid near the cell centre. Eukaryotes (meaning true nucleus) separate most of their genetic material into a well defined region, called the nucleus, surrounded by a double membrane sack known as the nuclear envelope. In addition to a cell membrane, prokaryotic cells also have a cell wall which is produced by the cell and resides on the outer surface of the cell membrane. Some eukaryotic cells also produce cell walls, but these are quite different to those of the prokaryotic cell. Animal cells do not have cell walls.

All other components of a cell are inside the cell, and are known as the cytoplasm. The cytoplasm contains all the molecules required for existence, in addition to well defined regions of function such as the organelles (meaning little organs).

1.1.1 The cell membrane

Biological membranes are the most common cellular structures in animals and plants. Membranes are involved in a number of cellular functions, and are complex and varied. A membrane is made mostly from a double layer of lipids (hydrophobic fatty acid chain molecules) and hydrophilic phosphorus molecules. Hence, the membrane is called a phospholipid bilayer. Lipids are water soluble, oily (greasy) organic substances, and are the most important storage forms of chemical energy in the body. A major component of the cell membrane are polar lipids. The cell membrane also is the basis for the capacitive nature of cells and tissues.

As seen in Figure 1.1, the phospho-heads cover the two surfaces of the bilayer and the fatty acid tails constitute the interior of the bilayer (Israelachvili, 1992). In Figure 1.2 the membrane embedded proteins, and sodium ionic channels are shown. The proteins are mostly involved with selective molecule transport across the membrane. Sodium ionic channels are involved in the electrogenic pump action explained below. Membranes commonly contain a number of proteins, a number of phospholipids and glycolipids with various

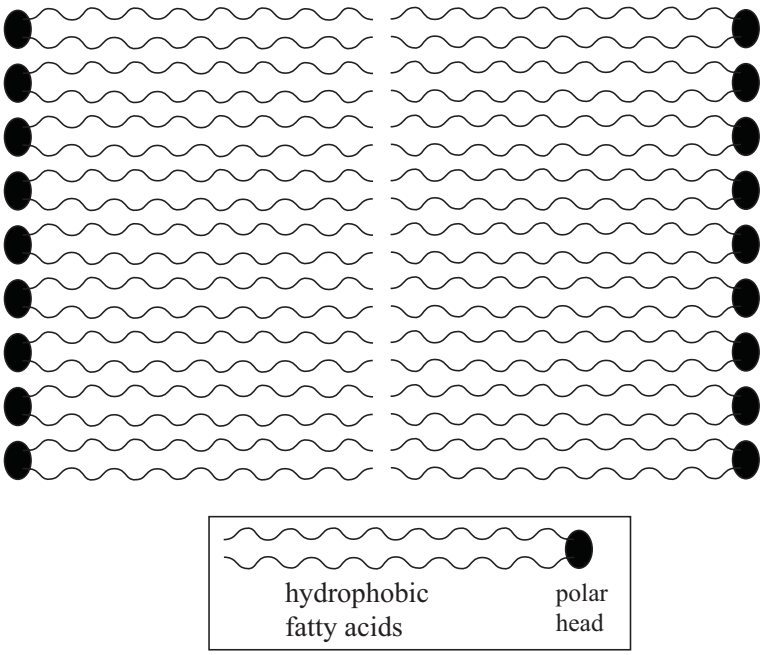

Figure 1.1: Bilayer lipid membrane (Adapted from (Israelachvili, 1992)).

headgroups, number of chains and chain lengths. In spite of the various complexities, membranes can be generalized to have the significant property that they exist as thin bilayer membranes. As the biological lipids tend to self-assemble, these structures are not fixed and are part of a very dynamic system.

A bilayer lipid membrane (BLM) has a very low electric conductivity and is thus closed for ion transport. The membrane thickness is about 5 nm, thus the membrane capacitance is very high, and the breakdown potential is low.

Membranes change their lipid composition in response to external stimuli. Under stress, a membrane may form a pore of a non-bilayer structure. More information on the membrane can be found in the book on intermolecular and surface forces by Israelachvili (1992).

1.1.2 Ion pumps

Ion pumps are sodium or potassium pumps that are embedded in the cell membrane. Each pump translocates a greater electric charge (three Na^+ ions per cycle) in one direction than in the other (two K^+ ions per cycle)(Grimnes and Martinsen, 2000). Many such pumps operate in parallel in the cell membrane, thus together they are capable of generating an electrical potential difference

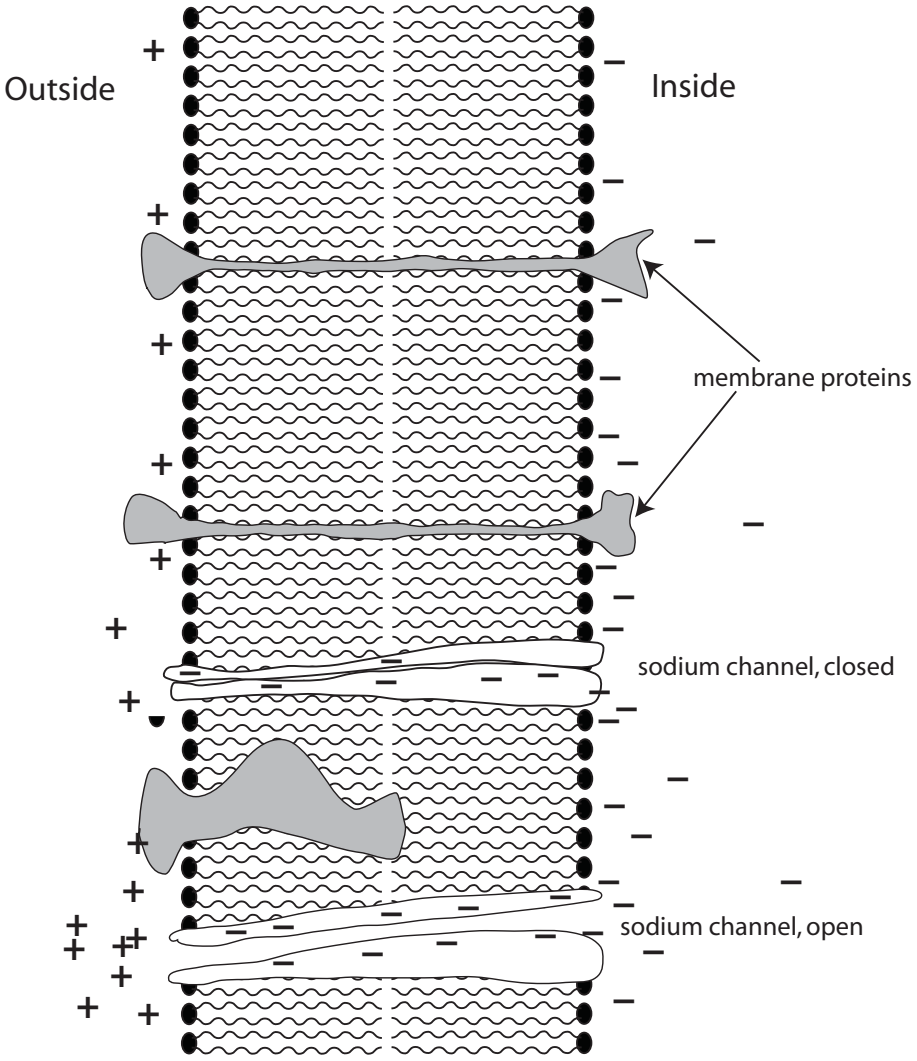

Figure 1.2: Bilayer lipid membrane with embedded proteins and sodium channels.

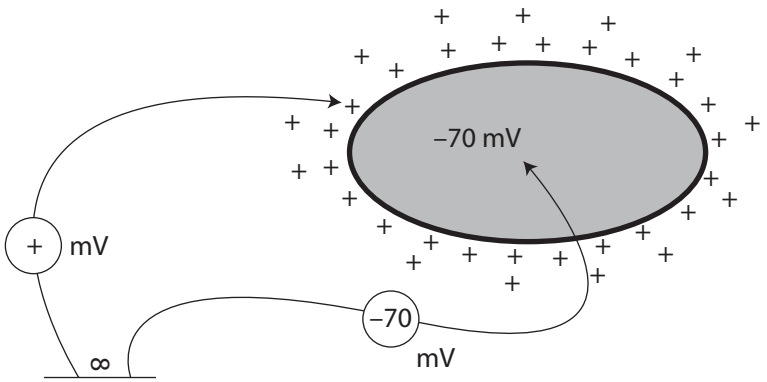

Figure 1.3: Rest potential: Intra and extra cellular potential of a cell under normal conditions.

of up to −90 to −40 mV across the membrane, the interior being at negative potential with respect to the extracellular liquid. As shown in Figure 1.3, for excitable cells (muscle and nerve cell) this potential is about −70 mV, for non-excitable cells only −10 to −20 mV (Grimnes and Martinsen, 2000). Excitable cells are those that can be stimulated to create a tiny electric current.

1.1.3 Tissue

When cells of a particular type are grouped together, they are known as cell tissue. For example, humans have skin, bone and lung tissue. The cells are of various sizes that perform different functions. Organization of tissue involves an extraordinary level of complexity.

1.2 DNA and Genetics

In section 1.1 it was described how all cells have some sort of genetic material. This genetic material is responsible for the biological information contained in an organism. Two different kinds of genetic material exist: deoxyribonucleic acid (DNA) and ribonucleic acid (RNA). Most organisms use DNA for their long-term information storage, but notable exceptions are some viruses that have RNA as their genetic material. In simple terms, DNA is an exceptionally long molecule that is a sequence of coded information. It is therefore genes or combinations of genes that characterize the biological make up of an organism. Genes determine the colour of eyes, the size of limbs and susceptibility to many ailments. When cells divide, all of the DNA in the parent cell is replicated to

both of the daughter cells. As in any other process, errors can happen during replication. Inherent cell replication systems correct and remove such errors, however any uncorrected errors may lead to changes in genes. The result may be a mutation in some physical characteristic (Curtis and Barnes, 1983). Most mutations are small and of little or no consequence. Typically it is when there is a change in the environment that mutations have an effect and they are then selected for or against by natural selection. Large mutations are rare and tend to be harmful. Many external conditions like chemical radiation can cause specific mutations that disrupt cell growth, lead to abnormal effects and even kill cells. Changes in genes can also be induced by some viruses. Due to advances in technology it is possible to include specific genetic material into cells and grow them to express that DNA. This is known as transfection. If the genetic transformation is maintained and carried on in their further progeny, the organism is called transgenic.

1.3 Electroporation

It is possible to break a hole in a cell membrane by applying a sufficiently strong electric field pulse. This is known as electroporation. Chapter 2 discusses this in detail. Polarization is one of the basic mechanisms of interactions of membranes with electric fields, leading to electroporation and related phenomenons of dielectrophoresis and electrofusion.

1.3.1 Polarization of membranes

Polarization of membranes underlies their destabilization. Polarization is due to restricted motion of charges: electric fields exert forces on charges. These charges can either move if they are free (material is conductive) or accumulate if they are limited in their movement. This charge redistribution in a particular limited space leads to polarization. Figure 1.4 shows polarization of a single cell due to restriction by the cell membrane to the motion of ions.

1.3.2 Electric field interaction with polarized membranes

The interaction of external electric field with the polarized membranes results in forces which can induce motions inside particles. This motion can result in

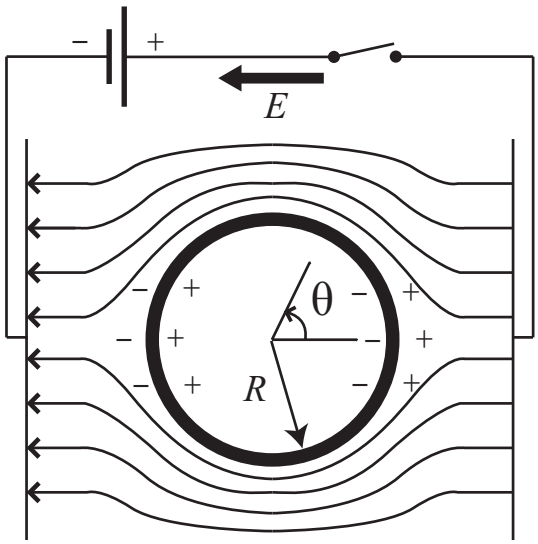

Figure 1.4: Spherical particle in electric field

structural rearrangement or fracture in the material. This can subsequently lead to electroporation and related phenomenon in case of cell membranes (Dimitrov, 1995). Membranes have low polarizability (relative dielectric constant about 5) and low conductivity (3×10^{-7} S/m) (Kotnik *et al.*, 1998). The cell is generally surrounded by a medium of high dielectric constant (about 80) and a high conductivity (about 1.2 S/m). Application of external fields leads to accumulation of charge at the membrane surface; this creates an electric field inside the membrane that is much stronger than the surrounding field. The polarized membrane interacts with this field, resulting in structural rearrangements which can cause membrane poration.

1.3.3 Applications of electroporation

There are many applications of electroporation/electropermeabilization (EP) in biotechnology, biochemistry, molecular biology, medicine and other biological research. Some of the applications are as follows:

1. Electrochemotherapy (ECT): In cancer chemotherapy, some drugs do not exhibit anti-tumour effects because of insufficient transport through the cell membrane (Miklavĉiĉ and Kotnik, 2004). A combined use of chemotherapeutic drugs and application of electric pulses is known as electrochemotherapy and is useful for local tumour control. Especially, bleomycin has been reported to have shown a 700-fold increased cytotox-

icity when used in ECT (Cemaẑar *et al.*, 1998; Serŝa, 2000). This helps to achieve a substantial anti-tumour effect with a small amount of drug, that limits its side effects (Serŝa *et al.*, 1993). Bleomycin and cisplatin have proven to be much more effective in electrochemotherapy than in standard chemotherapy when applied to tumour cell lines *in vitro*, as well as *in vivo* on tumours in mice (Mir *et al.*, 1991, 1995; Serŝa *et al.*, 1995). Clinical trials have been carried out with encouraging results (Glass *et al.*, 1996; Serŝa *et al.*, 2000; Gothelf *et al.*, 2003; Kranjc *et al.*, 2005; Tozon *et al.*, 2005; Snoj *et al.*, 2005).

2. Electrogenetransfection (EGT): Application of electroporation for transfer of DNA into cells to effect some form of gene therapy, often referred to as electrogenetransfection, is currently being applied in some pre-clinical trials (Mir, 2000). It is presently considered to have large potential as a non-viral method to deliver genetic material into cells, the process aimed at correcting genetic diseases (Budak-Alpdogan *et al.*, 2005; Bertino, 2008).

3. Electrofusion (EF): Under appropriate physical conditions, delivery of electric pulses can lead to membrane fusion in close-contact adjacent cells. EF results in the encapsulation of both original cells' intracellular material within a single enclosed membrane and can be used to produce genetic hybrids or hybridomas (Zimmermann, 1982). Hybridomas are hybrid cells produced by the fusion of an antibody secreting stimulated B-lymphocytes, with a tumour cell that grows well in culture. The hybridoma is then able to continue to grow in culture, and a large amount of specific desired antibodies can be recovered after processing. Electrofusion has proved to be a successful approach in the production of vaccines (Scott-Taylor *et al.*, 2000; Orentas *et al.*, 2001), antibodies (Schmidt *et al.*, 2001), and reconstructed embryos in mammalian cloning (Gaynor *et al.*, 2005).

4. Transdermal drug delivery (TDD): Application of high-voltage pulses to the skin allows a large increase in induced ionic and molecular transport across the skin barrier (Prausnitz *et al.*, 1993). This has been applied for transdermal delivery of drugs, such as metoprolol (Vanbever *et al.*, 1994), and also works for larger molecules, for example, DNA oligonucleotides

(Vanbever *et al.*, 1994).

5. Electroinsertion (EI): Another application of electroporation is insertion of molecules into the cell membrane. As the electric field induced membrane pores reseal, they entrap some of the transported molecules. Experiments on electroinsertion suggest the possibility of using the process to study certain physiological properties of these cells and understanding aspects of the lipid-protein interactions of the cell plasma membrane (Mouneimne *et al.*, 1992).

Chapter 2

Review of Electroporation

Electroporation also called *Electropermeabilization*, is the use of high magnitude electric field pulses to alter the permeability of a cell membrane. This change in permeability is achieved by using an electric field pulse to induce microscopic 'pores' in the cell membrane. These pores are commonly called 'electropores,' which is why the process is commonly referred to as *electroporation*.

Many biotechnological applications and research require transport of macromolecules such as genes, antibodies, and chemical drugs, into a host cell. For any particular application, choosing a given transfer process is based on its efficacy, ease of use and side effects. A characteristic shared by most of the chemical and biological techniques is that they are usually cell-type dependent and have relatively poor efficiencies. Therefore, methods which are both versatile and efficient are being searched for and investigated. Electroporation, first reported in 1982 (Neumann *et al.*, 1982), is one of the methods reported to be effective for such delivery. Since its inception, this method has been a valuable tool for *in vitro* delivery of small and large molecules into a large variety of cells. During this time, electroporation has been performed on living plants, animals, and humans (*in vivo* electroporation), with an increasing focus on therapeutic uses (Dev *et al.*, 2000; Smith and Nordstrom, 2000; Muramatsu *et al.*, 1998).

This chapter covers important aspects of electroporation including induced transmembrane potential, formation of pores, relation between pore radii and pore energy, pore density and current through electropores.

2.1 Overview of Electroporation

The phenomenon of the electric modification of cell membrane conductivity has been known since the 1940s (Cole, 1972). Sale and Hamilton (1967, 1968) observed that treatment of cells with intense electric field pulses led to cell lysis, and suggested that the cell membranes were damaged by the transmembrane potential induced by the applied electric field.

The transmembrane potential V_m was estimated from the equation, often referred to as the (steady-state) Schwan's equation (Schwan, 1957),

$$V_m = \frac{3}{2} E a \cos\theta, \tag{2.1}$$

where E is the applied external electric field, a is the radius of the cell, and θ is the angle between the direction of the field and the normal to the cell surface. The critical transmembrane potential built up for electroporation to occur was found to be about ± 1 V. The phenomenon was called 'electric breakdown' by Sale and Hamilton (1968).

It soon became apparent that a field-induced permeability increase is transient in nature although long-lived compared with the field duration. The term 'electropermeabilization' was used to explain the occurrence of permeability changes introduced by electrical impulses in vesicular membranes (Neumann and Rosenheck, 1972). It was later shown by Rosenheck *et al.* (1975) that the electric field induced change was transient. The resistance changes in the membrane were attributed to dielectric breakdown (Zimmermann *et al.*, 1973).

Subsequent studies showed that the cell membranes of pulse treated cells were permeable to molecules of a size smaller than a certain limit, suggesting the creation of a porous membrane structure (Neumann and Rosenheck, 1972; Zimmermann *et al.*, 1973; Kinosita and Tsong, 1977b). The term *electroporation* was born as a result of the observation that dielectric breakdown of the cell membrane appeared to generate 'holes' or 'pores' that material could pass through (Hofmann and Evans, 1986). It was also found that under appropriate conditions, the cells could recover, which implied that these electropores were resealable and could be induced without permanent damage to the cell (Zimmermann *et al.*, 1980), and the cytoplasmic macromolecular contents could be retained (Kinosita and Tsong, 1977a,b). Since then, a number of research groups have studied mechanisms of pore formation and detailed character-

istics of the cell membranes modified by electric fields (Abidor *et al.*, 1979; Chernomordik *et al.*, 1983; Glaser *et al.*, 1988; Schwister and Deuticke, 1985)

However, the pores themselves were not observed until the invention of rapid freezing electron microscopy in the 1990s. Chang and Reese (1990) were the first to observe them. Other aspects of electroporation, for example, vizualization of transmembrane potential and its evolution in space and time, resealing of pores and asymmetry in permeability of porated cells (sea urchin egg and liposomes) with the help of an optical microscope, were also reported (Kinosita *et al.*, 1992; Hibino *et al.*, 1993). These microscopes have a time resolution of sub-microseconds suitable for studying electroporation.

2.1.1 Important aspects of electroporation

During the formative years of modern micro- and molecular biology, chemical and biological techniques were developed to transfer selected material through cellular membranes (Ausubel *et al.*, 1990). The ability to perform transmembrane transport of material is critical to many areas of research. Much of this research requires transport of macromolecules such as DNA, RNA, antibodies, chemical drugs, metabolites, molecular probes and various vesicles.

Research that is closely associated with electroporation, and has attracted more study among cell biologists and biophysicists, is that high voltage electric pulses can induce fusion of cells. The viable giant cells were first obtained by Neumann *et al.* (1980) by simple electro-pulsing of a suspension of cells. Later, it was suggested to make use of the phenomenon of dielectrophoresis (Pohl, 1978), to acquire close contact between cells (Scheurich and Zimmermann, 1981). Dielectrophoresis is the movement of relatively nonconducting or charged particles (cells) in a non-uniform AC electric field (Pohl, 1978). If a number of particles are present, appropriate particle size, density of particles, electric field magnitude and frequency can induce cells to aggregate in long chains (pearl chain) in an alternating electric field (Zimmermann, 1982).

In 1982, transfection of a foreign gene into eukaryotic cells by the electroporation method was reported (Neumann *et al.*, 1982). Transfection involves opening transient pores in the cell plasma membrane, to allow the uptake of genetic material or even proteins such as antibodies. It was also reported that the transfected gene was expressed in the host cells (Neumann *et al.*, 1982). Since then, electroporation has become accepted as an effective technique for

introduction of foreign DNA into cells of any origin (Potter, 1988; Neumann *et al.*, 1989). The ease of the electroporation technique and its applicability to a variety of cells has led to investigations of DNA electrotransfer into various tissues. The utility of *in vivo* electroporation for entry of molecules has been demonstrated through an increasing number of new applications that have been developed each year (Jaroszeski *et al.*, 2000; Saulis and Ŝatkauskas, 2004b).

Experiments in 1989 on frog skin showed that electroporation could be made to occur repeatedly in a tissue without evident damage (Powell *et al.*, 1989). Further research has shown that the electroporation of the skin could be used to enhance transdermal drug delivery (Prausnitz *et al.*, 1993, 1994).

In 1989 it was reported that upon application of electric fields pulses on a suspension of cells in the presence of a selected membrane protein, implantation of the protein in the cell's plasma membrane was possible (Mouneimne *et al.*, 1989). This phenomenon is called electroinsertion. Later, electroporation of excitable membranes was observed (O'Neil and Tung, 1991). Electrically induced membrane breakdown of isolated cardiac cells was reported. Chen and Lee (1994) reported the asymmetrical electropermeabilization of frog skeletal muscle fibres with respect to the stimulation pulse polarity.

A method of electroporation has been applied *in vivo* to introduce anticancer drugs to tumorous tissue in order to obtain therapeutic effects (Mir *et al.*, 1991). The main factors that play a crucial role in obtaining high responses of the treatment are the drug used in the treatment and the appropriate electric pulses delivered to the tumour. This phenomenon is called electrochemotherapy.

Electroporation has been investigated and refined to an extent that, for most applications, it is simpler and more efficient than rival chemical and biological processes (Chang *et al.*, 1992a; Neumann *et al.*, 1989). However, the mechanisms of electroporation are still not fully understood and there are aspects of the process which are, as yet, suboptimal in their possible performance. Optimization of the parameters of electric pulses for any specific application is still needed (Jaroszeski *et al.*, 2000; Saulis and Ŝatkauskas, 2004b)

The scope of this thesis is to address some of these problems in an attempt to increase understanding and efficiency through optimization of parameters for electroporation.

2.2 Response of Cell to Electrical Field

From the electrical point of view, the cell can be described as an electrolyte (the cytoplasm) surrounded by an electrically insulating cover (the cell membrane). Under physiological conditions, extracellular space is also an electrolyte. As a simple approximation, one may treat the membrane as non-conducting (purely dielectric), and the intracellular and the extracellular space as purely conductive (having zero dielectric permittivity).

2.2.1 Membrane rest potential

Under physiological conditions, a potential in the range of -90 mV up to -40 mV (most commonly -70 mV) is always present on the cell membrane (Cole, 1972). This potential is caused by a tiny deficit of positive ions in the cytoplasm leading to a charge imbalance that is a consequence of the transport of specific ions (Na^+ and K^+) across the membrane. This transport is driven towards the electrical and ion concentration equilibrium. Once this equilibrium is reached, the electrical slope across the membrane determines the resting transmembrane potential. This is the normal physiological condition of any healthy cell. The unbalanced ions responsible for the membrane rest potential represent a very small fraction of all the ions in the cytoplasm, so that the osmotic pressure difference (hydrostatic pressure produced by a difference in concentration between solutions on the two sides of a semipermeable membrane) generated by this imbalance is negligible. The membrane also acts as a charged capacitor, with the unbalanced ions accumulating close to its surface, so that the cytoplasm can in general be viewed as electrically neutral.

2.2.2 Induced transmembrane potential

When a biological cell is exposed to an electric field, a local distortion of the field in the cell and its vicinity takes place. Due to the low membrane conductivity, the field is concentrated in the cell membrane, where it is several orders of magnitude larger than in the cytoplasm and the extracellular region. This results in an induced transmembrane potential V_m, that is stochastic. This transmembrane potential superimposes to the membrane rest potential (Kotnik, 2003). When an isolated spherical cell is exposed to a DC homogen-

eous electric field, the voltage induced on the cell membrane is determined by solving Laplace's equation. For the first approximation, the cell membrane can also be treated as initially nonconductive. Under these assumptions, the transmembrane potential is given by the Schwan's Equation, see Equation 2.1 (Schwan, 1957). Schwan's equation implies that the transmembrane potential varies proportionally to the cosine of the angle and the maximum potential is induced at the points where the electric field is perpendicular to the membrane, namely at $\theta = 0°$ and $\theta = 180°$, the points referred to as the 'poles' of the cell. The formula describes the static situation, and can safely be applied to yield the steady-state value of the induced transmembrane potential.

2.2.3 Effect of membrane rest potential on induced transmembrane potential

Recall that the transmembrane potential superimposes to the membrane rest potential. If an applied electric field produces a transmembrane potential of the same orientation of the inherent rest potential, then they add. Conversely, if the applied electric field produces a transmembrane potential in the opposite orientation of the inherent rest potential, then they subtract. Thus one pole is likely to experience a transmembrane potential about 140 mV (assuming a rest potential of -70 mV) lower than the other pole, and can result in asymmetry in breakdown around the cell.

2.3 Formation of Pores

Equation 2.1 for the transmembrane potential is valid only until pores are formed. Once enough pores are formed, the membrane conductivity changes and Schwan's equation is not valid any more. This phenomenon of electroporation has often been referred to as 'electrical breakdown' or electropermeabilization.

A few well observed and documented characteristics of the cell membrane electroporation can be summarised as follows:

1. The transmembrane potential must exceed a certain threshold value $V_{m(cr)}$ for electroporation to occur (Hibino *et al.*, 1991; Kinosita *et al.*, 1992).

2. It is thought, most probably, that it is the lipid part of the biological membrane which is transiently permeabilized by an electroporation pulse (Chernomordik *et al.*, 1987).

3. Electropermeabilization of cells can be asymmetrical: pore populations in two hemispheres may differ in the size and (or) number of pores (Kinosita *et al.*, 1992).

4. The change of the membrane permeability caused by the pore formation can be fully reversed. When the pulse parameters, number of pulses and the medium properties are properly chosen, electropores have a finite lifetime (Swezey and Epel, 1989; Kinosita and Tsong, 1977a,b; Saulis and Ŝatkauskas, 1977; Saulis *et al.*, 1991).

5. The increased permeability can be sufficient enough to allow ions and small molecules as well as macromolecules to enter or leave the cell (Kinosita and Tsong, 1977b; Liang *et al.*, 1988; Graziadei *et al.*, 1991; Sheng *et al.*, 1995; Swezey and Epel, 1989; Yumura *et al.*, 1995).

6. The uptake through pores is greater in a solution of low ionic strength (Kinosita and Tsong, 1977a; Rols and Teissié, 1989; Teissié and Tsong, 1981).

7. Permeability is bidirectional, that is, intracellular compounds (e.g., ions, glycine, ATP, proteins) can leak from electroporated cells (Moser *et al.*, 1995; Neumann and Rosenheck, 1972; Schwister and Deuticke, 1985), while foreign substances can enter the cell (Kinosita and Tsong, 1977a,b; Swezey and Epel, 1989; Zimmermann *et al.*, 1980).

8. Phospholipids in the membrane exhibit major structural changes under electroporation conditions (Neumann et al., 1992). There appears to be a rapid transition (within 1 μs) from hydrophobic to hydrophilic pores.

This dependence of pore number, size, and evolution characteristics are researched theoretically in this thesis with results reported in detail in Chapters 3 to 5. In early years a basic concept of the transient aqueous pore hypothesis was that they are membrane 'defects' or 'membrane perforations' (Neumann, 1989), that are created with rapidly increasing rate as transmembrane potential V_m is increased. If the magnitude of V_m increases from zero due to the

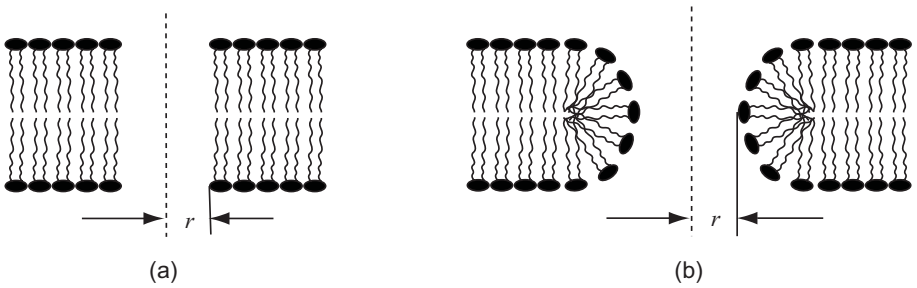

Figure 2.1: Types of electropores: (a) Hydrophobic (nonconduting pore), (b) Hydrophilic pore (conducting pore).

applied external electric field, then the additional membrane energy associated with V_m leads to increased pore creation probability. The rate of pore creation increases nonlinearly with larger V_m. A pore population described by a pore density function quickly increases with respect to increasing V_m, and gives the cell membrane rapidly changing electrical conductance thus reducing the rate at which pores can be created.

2.3.1 Types of pores and their characteristics

Based on the observation by Chang and Reese (1990) where a rapid freezing electron microscopy was used to show volcano-shaped pores in erythrocyte membranes exposed to an intense electric pulse (Weaver and Barnett., 1992; Kakorin *et al.*, 1996), it is currently thought that initial electroporation involves the rearrangement of clusters of lipids' pore structures (Tekle *et al.*, 2001; Saulis and Ŝatkauskas, 2004a) with minimum pore size in the order of a few nanometres. This is in agreement with the results obtained from other pore models. These pore models take into consideration energy changes in the bilayer membrane due to pore formation.

The pores are assumed to be hydrophobic or hydrophilic. The hydrophobic pores, as shown in Figure 2.1a (Abidor *et al.*, 1979; Neu and Krassowska, 1999; Glaser *et al.*, 1988), are simply gaps in the lipid bilayer of the membrane, formed as a result of thermal fluctuations. The primary pores that participate in electrical behaviour and molecular transport are thought to be hydrophilic pores, with a minimum radius of about 1 nm, and a reasonable probability of various pore sizes much larger (Weaver, 1993). The 'hydrophilic' or 'inverted pores,' as shown in Figure 2.1b, have their walls lined with the water-attracting heads of lipid molecules. Hence, the hydrophilic pores allow the passage of

water-soluble substances, such as ions, while the hydrophobic pores do not. In the remainder of this thesis, the hydrophilic pores will be referred to as conducting, and the hydrophobic pores, as nonconducting. Similar notation is used in the literature (Abidor *et al.*, 1979; Neu and Krassowska, 1999; Glaser *et al.*, 1988; Weaver and Chizmadzhev, 1996).

2.3.2 Relation between pore radius and pore energy

Research has established that pore radius and pore energy are related (Abidor *et al.*, 1979; Glaser *et al.*, 1988; Weaver and Chizmadzhev, 1996; Neu and Krassowska, 1999) as shown in Figure 2.2.

Energy of a pore:

The energy function consists of two parts, $u(r)$ for the energy of non-conducting pores and $w_c(r)$ the energy of conducting pores as shown in Figure 2.2a. The energy $w(r)$ of a pore of radius r is the lesser of $u(r)$ and $w_c(r)$ (see Figure 2.2b) (Neu and Krassowska, 1999). This is the pore energy in absence of an applied external V_m. The pore energy $w(r)$ has two maxima, at r_* and r_d, and a local minimum at r_m. The pore energies at r_*, r_m, and r_d are denoted by w_*= $w(r_*)$, w_m= $w(r_m)$, and w_d= $w(r_d)$. This plot in Figure 2.2 is calculated using the values of parameters in Table 2.1 and the form of $w(r)$ given by Neu and Krassowska (1999).

Energy of the nonconducting pores:

The energy $u(r)$ of the nonconducting pores is given in the literature in terms of Bessel functions, and is well approximated by the quadratic function (Neu and Krassowska, 1999),

$$u(r) = w_* \left(\frac{r}{r_*}\right)^2. \tag{2.2}$$

Energy of the conducting pores:

The energy $w_c(r)$ of conducting pores is given by (Neu and Krassowska, 1999)

$$w_c(r) = 2\pi w_{\mathrm{ed}} r - \pi \xi_0 r^2 + \left(\frac{w_{\mathrm{stc}}}{r}\right)^4. \tag{2.3}$$

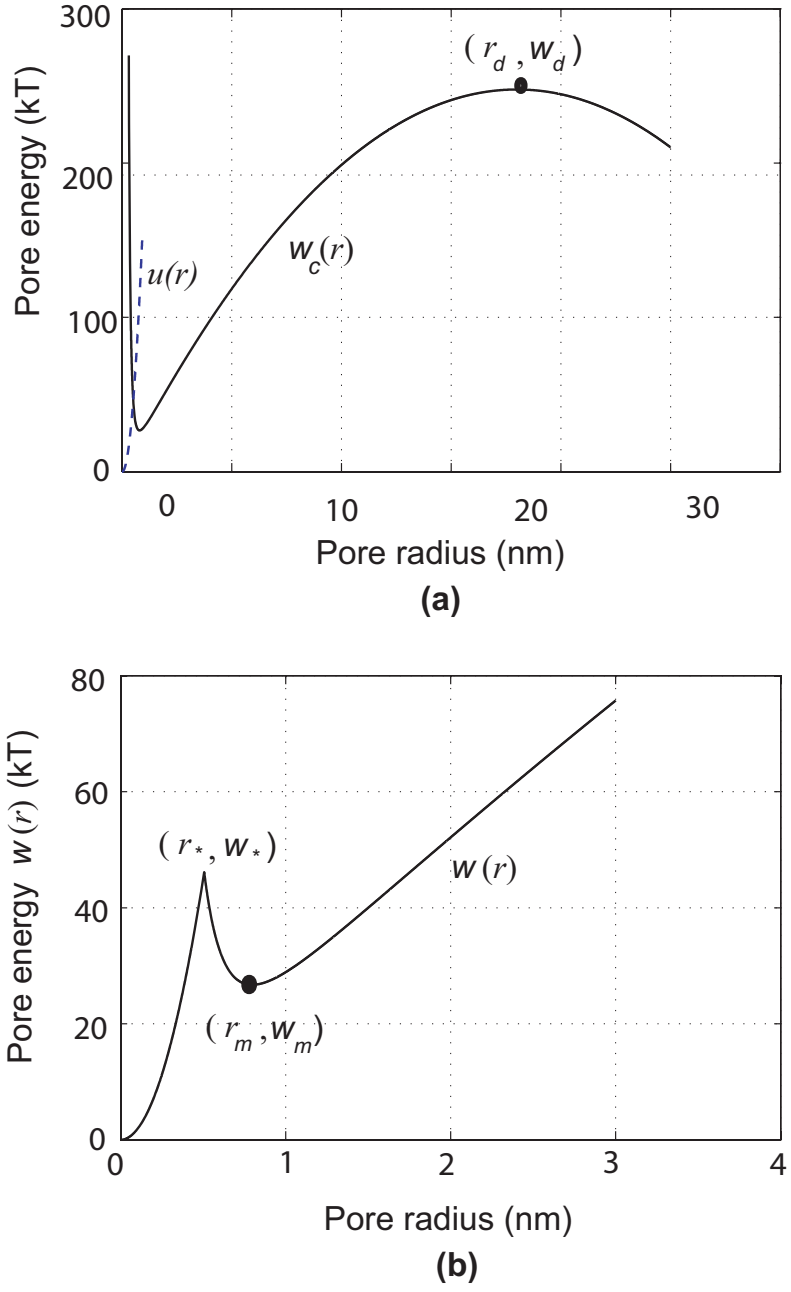

Figure 2.2: Pore-energy function at zero transmembrane potential: (a) The pore-energy function of a non-conducting (dotted line) and conducting (solid line) pore. Adapted from (Abidor *et al.*, 1979; Glaser *et al.*, 1988; Weaver and Chizmadzhev, 1996; Neu and Krassowska, 1999). (b) Lesser energy of the conducting and non-conducting pore. Pore-energy function is enlarged for a shorter range of radius.

The theory of electroporation of the cell membrane is similar to the theory of soap film rupture. If one imagines a membrane with surface tension ξ_0 and then cuts a hole of radius r, the energy change in the system due to the hole is given by the first two terms in Equation 2.3. The lipid head groups are assumed to line the pore interior, thus the pores are conducting. The appearance of a circular pore in a membrane with surface tension ξ_0 is balanced by the presence of two competing energy terms: increase in energy barrier by a linear edge component proportional to pore edge of length $2\pi r$ (Weaver and Powell, 1989; Glaser *et al.*, 1988; Abidor *et al.*, 1979) (first term Equation 2.3) and reduction in energy barrier proportional to removal of pore area πr^2 (second term in Equation 2.3). Here w_{ed} is the energy per unit length of the pore perimeter (pore edge energy) and ξ_0 is the tension of a membrane without pores.

The lipid head groups which line the pore interior, tend to repel each other due to steric and/or electrostatic interactions (Weaver and Chizmadzhev, 1996; Israelachvili, 1992) and are taken into account by adding the third term (Neu and Krassowska, 1999) of Equation 2.3. This steric repulsion is responsible for the increase in pore energy with shrinking radius (Weaver and Chizmadzhev, 1996; Neu and Krassowska, 1999), since it gives a local minimum of w at non-zero radius. Here w_{stc} is the steric repulsion energy constant. In absence of the steric repulsion term the pores would shrink to zero radius, whereas in reality their radii are about 0.76 nm, which corresponds to the local energy minimum (DeBruin and Krassowska, 1999; Neu and Krassowska, 2003; Krassowska and Filev, 2007).

Energy of a pore in the presence of non-zero transmembrane potential:

The existence of transmembrane potential diminishes the energy barrier to pore formation and thus the energy of a pore is modified in the presence of V_m as given by (Abidor *et al.*, 1979; Neu and Krassowska, 1999; Weaver and Mintzer, 1981)

$$w(r,t) = w(r) - \pi a_p {V_m}^2(t) r^2, \tag{2.4}$$

where the second term represents an energy drop across the capacitive membrane (Abidor *et al.*, 1979). The coefficient a_p is a property of the membrane and its aqueous environment. Here, the time dependence of the energy is due

Table 2.1: Values of parameters used to plot Figure 2.2

Symbol	Value	Description
r_*	0.51×10^{-9}(m)	minimum radius of hydrophilic pores[a]
r_m	0.76×10^{-9} (m)	minimum energy radius at V_m=0[a]
r_d	18 (nm)	radius at global maximum[a]
w_*	45 (kT)	energy at local maximum[a]
w_m	25.6 (kT)	energy at local maximum[a]
w_d	238 (kT)	energy at global maximum[a]
a_p	6.9×10^{-2} (Fm^{-2})	constant to calculate energy drop across membrane[b]
w_{stc}	$9.67 \times 10^{-15}(\mathrm{J}^{1/4}m)$	steric repulsion energy constant[b]
w_{ed}	1.8×10^{-11} (Jm^{-1})	edge energy[b]
ξ_0	1×10^{-3} (Jm^{-2})	tension of the bilayer without pores[b]

[a]Values taken from Glaser *et al.* (1988).
[b]Values taken from Neu and Krassowska (1999).

to the temporal variation of V_m. Also, as seen in Figure 2.3, the radius corresponding to the local energy minimum increases for higher transmembrane potential. All pores are initially created hydrophobic at a rate determined by their energy as shown in Figure 2.2 (Smith *et al.*, 2004). Most of them are quickly destroyed by lipid fluctuations. But if hydrophobic pores of radius $r > r_*$ are created, they spontaneously convert to long lived hydrophilic pores. The hydrophilic pores are created within a small range of radii just above r_* and immediately move (expand) toward minimum energy status of radius r_m (Glaser *et al.*, 1988; Neu and Krassowska, 1999, 2003; Smith *et al.*, 2004; Krassowska and Filev, 2007). This is the scenario considered in the model discussed in Chapter 3 of this thesis.

Bilayer membrane energy

The most important entity that affects the pore formation, growth and decay is the pore energy, $w(r)$ at any given time. This energy is a function of pore radius which is a function of space and time. Formation of pores cause dynamic changes in transmembrane potential V_m, that must be included. The pores also affect surface tension which also must be included. Theoretical accuracy of prediction of pores can be only as accurate as the correctness of pore energy, $w(r)$. This theory of the energy function $w(r)$ is applicable only to a single pore, as it does not account of any interactions between the pores. As the

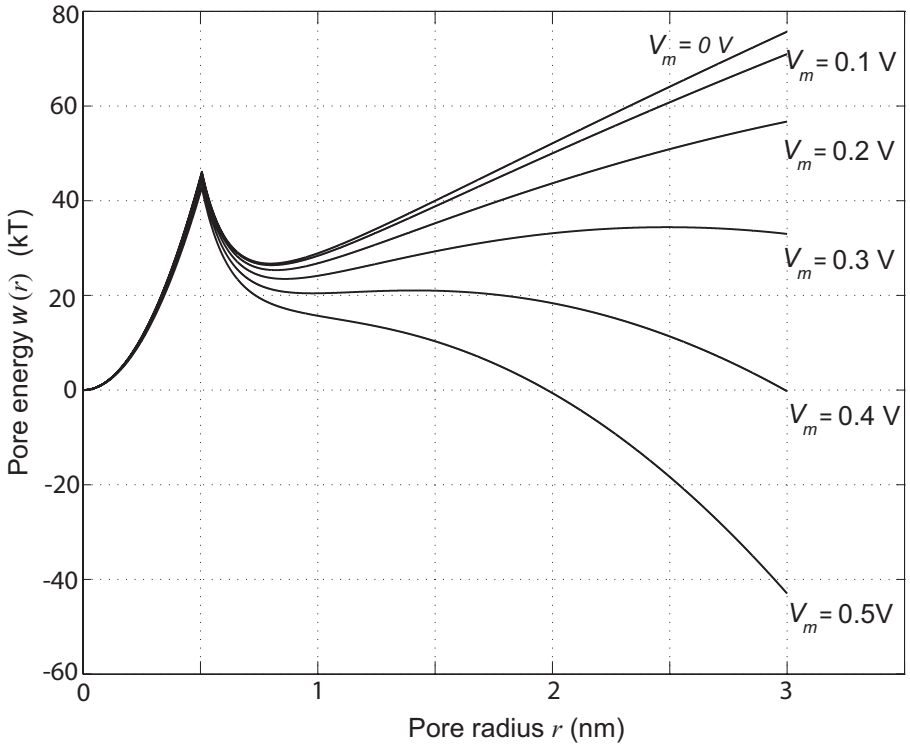

Figure 2.3: The pore-energy function of a pore at transmembrane potential $V_m = 0$, 0.1, 0.2, 0.3, 0.4, and 0.5 V based on references (Abidor *et al.*, 1979; Glaser *et al.*, 1988; Weaver and Chizmadzhev, 1996; Smith *et al.*, 2004). This plot uses the values of parameters in Table 2.1 as per literature (Neu and Krassowska, 1999)

.

radius of any pore of the cell increases, it relaxes the tension of the other pores, decreasing the effective tension experienced by each pore. It follows that pore formation will lead to variations in the tension. This is in agreement with Benachir and Lafleur (1996), whose experimental results suggested that the membrane surface tension must be variable. This tension coupling can be taken into account in terms of the total area A_p occupied by all the pores at any given time. Thus Equation 2.3 is suitably modified and reported by Smith *et al.* (2004), to accommodate pores of various sizes. The bilayer energy is then given by,

$$w_m = \sum_{q=1}^{Q} \left[w_{\mathrm{st}} \left(\frac{r_*}{r_q} \right)^4 + 2\pi w_{\mathrm{ed}} r_q - \pi \xi_{\mathrm{eff}}(A_p) r_q^2 + \int_0^{r_q} F_p(r_q, V_m) dr \right], \quad (2.5)$$

where summation is over the Q pores in the bilayer membrane. The terms in this equation are explained in the following paragraphs.

The lipid head groups which line the pore interior, tend to repel each other due to steric and/or electrostatic interactions (Weaver and Chizmadzhev, 1996; Israelachvili, 1992; Neu and Krassowska, 1999) and are taken into account by the first term in Equation 2.5, where w_{st} is the steric repulsion energy (Neu and Krassowska, 2003).

The appearance of a circular pore in a membrane is balanced by the presence of two competing energy terms: reduction in energy barrier proportional to removal of pore area $\pi {r_q}^2$ (third term in Equation 2.5) and increase in energy barrier by a linear edge component proportional to pore edge of length $2\pi r_q$ (Weaver and Powell, 1989; Glaser *et al.*, 1988; Abidor *et al.*, 1979) (second term in Equation 2.5). Here, w_{ed} is the pore edge energy, and ξ_{eff} is the effective tension of the membrane given by

$$\xi_{\mathrm{eff}}\left(A_p\right) = 2\xi' - \frac{2\xi' - \xi_0}{\left(1 - \frac{A_p}{A}\right)^2} \tag{2.6}$$

where ξ' is the energy per area of the hydrocarbon-water interface (Israelachvili, 1992; Neu and Krassowska, 2003), ξ_0 is the tension of a membrane without pores and A is the total area of the lipid bilayer. A varying value of the total area A_p occupied by the pores at any given time is given by

$$A_p = \sum_{q=1}^{Q} \pi r_q^2 \tag{2.7}$$

and contributes to a dynamic effect of pore formation both temporally and spatially.

The last term in Equation 2.5 is the contribution of the membrane potential to the bilayer energy (Neu and Krassowska, 2003). Assuming the inner surface of a pore as toroidal (Kandu$\hat{\mathrm{s}}$er *et al.*, 2003; Neu and Krassowska, 2003), the electric force F_p acting on the pore is given by

$$F_p(r, V_m) = \frac{F_{max}}{\left(1 + \frac{r_h}{r + r_t}\right)} V_m^2. \tag{2.8}$$

This equation is a heuristic approximation (Neu and Krassowska, 2003) of the

numerical solution which the authors have computed for the electrical force acting on a pore derived from first principles; r_h and r_t are constants taken from Neu and Krassowska (2003). This equation is thought to be appropriate for larger pores as it predicts that F_p approaches a constant value $F_{\max}$ as the pore radius increases, rather than increase linearly (Abidor *et al.*, 1979), or decrease to zero (Barnett and Weaver, 1991; Joshi *et al.*, 2002; Pastushenko and Chizmadzhev, 1982) as radius increases. The Equation 2.5 is used in the model developed in Chapter 5 of this thesis.

2.4 Calculation of Pore Density

The theoretical understanding of the electroporation process is based on the partial differential equation (PDE) known as the Smoluchowski equation (SE), (Freeman *et al.*, 1994; Barnett and Weaver, 1991; Pastushenko *et al.*, 1979; Weaver and Mintzer, 1981). The SE describes the evolution of membrane pore population density in terms of the number and size of the pores. Solution of this PDE requires several constants whose values can neither be measured directly nor are known accurately (Barnett and Weaver, 1991), thus the SE is useful in giving only a qualitative picture of electroporation, for a spatially clamped uniformly polarised membrane area (Neu and Krassowska, 1999).

As seen in Figure 2.2b and 2.3, the radius at the minimum pore energy r_m only weakly depends on the transmembrane potential V_m, hence can be considered to be independent of V_m. For the purpose of the mathematical model in Chapter 3, initially pores are assumed to be formed with the minimum-energy radius $r_m = 0.76$ nm (as measured from the graph in Figure 2.2b), at the rate given by DeBruin and Krassowska (1999); Smith *et al.* (2004); Krassowska and Filev (2007),

$$\frac{dN}{dt} = \psi e^{(V_m/V_{\text{ep}})^2} \left(1 - \frac{N}{N_{\text{eq}}(V_m)}\right), \tag{2.9}$$

where N is the pore density of the initial small pores formed, ψ is the creation rate coefficient and N_{eq} is the equilibrium pore density for a potential V_m given by

$$N_{\text{eq}}(V_m) = N_0 e^{b(V_m/V_{\text{ep}})^2}. \tag{2.10}$$

Here, N_0 is the initial pore density with no applied electric field, V_{ep} is the

characteristic voltage of electroporation and

$$b = (r_m/r_*)^2 \tag{2.11}$$

is the pore creation constant where r_* is the minimum radius of hydrophilic pores and r_m the minimum-energy radius (Neu and Krassowska, 2003).

In the model developed in later chapters the value of constant V_{ep} given by DeBruin and Krassowska (1999), who had chosen it to fit experimental data, is used. Further details of this equation are given by Neu and Krassowska (1999), who take the pore density equation to be a result of the asymptotic model that is an approximation to the Smoluchowski Equation (SE)-based models. The asymptotic ordinary differential equation (ODE) described here is easier to solve, requires constants which can be easily related to experimental measurements, and has been shown to be valid even if the applied electric field has frequency in the megahertz range (Neu and Krassowska, 1999).

2.4.1 Current through a single pore

In order to model the response of a single cell to an applied electric field, it is important to be able to find the value of electric current i_{sml}, that flows through each pore of the cell membrane. As mentioned above, the cell membrane is embedded in an electrolytic solution. Figure 2.4 shows a cross section of the membrane through the centre of a pore. As mentioned by Barnett and Weaver (1991) and Glaser *et al.* (1988), the mathematical formulation of this three dimensional problem consists of a set of coupled differential equations that cannot be solved analytically. However, if the potential across the membrane can be found, then the Nernst-Planck equation of the corresponding one dimensional problem can be reduced and further used to solve the three dimensional case. The following discussion in this section draws heavily upon Barnett and Weaver (1991), Glaser *et al.* (1988) and DeBruin and Krassowska (1999). The Nernst-Planck equation for the current density in the pore is

$$j_x = -z_x F D_f \left(\nabla \kappa_x + \frac{z_x F \kappa_x}{RT} \nabla \Phi \right) \tag{2.12}$$

for an ion species x with valence z_x where D_f is the diffusion constant, F is Faraday's constant, R is the universal gas constant, T is the absolute temperature, $\kappa_x(x, y, z)$ is the concentration of the ion species and $\Phi(x, y, z)$ is the

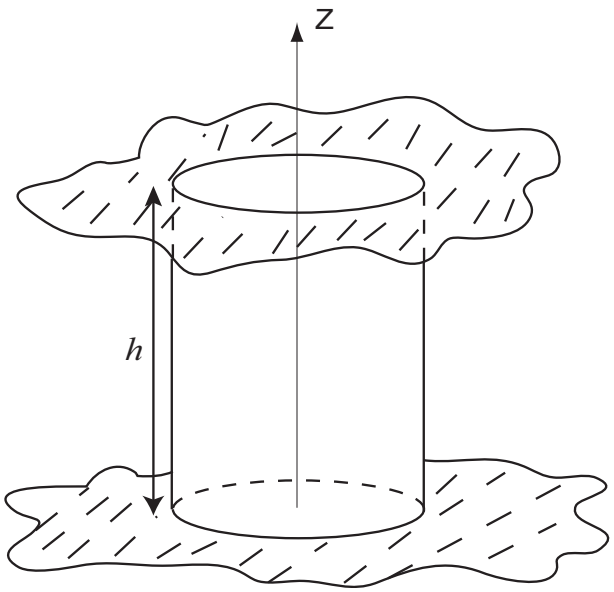

Figure 2.4: Cross section of a pore in the membrane.

electric potential. In order to model the interior of a pore in a cell membrane, we take the z-axis perpendicular to the membrane and assume cylindrical symmetry around the z-axis. Thus $\kappa = \kappa(z)$ and $\Phi = \Phi(z)$. Now the z-component of Equation 2.12 is,

$$j_x = M\left(\frac{d\kappa}{dz} + \varrho\kappa\frac{d\Phi}{dz}\right)$$
$$= M\exp[-\varrho\Phi]\frac{d}{dz}\left(\kappa\exp[\varrho\Phi]\right) \qquad (2.13)$$

where $M = -z_x F D_f$ and $\varrho = z_x F/RT$. Hence

$$\frac{j_x}{M}\int_0^h \exp[\varrho\Phi]\,dz = \int_0^h \frac{d}{dz}\left(\kappa\exp[\varrho\Phi]\right)dz$$
$$= \kappa(h)\exp[\varrho\Phi(h)] - \kappa(0)\exp[\varrho\Phi(0)] \qquad (2.14)$$

where h is the thickness of the cell membrane, $z = 0$ is taken to be the inner surface of the membrane and $z = h$ the outer surface. Thus

$$\begin{aligned} j_x &= M\frac{\kappa(h)\exp[\varrho\Phi(h)] - \kappa(0)\exp[\varrho\Phi(0)]}{\int_0^h \exp[\varrho\Phi(z)]\,dz} \\ &= M\frac{\kappa(h) - \kappa(0)\exp[\varrho\Phi(0) - \varrho\Phi(h)]}{\int_0^h \exp[\varrho\Phi(z) - \varrho\Phi(h)]\,dz} \\ &= z_x D_f F\frac{[x]_{\text{in}}\exp(\frac{z_x F}{RT}[\Phi(0) - \Phi(h)]) - [x]_{\text{ex}}}{\int_0^h \exp(\frac{z_x F}{RT}[\Phi(z) - \Phi(h)])}\,dz \end{aligned} \tag{2.15}$$

where $\kappa(0) \equiv [x]_{\text{in}}$ is the internal concentration of ion x and $\kappa(h) \equiv [x]_{\text{ex}}$ is the external concentration. To evaluate the integral in the denominator one must know the form $\Phi(z)$ takes. Let us assume $\Phi(z) = \Phi_{\text{ext}}(z) + \Phi_B(z)$, namely the sum of the potential due to the applied electric field and the Born energy caused by the interactions of the ions with the pore walls. Φ_{ext} can be taken to be varying linearly across the membrane, with $\Phi_{\text{ext}}(0) = \Phi_{\text{in}}$ and $\Phi_{\text{ext}}(h) = \Phi_{\text{ex}}$. Thus

$$\Phi_{\text{ext}}(z) \;=\; \Phi_{\text{in}} - [\Phi_{\text{in}} - \Phi_{\text{ex}}]\frac{z}{h}. \tag{2.16}$$

So

$$\begin{aligned} \frac{z_x F}{RT}[\Phi_{\text{ext}}(z) - \Phi_{\text{ext}}(h)] &= \frac{z_x F}{RT}[\Phi_{\text{in}} - \Phi_{\text{ex}}]\left(1 - \frac{z}{h}\right) \\ &= z_x v_m\left(1 - \frac{z}{h}\right) \end{aligned} \tag{2.17}$$

As for the Born energy, we follow Glaser *et al.* (1988), and assume $\Phi_B(z) = z_x t_B(z)$, where $t_B(z)$ is a trapezoidal function. This is based on the assumption that the interactions of the ion type x with the walls of the pore are described by an energy barrier given by,

$$w(z) = \frac{F}{RT}[t_B(z) - t_B(h)] = \begin{cases} w_0\frac{z}{d} & 0 \le z < d \\ w_0 & d \le z < h - d \\ w_0\frac{h-z}{d} & h - d \le z \le h, \end{cases} \tag{2.18}$$

where w_0 is the energy barrier within the pore. The Born energy function is shown in Figure 2.5. Thus

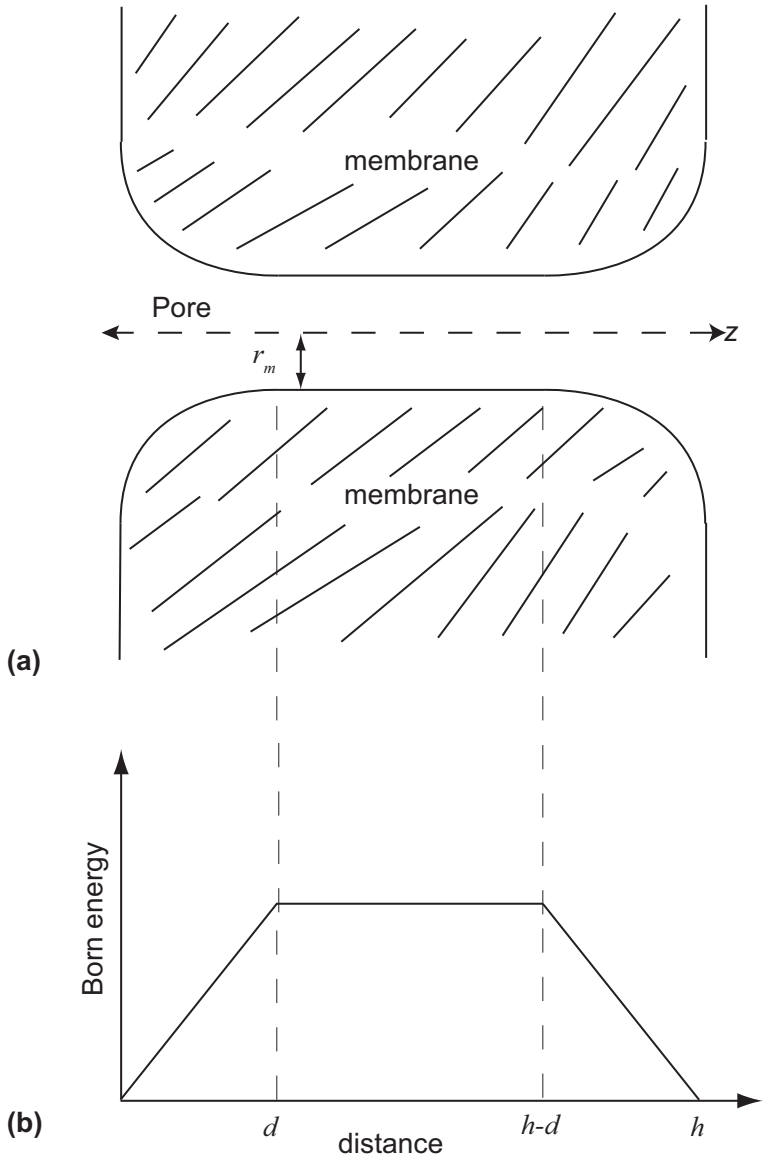

Figure 2.5: Born energy of a pore: (a) Cross section of a pore (b) Energy profile of a hydrophilic pore as a function of its position along the axis of the pore.

$$\frac{z_x F}{RT}[\Phi_B(z) - \Phi_B(h)] = z_x^2 w(z). \tag{2.19}$$

Now, using these assumptions in Equations 2.16 to 2.19, the integral in the denominator of Equation 2.15 can be evaluated as follows.

$$\begin{aligned} I &= \int_0^h \exp\left(\frac{z_x F}{RT}[\Phi(z) - \Phi(h)]\right) dz \qquad (2.20)\\ &= \int_0^d \exp\left(z_x v_m - z_x\left[\frac{v_m}{h} - \frac{z_x w_0}{d}\right] z\right) dz \\ &\quad + \int_d^{h-d} \exp\left(z_x v_m + z_x^2 w_0 - \frac{z_x v_m}{h} z\right) dz \\ &\quad + \int_{h-d}^{h} \exp\left(z_x v_m + \frac{z_x^2 w_0 h}{d} - z_x\left[\frac{v_m}{h} + \frac{z_x w_0}{d}\right] z\right) dz \\ &= \frac{hn}{z_x^2 w_0 - z_x v_m n}\left(\exp[z_x v_m + z_x^2 w_0 - n z_x v_m] - \exp[z_x v_m]\right) \\ &\quad - \frac{hn}{z_x v_m n}\left(\exp[z_x^2 w_0 + n z_x v_m] - \exp[z_x v_m + z_x^2 w_0 - n z_x v_m]\right) \\ &\quad - \frac{hn}{z_x^2 w_0 + z_x v_m n}\left(1 - \exp[z_x^2 w_0 + n z_x v_m]\right), \qquad (2.21) \end{aligned}$$

where $n = d/h$, is the relative entrance length of the pore as shown in Figure 2.5. This expression simplifies to

$$\begin{aligned} I = \frac{h}{z_x v_m}\left(\frac{w_0 z_x \exp[z_x(w_0 z_x - n v_m)] - n v_m}{w_0 z_x - n v_m}\right)\exp(z_x v_m) \\ - \frac{h}{z_x v_m}\left(\frac{w_0 z_x \exp[z_x(w_0 z_x + n v_m)] + n v_m}{w_0 z_x + n v_m}\right). \qquad (2.22) \end{aligned}$$

The total current i_{sml} through the pore is the current density in the pore multiplied by the cross sectional area of the pore. Further simplification using the Nernst-Einstein equation gives

$$i_{\text{sml}} = \frac{\pi r_m^2 \sigma_{ps} v_m RT}{Fh} \frac{(e^{v_m} - 1)}{\left(\frac{w_0 e^{w_0 - n v_m} - n v_m}{w_0 - n v_m} e^{v_m} \quad - \quad \frac{w_0 e^{w_0 + n v_m} + n v_m}{w_0 + n v_m}\right)}, \tag{2.23}$$

where r_m is the radius of the pore at its narrowest part, σ_{ps} is the conductivity of the aqueous solution that fills the pore, $v_m = z_x V_m/RT$, and $V_m = \Phi_{\text{in}} - \Phi_{\text{ex}}$ is the transmembrane potential. Thus the formula for pore current is valid only for small pores up to 1 nm radius, and accounts only for the diffusion current due to interaction of ions with the pore walls. Current through larger pores has to be modelled differently. The above derivation for pore current is based upon those of Barnett and Weaver (1991), Glaser *et al.* (1988) and DeBruin and Krassowska (1999). Equation 2.23 for current through small pores is used in the model developed as discussed in Chapters 3 and 6 of this thesis. A model based on the assumption of all created pores being small in radius, is useful for comparing onset of pore density depending on various independent parameters like cell radius, peak electric field, extracellular and intracellular fluid conductivity. The next chapter deals with a method to model the pore density response of a single cell to an arbitrary applied electric field.

2.5 Calculation of Transmembrane Potential

Small spherical particles in the size range 1 μm–1000 μm are very important in today's world. They are used in manufacturing operations like powder coating, and powder injection molding. A number of raw materials used in the agricultural, food, mining, and metallurgical industries are received in particulate form, and are to be processed further. Particles of biological origin, such as cells and DNA are of common interest, for further use in biomedical applications. This section introduces the reader to some of the mathematical formulae related to the effect of the electric field on biological cells. These formulae are used in further chapters to build and extend models of electroporation of a single spherical cell.

2.5.1 Electric field interaction with a cell as a particle

Further discussion in this section is heavily based on the text by Jones (1995). Imagine a spherical particle of radius R, suspended in a dielectric fluid and subject to a uniform electric field E_0 orientated in the z-direction as illustrated in Figure 2.6. The dielectric permittivity inside and outside the cell is ε_{in} and ε_{ex}, respectively. The field polarizes the particle, inducing a moment in it. The effective dipole moment P_{eff}, is defined as the moment of an equivalent, point

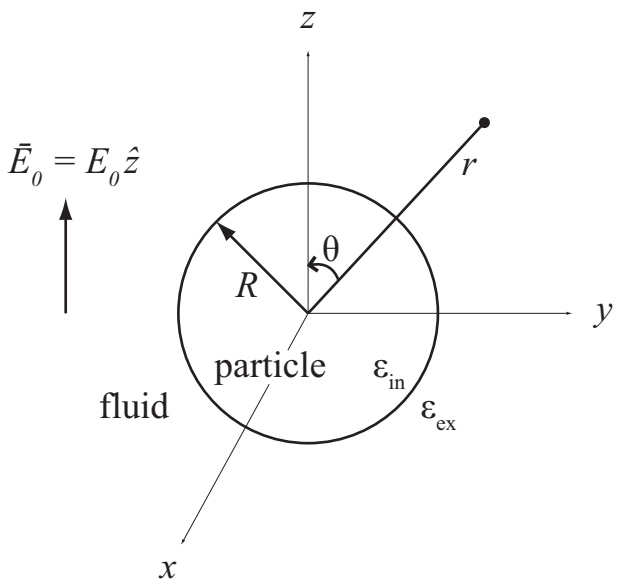

Figure 2.6: Spherical particle in electric field

dipole that, when immersed in the same dielectric medium and positioned at the centre of the original particle, produces the same electrostatic potential. The electrostatic potential Φ due to a point dipole of moment P_{eff} in a dielectric medium of permittivity ε_{ex} is

$$\Phi(r,\theta) = \frac{P_{\text{eff}}\cos\theta}{4\pi\varepsilon_{\text{ex}}r^2}, \tag{2.24}$$

where θ is the polar angle measured from the positive pointing pole of the dipole and r is the distance from the origin. This is the standard solution of Laplace's equation in the far-field of a dipole source. This approximation may have to be modified if the potential at the centre of the cell is to be calculated. However, modelling in this thesis requires the potential, just inside and outside the cell membrane, thus the approximation is valid.

2.5.2 Effective dipole moment of a dielectric sphere in a dielectric medium

This electric potential due to the effective dipole moment can be determined by solving the boundary value problem as follows. The following assumptions are made: that there is an applied external uniform electric field E_0; that there is no free charge anywhere in the sphere or dielectric liquid; and that the presence

of the particle does not disturb the system of source charges that create E_0. With these assumptions the electrostatic potential satisfies Laplace's equation everywhere. The solutions for the potential outside Φ_{ex}, and inside Φ_{in} the sphere, of radius a take the form:

$$\Phi_{\text{ex}}(r,\theta) = -E_0 r\cos\theta + \frac{A\cos\theta}{r^2}, \qquad r > a \tag{2.25}$$

$$\Phi_{\text{in}}(r,\theta) = -Br\cos\theta, \qquad r < a \tag{2.26}$$

where A and B are coefficients, that can be determined using the boundary conditions. The first term in Equation 2.25 is the imposed uniform electrostatic field, and the second term is the induced dipole of the particle. Comparing Equation 2.24 with this second term links the coefficient A and the effective dipole moment, by the equation,

$$P_{\text{eff}} = 4\pi\varepsilon_{\text{ex}}A. \tag{2.27}$$

The boundary conditions are applied at the surface of the particle. The first condition is that the potential must be continuous across the surface of the cell, namely

$$\Phi_{\text{ex}}(a,\theta) = \Phi_{\text{in}}(a,\theta). \tag{2.28}$$

The second condition is that, the normal component of the displacement flux must be continuous across the boundary, hence

$$\varepsilon_{\text{ex}}\frac{\partial\Phi_{\text{ex}}}{\partial r} = \varepsilon_{\text{in}}\frac{\partial\Phi_{\text{in}}}{\partial r}, \tag{2.29}$$

where ε_1 is the extracellular permittivity, and ε_2 is the intracellular permittivity. Equations 2.25, 2.26, 2.28 and 2.29 are solved by Jones (1995) to obtain

$$A = \frac{(\varepsilon_{\text{in}} - \varepsilon_{\text{ex}})}{(\varepsilon_{\text{in}} + 2\varepsilon_{\text{ex}})}a^3E_0 \qquad \text{and} \qquad B = \frac{3\varepsilon_{\text{ex}}}{(\varepsilon_{\text{in}} + 2\varepsilon_{\text{ex}})}E_0. \tag{2.30}$$

Thus the effective dipole moment can be written as

$$P_{\text{eff}} = 4\pi\varepsilon_{\text{ex}}\frac{(\varepsilon_{\text{in}} - \varepsilon_{\text{ex}})}{(\varepsilon_{\text{in}} + 2\varepsilon_{\text{ex}})}a^3E_0. \tag{2.31}$$

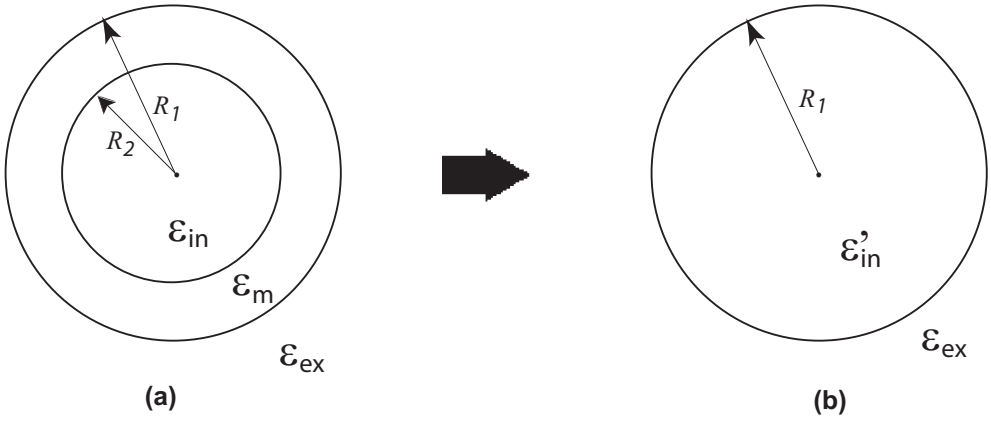

Figure 2.7: Spherically concentric dielectric shell and its homogeneous equivalent (a) cell with membrane (b) equivalent cell

In general form, for a homogeneous dielectric sphere the expression for the effective dipole moment is

$$P_{\text{eff}} = 4\pi\varepsilon_{\text{ex}} K a^3 E_0. \tag{2.32}$$

where K, known as the Clausius-Mossotti function, provides a measure of the strength of the effective polarization of a spherical particle. As seen, K is a function of the permittivities of the sphere and the fluid in which the sphere is immersed, viz

$$K(\varepsilon_{\text{in}}, \varepsilon_{\text{ex}}) = \frac{\varepsilon_{\text{in}} - \varepsilon_{\text{ex}}}{\varepsilon_{\text{in}} + 2\varepsilon_{\text{ex}}}. \tag{2.33}$$

2.5.3 Multilayered particles

The above model of the cell is over simplified—in reality the biological cell has at least an outer cell wall, known as the membrane. The membrane should be modelled as an extra layer. To calculate the effective dipole moment of a layered particle, we assume that the particle is spherically symmetrical as shown in Figure 2.7. Here, ε_{ex} is the extracellular permittivity, ε_m is the membrane permittivity and ε_{in} is the intracellular permittivity. R_1 and R_2 are the outer and inner radii respectively, of the particle. We can approximate the three layer model (ε_{ex}, ε_m, ε_{in}) with a two layer model (ε_{ex}, $\varepsilon_{\text{in}}^{\cdot}$) where $\varepsilon_{\text{in}}^{\cdot}$ is a revised ε_{in} from this simplification. We only need the potential Φ at the membrane boundary, as the membrane is very thin compared with the cell radius, thus this approximation is suitable. The effective permittivity of the

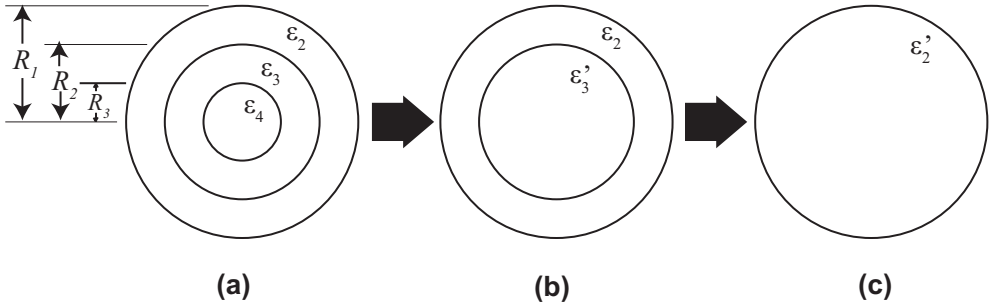

Figure 2.8: Multilayered spherical concentric dielectric shell and its homogeneous equivalent (a) Multilayered shell (b) Intermediate equivalent particle (c) Equivalent particle.

equivalent particle as given by Jones (1995) is

$$\varepsilon_{\text{in}}^{\text{'}} = \varepsilon_m \left\{ \frac{a_r^3 \; + \; 2\left(\dfrac{\varepsilon_{\text{in}} - \varepsilon_m}{\varepsilon_{\text{in}} + 2\varepsilon_m}\right)}{a_r^3 \; - \; \left(\dfrac{\varepsilon_{\text{in}} - \varepsilon_m}{\varepsilon_{\text{in}} + 2\varepsilon_m}\right)} \right\}, \tag{2.34}$$

where

$$a_r = \frac{R_1}{R_2}.$$

This method can be easily applied to multilayered shells using the approach illustrated in Figure 2.8. One starts at the innermost layer and by repeatedly applying Equation 2.34, eventually arrives at the expression for the permittivity of the equivalent homogeneous sphere.

2.5.4 Lossless spherical shell in a uniform field, calculation of potentials

Consider a layered spherical particle as in Figure 2.7, subjected to an applied uniform electric field E_0, oriented in the z-direction. Assume that there is no free electric charge anywhere. To solve this boundary value problem, we solve Laplace's equation for the electrostatic potential in the three regions. Then Φ_{ex} the extracellular potential, Φ_m the potential in the membrane, and Φ_{in} the

intracellular potential are given by,

$$\Phi_{\text{ex}}(r,\theta) = \left(-E_0 r + \frac{A}{r^2}\right)\cos\theta, \qquad r > R_1 \tag{2.35}$$

$$\Phi_m(r,\theta) = \left(-Br + \frac{C}{r^2}\right)\cos\theta, \qquad R_1 > r > R_2 \tag{2.36}$$

$$\Phi_{\text{in}}(r,\theta) = -Dr\cos\theta, \qquad r < R_2. \tag{2.37}$$

where A, B, C and D are unknown coefficients to be determined using the boundary conditions. The boundary conditions at the two dielectric surfaces are

$$\Phi_{\text{ex}} = \Phi_{\text{in}} \quad \text{and} \quad \varepsilon_{\text{ex}}\frac{\partial\Phi_{\text{ex}}}{\partial r} = \varepsilon_m\frac{\partial\Phi_m}{\partial r} \quad \text{at} \quad r = R_1 \tag{2.38}$$

$$\Phi_m = \Phi_{\text{in}} \quad \text{and} \quad \varepsilon_m\frac{\partial\Phi_m}{\partial r} = \varepsilon_{\text{in}}\frac{\partial\Phi_{\text{in}}}{\partial r} \quad \text{at} \quad r = R_2. \tag{2.39}$$

The above solutions and the boundary conditions can be solved to give,

$$A = \frac{\varepsilon_{\text{in}}^{'} - \varepsilon_{\text{ex}}}{\varepsilon_{\text{in}}^{'} + 2\varepsilon_{\text{ex}}} R_1^3\ E_0, \tag{2.40}$$

$$B = \frac{-3\varepsilon_{\text{ex}} a_r^3}{(\varepsilon_{\text{in}}^{'} + 2\varepsilon_{\text{ex}})(a_r^3 - K)} E_0, \tag{2.41}$$

$$C = \frac{-3\varepsilon_{\text{ex}} K a_r^3}{(\varepsilon_{\text{in}}^{'} + 2\varepsilon_{\text{ex}})(a_r^3 - K)} E_0, \tag{2.42}$$

$$D = \frac{-3\varepsilon_{\text{ex}}(1-K) a_r^3}{(\varepsilon_{\text{in}}^{'} + 2\varepsilon_{\text{ex}})(a_r^3 - K)} E_0, \tag{2.43}$$

where

$$a_r = \frac{R_1}{R_2} \quad \text{and} \quad K = \frac{\varepsilon_{\text{in}}^{'} - \varepsilon_{\text{ex}}}{\varepsilon_{\text{in}}^{'} + 2\varepsilon_{\text{ex}}}. \tag{2.44}$$

2.5.5 Spherical shell with ohmic loss in uniform field

Typically cells are multilayered and have finite conductivities. In such cases, an effective complex permittivity may be substituted for any layered sphere. In the preceding sections, the spherical particle and the medium have been assumed to be perfectly dielectric (zero conductivity). In fact, biological cells and the medium have finite conductivities (σ_{in} and σ_{ex}) in addition to their

dielectric permittivities. This contributes to losses in the system and influences the cell behaviour in an electric field. When loss is present, the dipole moment of a particle in a field exhibits either a time delay when the electric field is suddenly applied or a phase lag when the electric field is a continuous time varying cyclic signal. Imagine the layered dielectric sphere in Figure 2.7 with permittivities ε_{in}, ε_m and ε_{ex} and conductivities σ_{in}, σ_m and σ_{ex} . Then, as shown in Figure 2.9, in each of the n separate dielectric layers, where ε is the dielectric permittivity, σ is the dielectric conductivity and $i = \sqrt{-1}$, the complex permittivity can be used as

$$\bar{\varepsilon}_n = \varepsilon_n + \frac{\sigma_n}{i\omega} \qquad n \in \{\text{in}, \text{m}, \text{ex}\}. \tag{2.45}$$

The boundary conditions in Equations 2.28 and 2.29 are modified by replacing the permittivities with their complex equivalents. Solving Laplace's equation for the three region problem with complex permittivities, results in new coefficients, $\bar{A}$, $\bar{B}$, $\bar{C}$, and $\bar{D}$ to be used in the solutions for Φ_{in}, Φ_m and Φ_{ex}. They are:

$$\bar{A} = \frac{\bar{\varepsilon}^{\text{'}}_{\text{in}} - \bar{\varepsilon}_{\text{ex}}}{\bar{\varepsilon}^{\text{'}}_{\text{in}} + 2\bar{\varepsilon}_{\text{ex}}} R_1^3 \; E_0 \tag{2.46}$$

$$\bar{B} = \frac{-3\bar{\varepsilon}_{\text{ex}} a_r^3}{(\bar{\varepsilon}^{\text{'}}_{\text{in}} + 2\bar{\varepsilon}_{\text{ex}})(a_r^3 - K)} E_0 \tag{2.47}$$

$$\bar{C} = \frac{-3\bar{\varepsilon}_{\text{ex}} K a_r^3}{(\bar{\varepsilon}^{\text{'}}_{\text{in}} + 2\bar{\varepsilon}_{\text{ex}})(a_r^3 - K)} E_0 \tag{2.48}$$

$$\bar{D} = \frac{-3\bar{\varepsilon}_{\text{ex}} (1 - K) a_r^3}{(\bar{\varepsilon}^{\text{'}}_{\text{in}} + 2\bar{\varepsilon}_{\text{ex}})(a_r^3 - K)} E_0 \tag{2.49}$$

where

$$a_r = \frac{R_1}{R_2} \quad \text{and} \quad K = \frac{\varepsilon^{\text{'}}_{\text{in}} - \varepsilon_{\text{ex}}}{\varepsilon^{\text{'}}_{\text{in}} + 2\varepsilon_{\text{ex}}}. \tag{2.50}$$

The effective homogeneous dielectric permittivity is replaced by its complex equivalent as follows:

$$\bar{\varepsilon}^{\text{'}}_{\text{in}} = \bar{\varepsilon}_m \left\{ \frac{a_r^3 \; + \; 2\left(\dfrac{\bar{\varepsilon}_{\text{in}} - \bar{\varepsilon}_m}{\bar{\varepsilon}_{\text{in}} + 2\bar{\varepsilon}_m}\right)}{a_r^3 \; - \; \left(\dfrac{\bar{\varepsilon}_{\text{in}} - \bar{\varepsilon}_m}{\bar{\varepsilon}_{\text{in}} + 2\bar{\varepsilon}_m}\right)} \right\} = \varepsilon^{\text{'}}_{\text{in}} + \frac{\sigma^{\text{'}}_{\text{in}}}{i\omega} \tag{2.51}$$

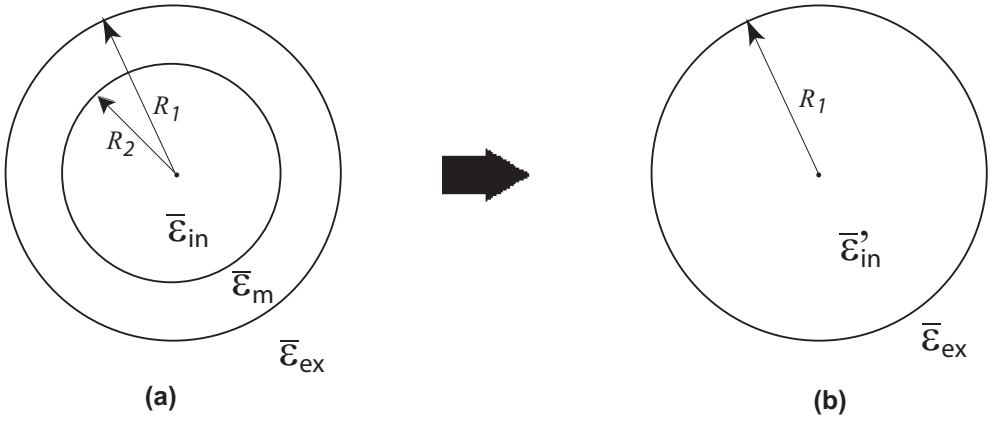

Figure 2.9: Multilayered spherical concentric lossy shell and its homogeneous equivalent (a) Multilayered shell (b) Equivalent particle.

2.5.6 Transient response of lossy dielectric sphere to a suddenly applied electric field

Imagine an ohmic sphere exposed to an electric field that is suddenly turned on, namely, $E(t) = E_0 u(t)$, where $u(t)$ is the unit step function. It turns out that the potentials inside and outside are unchanged in their form; the coefficients just become functions of time, namely A is replaced by $A(t)$ and B replaced by $B(t)$.

The boundary conditions are as usual (and true for all time)

$$\Phi_{\text{ex}}(a,\theta) = \Phi_{\text{in}}(a,\theta). \tag{2.52}$$

Now Equation 2.29 must be replaced by a charge continuity condition because finite conductivity allows accumulation of free electrical charge on a surface. The instantaneous charge conservation condition is

$$\sigma_{\text{ex}}\left(-\frac{\partial\Phi_{\text{ex}}}{\partial r}\right) - \sigma_{\text{in}}\left(-\frac{\partial\Phi_{\text{in}}}{\partial r}\right) + \frac{\partial\sigma_f}{\partial t} = 0 \quad \text{at} \quad r = a, \tag{2.53}$$

where σ_f is the free electric surface charge as defined by

$$\varepsilon_f = \varepsilon_{\text{ex}}\frac{\partial\Phi_{\text{ex}}}{\partial r} - \varepsilon_{\text{in}}\frac{\partial\Phi_{\text{in}}}{\partial r} \quad \text{at} \quad r = a. \tag{2.54}$$

Here, $\frac{\partial \Phi_{\text{ex}}}{\partial r}$ and $\frac{\partial \Phi_{\text{in}}}{\partial r}$ are the normal components of the ohmic current outside and inside of the sphere respectively. Combining these equations give a set of differential equations that can be solved for the time dependent coefficient $A(t)$ to give

$$A(t) = \frac{\sigma_{\text{in}}^{,} - \sigma_{\text{ex}}}{\sigma_{\text{in}}^{,} + 2\sigma_{\text{ex}}} R_1^3 E_0 \left(1 - \exp\left(\frac{-t}{\tau_{mw}}\right)\right) + \frac{\varepsilon_{\text{in}}^{,} - \varepsilon_{\text{ex}}}{\varepsilon_{\text{in}}^{,} + 2\varepsilon_{\text{ex}}} R_1^3 E_0 \exp\left(\frac{-t}{\tau_{mw}}\right) \quad (2.55)$$

where

$$\tau_{mw} = \frac{\varepsilon_{\text{in}}^{,} + \varepsilon_{\text{ex}}}{\sigma_{\text{in}}^{,} + 2\sigma_{\text{ex}}} \quad (2.56)$$

is the membrane relaxation time constant.

By careful observation of Equations 2.40 and 2.55, by analogy the time dependent coefficient $D(t)$ is

$$D(t) = -\frac{3\sigma_{\text{ex}}(1 - K_I)}{(\sigma_{\text{in}}^{,} + 2\sigma_{\text{ex}})(a_r^3 - K_I)} a_r^3 E_0 \left(1 - \exp\left(\frac{-t}{\tau_{mw}}\right)\right) - \frac{3\varepsilon_{\text{ex}}(1 - K_R)}{(\varepsilon_{\text{in}}^{,} + 2\varepsilon_{\text{ex}})(a_r^3 - K_R)} a_r^3 E_0 \exp\left(\frac{-t}{\tau_{mw}}\right), \quad (2.57)$$

where K_I and K_R are the imaginary and real component of K respectively. These equations for $A(t)$ and $D(t)$ are used in the model described in Chapter 3 to calculate transmembrane potential defined as the potential across the membrane, given by

$$V_m = \Phi_{\text{in}} - \Phi_{\text{ex}}. \quad (2.58)$$

As seen from Equations 2.35 and 2.37, to calculate Φ_{in} and Φ_{ex} we only need the constants $A(t)$ and $D(t)$, thus the other two constants $B(t)$ and $C(t)$ are not relevant.

2.5.7 Analytical solutions for transmembrane potential

Assuming the cell dielectric properties are known, here I detail the analytical solutions for the potentials inside and outside a spherical cell as available in literature (Schwan, 1989). These are used in Chapter 3 for validating the results from the model developed earlier in the same chapter. Once again, consider a spherical cell with external radius R_1 and internal radius R_2 as in

the previous section. The cell membrane thickness is then $h = R_1 - R_2$. Assume E_0 is the external applied electric field. Imagine the cell with permittivities (ε_{in}, ε_m, ε_{ex}) and conductivities (σ_{in}, σ_m, σ_{ex}). Then in each of the separate dielectric regions, the specific admittivity is given by

$$\varpi = \sigma - i\omega\varepsilon \tag{2.59}$$

to give the specific admittivities ϖ_{in}, ϖ_m and ϖ_{ex}. Potentials just inside and outside the cell membrane are given by

$$\Phi_{\text{in}} = \vartheta R_2, \tag{2.60}$$

$$\Phi_{\text{ex}} = E_0(R_1 - \nu/(R_1)^2). \tag{2.61}$$

The constants ϑ and ν are calculated as,

$$\vartheta = 9\varpi_{\text{ex}}\varpi_m E_0/\varsigma, \tag{2.62}$$

where

$$\varsigma = ((\varpi_m + 2\varpi_{\text{ex}})(2\varpi_m + \varpi_{\text{in}}) + 2(R_2/{R_1}^3)(\varpi_m - \varpi_{\text{ex}})(\varpi_{\text{in}} - \varpi_m)), \tag{2.63}$$

and

$$\nu = (({R_1})^3(2\varpi_m + \varpi_{\text{in}})(\varpi_{\text{ex}} - \varpi_m) + {R_2}^3(2\varpi_m + \varpi_{\text{ex}})(\varpi_m - \varpi_{\text{in}}))/\varsigma. \tag{2.64}$$

Equations 2.59 to 2.64 can be used to calculate transmembrane potential as a passive response to an applied sinusoidal electric field.

If the cell membrane parameter is specified as specific membrane capacitance C_m and only the intracellular and extracellular conductivities for a cell of radius a are known, then the following Equation 2.65 by Holzapfel *et al.* (1982) can be used to calculate analytical solution for the induced transmembrane potential as a passive response to an applied sinusoidal electric field.

$$V_m(t) = \frac{1.5Ea}{1 + (\omega\tau_r)^2}(cos\omega t + \omega\tau_r sin\omega t) \tag{2.65}$$

where the membrane relaxation time constant is

$$\tau_r = aC_m \left(\frac{1}{\sigma_{\text{in}}} + \frac{1}{2\sigma_{\text{ex}}} \right). \tag{2.66}$$

Chapter 3

Response of a Single Cell to an Applied Arbitrary Electric Field

Electroporation is now a common tool in biotechnology and is used in a number of medical treatments. Until recently, the development of theoretical models of electroporation has lagged behind experimental research. In order to optimize the efficiency of electroporation, it is important to consider as many biological and physical aspects as possible and it is a necessity that a variety of electric pulse parameters be tested. Thus a comprehensive model which can predict electropermeabilization as a result of any form of applied electric field and other important electroporation parameters is necessary.

This chapter initially gives a literature review of existing models for electropermeabilization and comments on their respective limitations and specialities and, thus, the need for a new model. The chapter then describes the numerical model I developed for a single cell electroporated by application of arbitrary external electric field pulses. The model is used to compare the transmembrane potential V_m, and pore density N, developed in response to the pulses. Transmembrane potential and pore density are calculated via a piece-wise step response method that enables solutions to be obtained for any practical applied electric field waveform. Pore density is shown to increase so long as a threshold transmembrane potential is maintained by the electric field, and effectively clamps the transmembrane potential to just over 1 V while pore density is increasing. Short unipolar pulses are also shown to create asymmetrical pore density between the two cell polar regions, whereas bipolar pulses result in a symmetrical pore density.

The model presented here helps predict dynamic non-linear results of electropermeabilization, given any form of applied electric field and other important electroporation system parameters. This model can be used as a tool for the determination of starting parameters in biological applications.

3.1 Background

Exposure of biological cells to electric fields can lead to a variety of biophysical and biochemical responses (Pavlin *et al.*, 2002; Neumann, 1989; Mir, 2000; Neumann *et al.*, 1998; Neumann and Kakorin, 2002; Griese *et al.*, 2002; Miklavĉiĉ and Kotnik, 2004). Electroporation is an application in biotechnology and is used in a number of medical treatments (DeBruin and Krassowska, 1999; Dev *et al.*, 2000; Kotnik *et al.*, 2003; Miklavĉiĉ and Kotnik, 2004; Snoj *et al.*, 2005; Schmidt *et al.*, 2001; Tozon *et al.*, 2005). However, the process of electroporation is still not completely understood. Until recently, the development of theoretical models of electroporation has lagged behind experimental research (DeBruin and Krassowska, 1999; Smith *et al.*, 2004; Krassowska and Filev, 2007).

In order to optimize the efficiency of electroporation, it is important to consider as many biological and physical aspects as possible and it is necessary that a variety of electric pulse parameters tested. The most common form of electric pulses used in conventional electroporation and electrofusion are in the form of rectangular or exponentially decreasing (capacitive discharge) unipolar pulses. The unipolar nature of these pulses is known to contribute to asymmetrical poration due to the inherent transmembrane potential (rest potential) of living cells, and induce variable membrane permeability with respect to the position of the membrane relative to the direction of the applied electric field (DeBruin and Krassowska, 1999; Kotnik *et al.*, 2001b; Valic *et al.*, 2004). The rest potential of a cell is the transmembrane potential that would usually be maintained by normal cellular function in the absence of any externally applied electric field. In most cells the rest potential has a negative value of around -50 to -90 mV (Cole, 1972). There is also a possibility that if an upper limit of pore density is reached, the cell membrane may be irreversibly damaged leading to loss of cell viability (Kotnik *et al.*, 2003). Researchers have recommended using electric field pulses symmetric about zero volts as a solution for asymmetrical poration (Kotnik *et al.*, 2003; Gaynor and Bodger, 1995; Tekle

et al., 1991) and to provide more uniform electropermeabilization over a wider range of cell sizes resulting in improved control and better cell survival (Gaynor and Bodger, 1995; Tekle *et al.*, 1991). Experiments have been reported on using a pulsed radio frequency electric field for electroporation and electrofusion (Chang *et al.*, 1992b), and indicated that a proper choice of frequency can counterbalance the effect of cell size on electroporation efficiency.

A recent study (Kotnik *et al.*, 2001a) involving an empirical electropermeabilization result using symmetric bipolar rectangular pulses has reported increased efficiency of electroporation. The reasons suggested for this were: (1) counterbalancing the asymmetry of electropermeabilized area at the poles of the cell which is introduced by the rest potential, and (2) increased odds of permeabilization for cells having non-spherical shape (Kotnik *et al.*, 2001a). Improved electroporation efficiency was also observed using similar bipolar rectangular pulses in an earlier investigation (Tekle *et al.*, 1991). Another empirical study looked at the role of three bipolar pulse shapes, triangular, sine, and rectangular, in electropermeabilization (Kotnik *et al.*, 2003). The study found that the level of electropermeabilization is primarily attributed to the duration that the pulse amplitude exceeds a value that induces pore formation.

Kotnik *et al.* (1998) developed a model that analyses the time course of induced V_m when a cell is exposed to different time varying electric field shapes. This model uses passive complex dielectric material based Laplace transforms to describe the transmembrane potential of the model cell. Electropermeabilization is estimated to occur when transmembrane potential exceeds approximately 1 V. While this model is capable of producing results for arbitrary waveforms, it does not include the non-linear effects of membrane electropermeabilization on transmembrane potential V_m and on pore density, N. Another theoretical model has been developed for single cell electroporation when exposed to a unipolar square shape electric field pulse (DeBruin and Krassowska, 1999). This model considers electropermeabilization as a dynamic process and describes the evolution of transmembrane potential and pore density, assuming a set of defined electroporation parameters. While this model includes the non-linear effects of membrane breakdown, it did not use arbitrary pulse waveforms.

Another recent and substantially novel model based on nodal circuit analysis techniques includes both basic non-linear effects of electroporation and can provide results for arbitrary pulse waveforms in both single cell and tissue-

like systems (Gowrishankar and Weaver, 2003). This model was primarily created to investigate the general response of cells to electric fields, so it does not specifically concentrate on the finer temporal or spatial components of electroporation.

Another recent model by Ellappan and Sundararajan (2005) based on circuit simulator techniques considers a biological cell as an electrical model using resistors and capacitors. This model focuses primarily on studying the transmembrane potential induced in a biological cell as a function of the media resistance and the frequency of the applied electric field, so it does not include the temporal or spatial components of electroporation. They conclude that high frequency alternating electric field might also be useful for electroporation and that more work needs to be done to explore these possibilities.

With the wide variety of electroporation parameters and empirical techniques, the literature on electropermeabilization is difficult to compare, and prediction of electropermeabilization results becomes ambiguous. The model presented here helps predict accurate non-linear results of electropermeabilization, given any form of applied electric field and other important electroporation system parameters such as external medium, membrane, and cytoplasm complex dielectric properties. The non-linear behaviour of electroporation is primarily due to the dynamics of membrane pore formation and is described further in the following section.

3.2 Mathematical Model

Fundamentally important features of the model presented here are; it provides solutions for arbitrary electric field pulse waveforms and includes the non-linear dynamic effects of membrane electropermeabilization.

3.2.1 Step response method

To be able to provide solutions for an electric field varying arbitrarily with time, a piece-wise step response method was used. The electric field signal is approximated by a number of consecutive small discrete step signals. This is exactly the same process as used for an analogue to digital signal conversion. The effect of each consecutive discrete step is calculated using standard step function response analysis. The result of the immediately previous time step

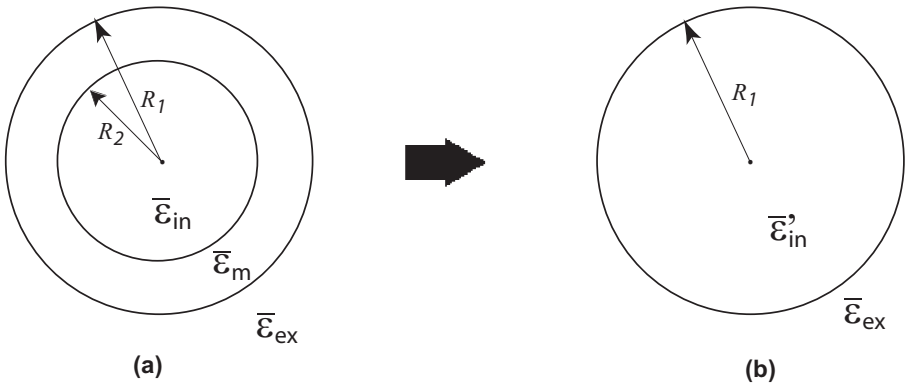

Figure 3.1: (a) Layered spherical cell (b) Equivalent homogeneous sphere.

is used for the required initial conditions of each following step, in accordance with the electropermeabilization dynamics discussed in following paragraphs. This method allows numerical calculation of the dynamic evolution of electropermeabilization. The temporal resolution of the method depends on the size of the time step used. All the results presented here use a time step small enough to provide an accuracy that does not noticeably improve with smaller time steps.

3.2.2 Model of a multilayered cell

This section draws upon mathematical expressions presented in sections 2.5.4 and 2.5.5. The cell is modelled as a multilayered lossy dielectric spherical structure. A homogeneous sphere with complex permittivity $\bar{\varepsilon}^{'}_{\text{in}}$ and radius R_1 can be substituted for the original multilayered cell with outer cell radius and core radius of R_1 and R_2 respectively as shown in Figure 3.1 (Jones, 1995). In each of the n separate dielectrics, where ε is the dielectric permittivity, σ is the dielectric conductivity and $i = \sqrt{-1}$, the complex permittivity is defined as,

$$\bar{\varepsilon}_n = \varepsilon_n + \frac{\sigma_n}{i\omega}. \tag{3.1}$$

where ω is the angular frequency of the applied electric field. The complex permittivity value $\bar{\varepsilon}^{'}_{\text{in}}$ is given by Equation 2.51, reproduced here for ease of the reader.

$$\bar{\varepsilon}^{'}_{\text{in}} = \bar{\varepsilon}_m \left\{ \frac{a_r^3 \; + \; 2\left(\dfrac{\bar{\varepsilon}_{\text{in}} - \bar{\varepsilon}_m}{\bar{\varepsilon}_{\text{in}} + 2\bar{\varepsilon}_m}\right)}{a_r^3 \; - \; \left(\dfrac{\bar{\varepsilon}_{\text{in}} - \bar{\varepsilon}_m}{\bar{\varepsilon}_{\text{in}} + 2\bar{\varepsilon}_m}\right)} \right\} = \varepsilon^{'}_{\text{in}} + \frac{\sigma^{'}_{\text{in}}}{i\omega} \tag{3.2}$$

where

$$a_r = \frac{R_1}{R_2}.$$

The transmembrane potential V_m is given by

$$V_m = \Phi_{\text{in}} - \Phi_{\text{ex}}, \tag{3.3}$$

with the intracellular potential Φ_{in}, given by the solution to Laplace's equation in the inner region, (Jones, 1995), as presented in Equation 2.37 is

$$\Phi_{\text{in}} = -Dr\cos\theta \quad \text{for} \quad r < R_2, \tag{3.4}$$

where θ is the polar angle measured with respect to the direction of the applied field. The coefficient D as given by Equation 2.46 is,

$$D = \frac{-3\bar{\varepsilon}_{\text{ex}}(1-K)a_r^3}{(\bar{\varepsilon}_{\text{in}}^{,} + 2\bar{\varepsilon}_{\text{ex}})(a_r^3 - K)} E_0, \tag{3.5}$$

where

$$K = \frac{\bar{\varepsilon}_{\text{in}}^{,} - \bar{\varepsilon}_{\text{ex}}}{\bar{\varepsilon}_{\text{in}}^{,} + 2\bar{\varepsilon}_{\text{ex}}} \tag{3.6}$$

is the Clausius-Mossotti factor, and E_0 is the applied electric field magnitude. The extracellular potential given by the solution to Laplace's equation in the outer region is (Jones, 1995), as presented in Equation 2.37 is,

$$\Phi_{\text{ex}} = \left(-E_0 r + \frac{A}{r^2}\right)\cos\theta \quad \text{for} \quad r > R_1, \tag{3.7}$$

where the constant A as presented in Equation 2.46 is,

$$A = \frac{\bar{\varepsilon}_{\text{in}}^{,} - \bar{\varepsilon}_{\text{ex}}}{\bar{\varepsilon}_{\text{in}}^{,} + 2\varepsilon_{\text{ex}}^{-}} R_1^3 \; E_0. \tag{3.8}$$

3.2.3 Electric field step response

The transient response of a lossy dielectric spherical cell to a constant electric field weighted unit step function, $E_0 u(t)$, is found by using the solution for the effective dipole moment (Jones, 1995). The coefficients now are functions of

time and as presented in section 2.5.6 are given by,

$$D(t) = -\frac{3\sigma_{\text{ex}}(1-K_I)}{(\sigma_{\text{in}}^{'}+2\sigma_{\text{ex}})(a_r^3-K_I)}a_r^3E_0\left(1-\exp\left(\frac{-t}{\tau_{mw}}\right)\right) - \frac{3\varepsilon_{\text{ex}}(1-K_R)}{(\varepsilon_{\text{in}}^{'}+2\varepsilon_{\text{ex}})(a_r^3-K_R)}a_r^3E_0\exp\left(\frac{-t}{\tau_{mw}}\right) \quad (3.9)$$

$$A(t) = \frac{\sigma_{\text{in}}^{'}-\sigma_{\text{ex}}}{\sigma_{\text{in}}^{'}+2\sigma_{\text{ex}}}R_1^3E_0\left(1-\exp\left(\frac{-t}{\tau_{mw}}\right)\right) + \frac{\varepsilon_{\text{in}}^{'}-\varepsilon_{\text{ex}}}{\varepsilon_{\text{in}}^{'}+2\varepsilon_{\text{ex}}}R_1^3E_0\exp\left(\frac{-t}{\tau_{mw}}\right) \quad (3.10)$$

where K_I and K_R are the imaginary and real components of K respectively, and

$$\tau_{mw} = \frac{\varepsilon_{\text{in}}^{'}+\varepsilon_{\text{ex}}}{\sigma_{\text{in}}^{'}+2\sigma_{\text{ex}}} \quad (3.11)$$

is the membrane relaxation time constant (Jones, 1995).

3.2.4 Response to a continuous arbitrary electric field

Basic calculus theory states that any continuous and well behaved function can be accurately approximated by a series of small enough consecutive discrete steps (Garcia, 1994). This concept is directly used in the analogue to digital conversion of continuous signals. The electric field signal is discretized in this manner. The step response equations defined above are then used to approximate the response of a cell exposed to an arbitrary electric field. The time step of each step response must be much smaller than the reciprocal of the highest frequency component of the arbitrary electric field waveform. This is carried out with a time step of 1 ns for waveforms with frequency components in the few MHz range.

The cell is assumed to have both passive and dynamic membrane kinetics. By passive I mean the response of the cell in the absence of any pore formation, and by dynamic I mean the response of the cell membrane when changes due to pore formation are considered. Passive transmembrane ionic current density J_{ion} is given by (DeBruin and Krassowska, 1999),

$$J_{\text{ion}} = g_m(V_m - V_{\text{rest}}), \tag{3.12}$$

where g_m is the specific membrane conductance (S/m^{-2}) and V_{rest} is the intrinsic rest potential. There is a threshold value of transmembrane potential above which formation of pores becomes energetically favourable (DeBruin and Krassowska, 1999; Kotnik *et al.*, 1998). The current density through these small pores, J_{sml}, is given by,

$$J_{\text{sml}} = N i_{\text{sml}}, \tag{3.13}$$

where N is the pore density of the initial small pores formed and $i_{\text{sml}}(r)$ is the diffusion current through a single pore of radius r (true for small pores only), as explained in Section 2.4.1 about current through a single pore. The expression for i_{sml} due to DeBruin and Krassowska (1999), based upon the Nernst-Planck equation models, and given in section 2.4.1, is used for pore radius below 1 nm. We repeat Equation 2.23 here for completeness:

$$i_{\text{sml}} = \frac{\pi r^2 \sigma_{\text{ps}} v_m RT}{Fh} \cdot \frac{(e^{v_m} - 1)}{(G_- e^{v_m} - G_+)} \tag{3.14}$$

with

$$G_\pm = \frac{w_0 e^{w_0 \pm n v_m} \pm n v_m}{w_0 \pm n v_m}. \tag{3.15}$$

This equation for pore current i_{sml} (Equation 3.14) accounts for the electrical interactions between the ions and the pore wall (DeBruin and Krassowska, 1999). The pore density is governed by a first order differential equation (DeBruin and Krassowska, 1999), as already discussed in section 2.4. The Equation 2.9 is presented here for completeness:

$$\frac{dN}{dt} = \psi e^{(V_m/V_{\text{ep}})^2} \left(1 - \frac{N}{N_{\text{eq}}(V_m)}\right), \tag{3.16}$$

Once the pores are electrically induced, the specific membrane conductance increases because of the increased number of conductive pores, and can be mathematically modelled as:

$$J_{\text{sml}} = N i_{\text{sml}} = g_p V_m, \tag{3.17}$$

where g_p is the specific conductance due to electroporation. As an effect, the

electropermeabilized membrane conductivity σ_m^p is modified to

$$\sigma_m^p = \sigma_m + \sigma_p, \tag{3.18}$$

where σ_p is the specific conductivity due to electroporation and is dynamically altered at each time step as the pore density changes. Formation of individual pores increases while the membrane potential is maintained above the threshold for electroporation (DeBruin and Krassowska, 1999).

3.3 Numerical Implementation and Methodology

The model is implemented in MATLAB. The Euler method is used for solving the first order differential equation (Garcia, 1994). A time step of 1 ns gave repeatable results. To confirm the accuracy of the piece-wise step method, the model results for V_m were initially compared with results obtained by calculating V_m using analytical solutions of the Laplace equation given by Schwan (1989) as presented in section 2.5.7. Solutions to the numerical model and the analytical model were obtained for applied bipolar sinusoidal pulse electric fields (10 kV/m, 20 kV/m and 30 kV/m at a frequency of 100 kHz and 1 MHz), each amplitude less than that required for onset of electroporation, as the analytical solution from Schwan (1989) does not model the non-linear effects of membrane electroporation. As seen in Figure 3.2 and Figure 3.3, it was found that these results matched very closely. This confirmed that the developed piece-wise step method is a valid numerical calculation technique.

It is well known that electric field frequency higher than 1 MHz is too fast compared to the cell membrane relaxation time, thus reducing the effect of membrane electroporation. However, Equations 2.65 and 2.66 used to calculate the induced transmembrane potential for an applied sinusoidal electric field suggest that the dependence on radius of the transmembrane potential is eliminated if either the frequency or relaxation time constants are large enough. To achieve this a frequency of 100 kHz is needed. To confirm radial independence through dynamic modelling of electroporation, frequencies of 100 kHz and 1 MHz are used for simulations in this thesis.

Most mammalian cell radii are in the range of 5 μm to 15 μm, thus the two

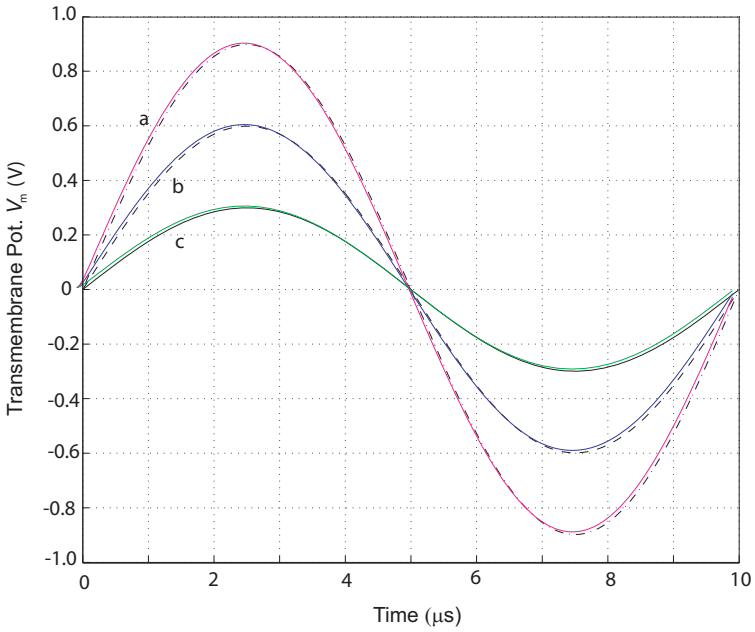

Figure 3.2: Cell response to 100 kHz bipolar sinusoidal pulse: Superposition of the analytical and numerical model solutions for the induced transmembrane potential (a) For peak electric field of 30 kV/m: analytical (black dash dot) and numerical model (magenta) (b) For peak electric field of 20 kV/m: analytical (black dash) and numerical model(blue) (c) For peak electric field of 10 kV/m: analytical (black solid) and numerical model (green).

cell radii of 7.5 μm and 15 μm are used for simulations in this thesis. Specific model parameters used are listed in Table 3.1.

3.4 Results and Discussion

3.4.1 Electropermeabilization response of a spherical cell exposed to different electric field waveforms

The piece-wise step response model presented here was used to simulate cell response to several different applied electric field wave-shape pulses including a unipolar square wave, bipolar square wave, bipolar sine wave, bipolar rectangular wave (rectangular pulse train), and a bipolar triangular wave. Figure 3.4 shows that upon application of a 52 kV/m unipolar square pulse at time $t = 0$, the induced transmembrane potential rises to a threshold of around 1.2 V at which point the electroporation dynamics of the model are initiated. The

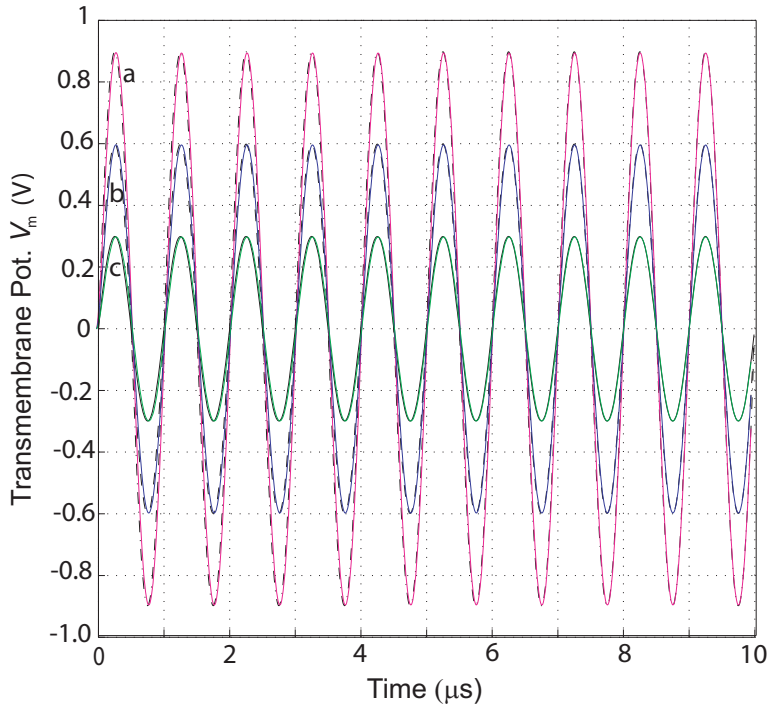

Figure 3.3: Cell response to 1 MHz bipolar sinusoidal pulse: Superposition of the analytical and numerical model solutions for the induced transmembrane potential (a) For peak electric field of 30 kV/m: analytical (black dash dot) and numerical model (magenta) (b) For peak electric field of 20 kV/m: analytical (black dash) and numerical model (blue) (c) For peak electric field of 10 kV/m: analytical (black solid) and numerical model (green).

corresponding increase in pore density increases the membrane conductance, clamping the membrane potential to a maximum of around 1.2 V. The equivalent transmembrane potential that do not consider the non-linear effects of membrane electroporation is also shown in Figure 3.4. Using the fraction of membrane area occupied by the pores as defined by Hibino *et al.* (1991), a pore density of about 3×10^{13} pores/m^2 is calculated as being an appropriate level of electroporation (Hibino *et al.*, 1991; Gowrishankar and Weaver, 2003), and the pulse amlpitude and duration chosen accordingly.

Figure 3.5 shows similar plots for a 1 μs, bipolar square wave (1 MHz), applied electric field of the same peak amplitude and total application time as the unipolar pulse. Clamping of the membrane potential still occurs at around 1.2 V and pore density rises to a similar value as observed with the unipolar pulse application. Reversal of the applied electric field at 0.5 μs has very little effect

Table 3.1: Geometric, electrical and electroporation parameters.

Symbol	Value	Description
a	15.0 (μm)	cell radius
r_*	0.51 (nm)	minimum radius of hydrophilic pores[a]
r_m	0.76 (nm)	minimum energy radius at V_m=0 [a]
h	5.0 (nm)	membrane thickness[b]
g_m	1.9 (Sm^{-2})	specific membrane conductance[b]
V_{rest}	–80 (mV)	membrane rest potential[b]
σ_{in}	0.3 (Sm^{-1})	intracellular conductivity[c]
σ_m	3×10^{-7}(Sm^{-1})	membrane conductivity[c]
σ_{ex}	1.2 (Sm^{-1})	extracellular conductivity[d]
$\varepsilon_{\mathrm{in}}$	7.1×10^{-10} (Fm^{-1})	intracellular permittivity[c]
ε_m	4.4×10^{-11} (Fm^{-1})	membrane permittivity[c]
$\varepsilon_{\mathrm{ex}}$	7.1×10^{-10}(Fm^{-1})	extracellular permittivity[c]
T	295 (K)	absolute temperature[b]
n	0.15	Relative entrance length of pores[b]
b	2.46	pore creation constant[b]
ψ	1×10^9 ($\mathrm{m}^{-2}\mathrm{s}^{-1}$)	creation rate coefficient [b]
V_{ep}	258 (mV)	characteristic voltage of electroporation[b]
N_o	1.5×10^9(m^{-2})	equivalent pore density when $V_m = 0$ mV[b]
w_o	2.65	energy barrier within pore[b]

[a]Values taken from Glaser *et al.* (1988).
[b]Values taken from DeBruin and Krassowska (1999).
[c]Values taken from Kotnik *et al.* (1998).
[d]Values taken from Kotnik and Miklavĉiĉ (2000).

on the growth of pore density. Figure 3.7 shows the response to a 1 μs, bipolar sinusoidal wave (1 MHz), electric field again of the same peak amplitude and total application time as in Figure 3.5. Compared to the square wave pulse, the poration threshold is achieved much later at around 0.25 μs. Additionally, transmembrane potential drops below the poration threshold about 0.2 μs later. Correspondingly, the resultant pore density is also lower. The pore density is seen to increase significantly at the second peak of the applied sinusoid where the transmembrane potential threshold is again exceeded. This is due to the lower pore density created by the first peak of the applied sinusoid. Note that the poration scale on figures is not on the same scale.

Figure 3.6 shows the response to a 1 μs, bipolar rectangular wave (1 MHz), electric field pulse, where the pulse peak duration is 0.2 μs shorter than the square wave pulse peak duration. The pore density can again be seen to rise noticeably at the second pulse peak owing to the lower pore density created

by the first pulse peak.

Figure 3.8 shows the response to a 1 μs, bipolar triangular wave (1 MHz), electric field pulse, where the pulse peak duration above the threshold for electroporation is shorter compared to all other types of electric field pulses. The result is the lowest mean pore density and the most significant rise for the second pulse peak compared to the other pulse waveforms.

The common trend for transmembrane potential shows that it initially follows the analytically derived induced potential with the same membrane time constant until a threshold value for electroporation is reached. During this initial phase the membrane has a small baseline pore density, N_0 (DeBruin and Krassowska, 1999). Once transmembrane potential exceeds the threshold value for electroporation (super-threshold), a steep rise in the pore density is seen. It is also seen from Figures 3.4 to 3.8 that the transmembrane potential could be up to 20 % reduced compared to that simulated without considering the dynamic changes due to electroporation while simulating.

Depending on the amplitude of the pulses, electropermeabilization can either occur fully in the first pulse or it can occur in steps at each subsequent electric field peak. This increase in pore density with multiple pulses offers better control over the degree of membrane permeability and is reflected in experimental situations by reported increases in electroporation effectiveness with multiple pulse applications (Lebar and Miklavĉiĉ, 2001; Gehl and Mir, 1999; Ŝatkauskas *et al.*, 2002).

For the same set of cell parameters and same peak to peak value of electric field amplitude, the pore density is the highest for the square wave pulse, reducing to the lowest for the triangular wave field. This agrees with reported experimental results (Kotnik *et al.*, 2003). The super-threshold duration is longer for a square pulse and shorter for the triangular pulse than a sine-wave pulse at the same pulse application time and peak amplitude. Alternately, if interested in creating equivalent electroporation conditions for different field waveforms, then for the same pore density formation to be achieved, the peak field intensity required follows the inequality, $E_{\mathrm{sq}} < E_{\mathrm{sin}} < E_{\mathrm{tri}}$, assuming that each waveform is applied for the same duration.

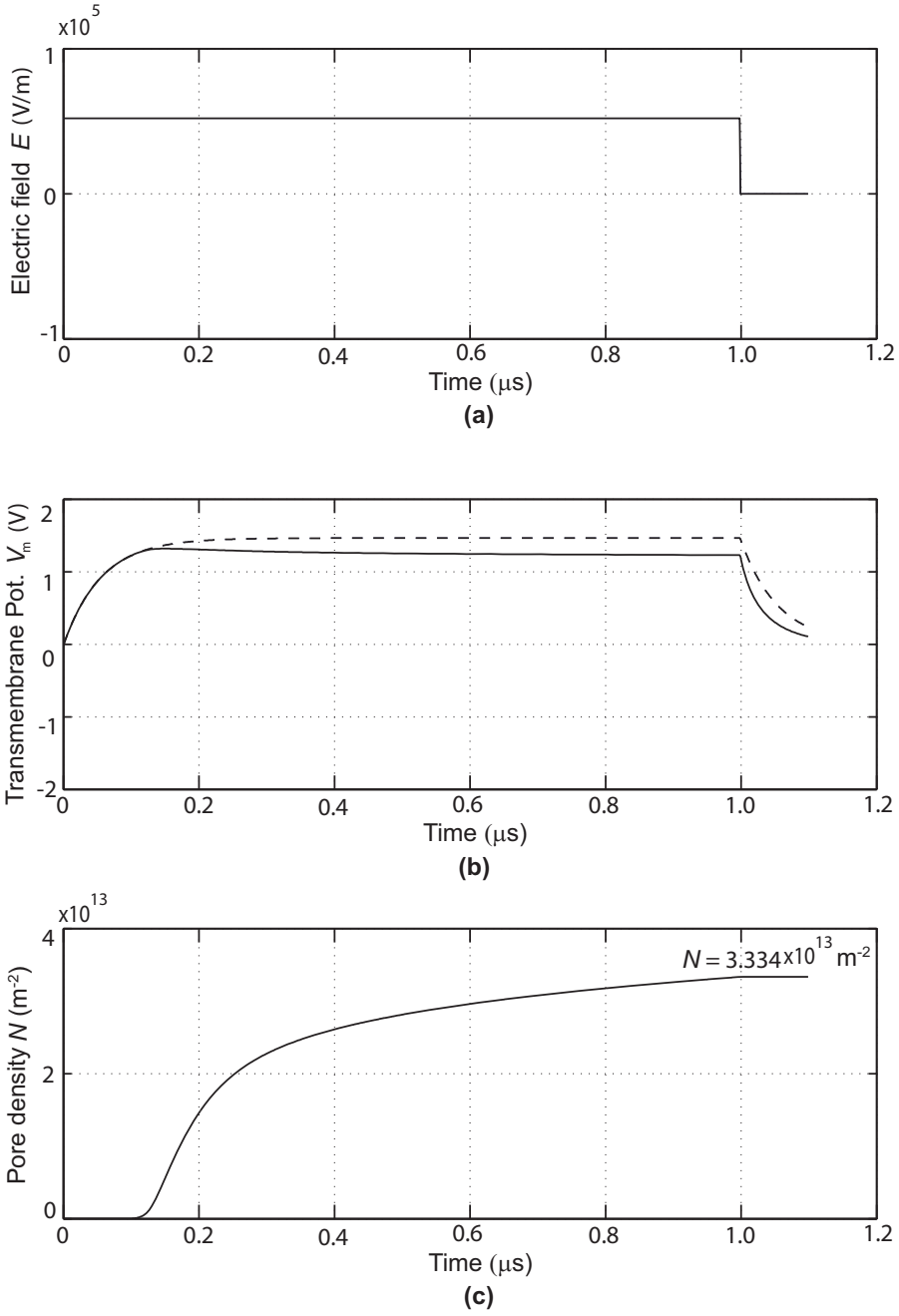

Figure 3.4: Cell response to unipolar square pulse: (a) Applied electric field waveform (unipolar square pulse) (b) Induced transmembrane potential for the piece-wise step response method (i) Including the non-linear effects of membrane electroporation (solid line), (ii) Not including the non-linear effects of membrane electroporation (dashed line) (c) Associated change in pore density, with the maximum pore density given.

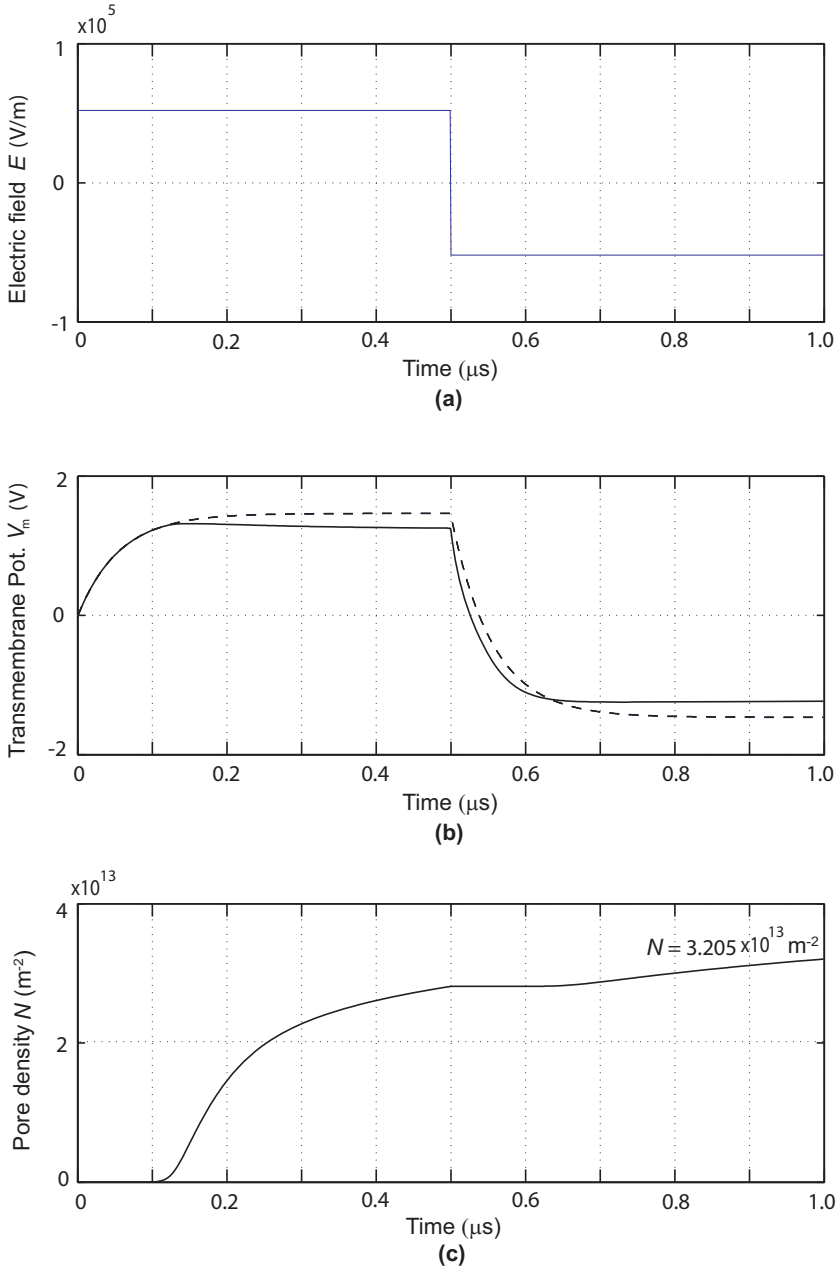

Figure 3.5: Cell response to bipolar square pulse: (a) Applied electric field waveform (bipolar square pulse) (b) Induced transmembrane potential for the piece-wise step response method (i) Including the non-linear effects of membrane electroporation (solid line), (ii) Not including the non-linear effects of membrane electroporation (dashed line) (c) Associated change in pore density, with the maximum pore density given.

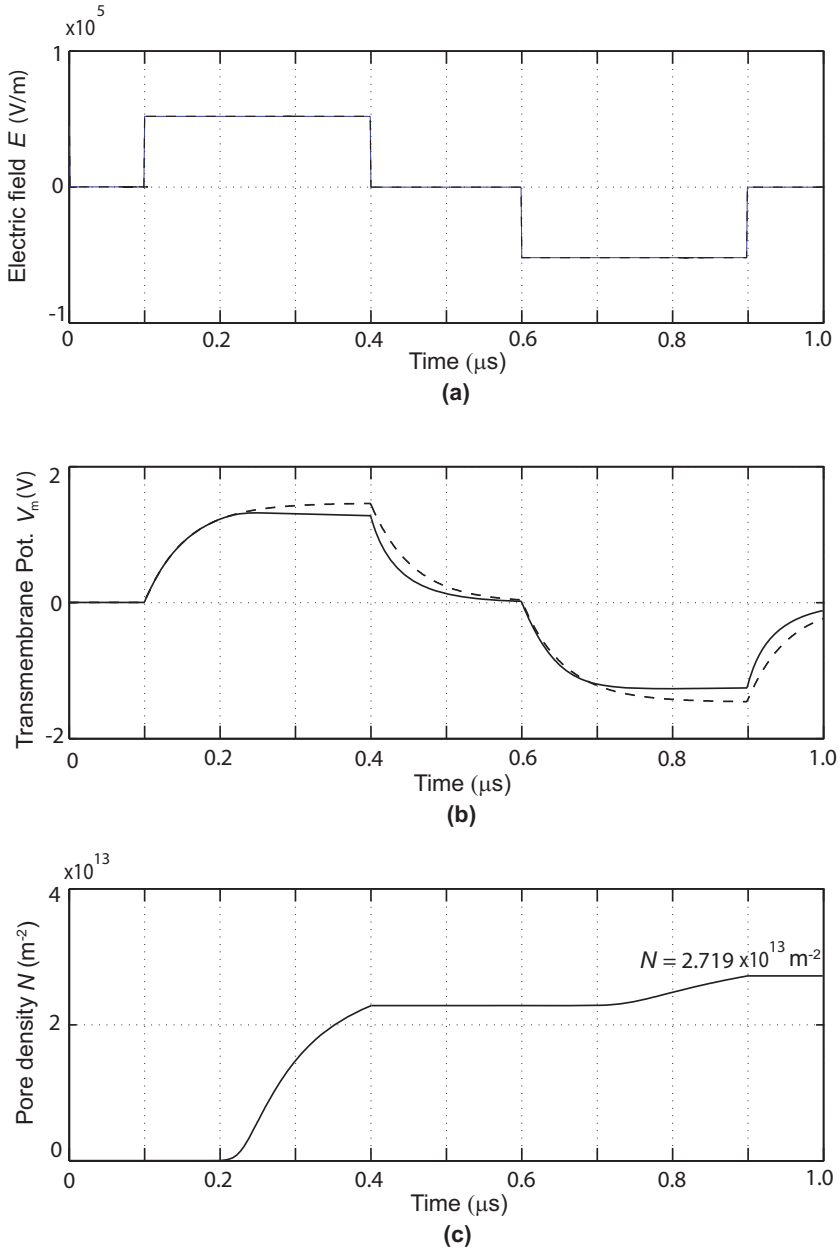

Figure 3.6: Cell response to bipolar rectangular pulse: (a) Applied electric field waveform (bipolar rectangular pulse) (b) Induced transmembrane potential for the piece-wise step response method (i) Including the non-linear effects of membrane electroporation (solid line), (ii) Not including the non-linear effects of membrane electroporation (dashed line) (c) Associated change in pore density, with the maximum pore density given.

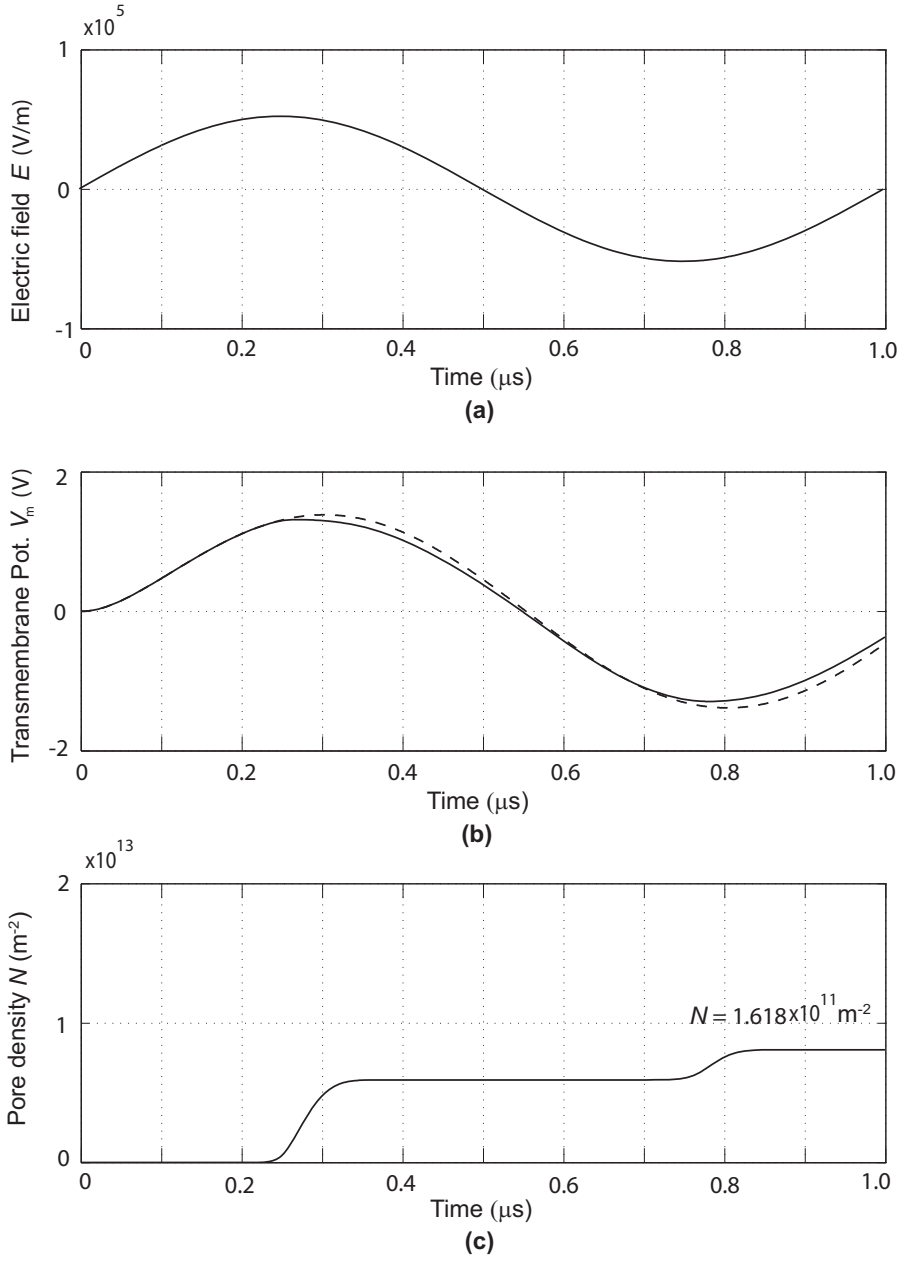

Figure 3.7: Cell response to bipolar sinusoidal pulse: (a) Applied electric field waveform (bipolar sinusoidal pulse) (b) Induced transmembrane potential for the piece-wise step response method (i) Including the non-linear effects of membrane electroporation (solid line), (ii) Not including the non-linear effects of membrane electroporation (dashed line) (c) Associated change in pore density, with the maximum pore density given.

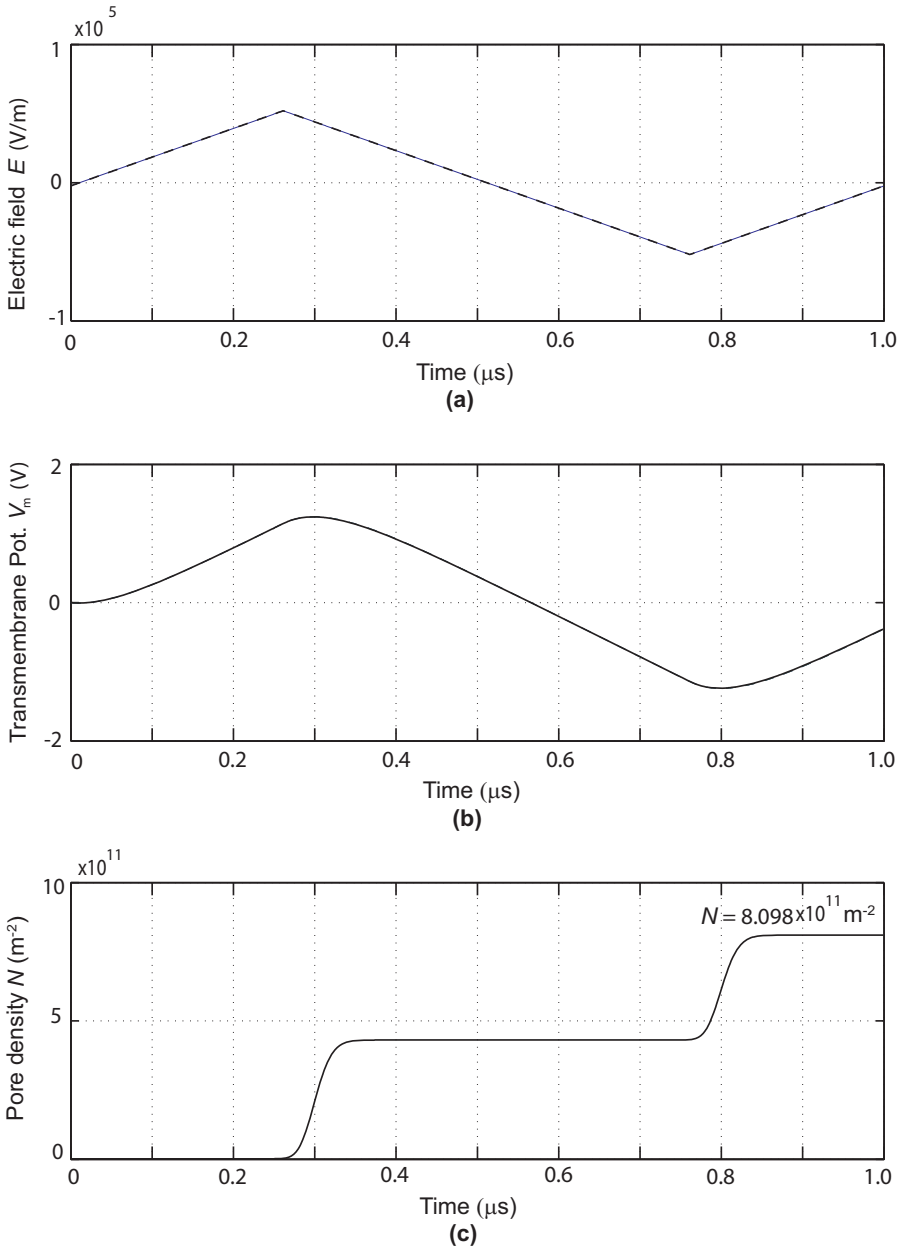

Figure 3.8: Cell response to bipolar triangular pulse: (a) Applied electric field waveform (bipolar triangular pulse) (b) Induced transmembrane potential for the piece-wise step response method (i) Including the non-linear effects of membrane electroporation (solid line), (ii) Not including the non-linear effects of membrane electroporation (dashed line) (c) Associated change in pore density, with the maximum pore density given.

3.4.2 Transmembrane potential and pore density about the spherical cell

A spherical cell exposed to a unipolar square external electric field is polarized such that maximum transmembrane potentials occurs at the anode end ($\theta = 0°$) and the cathode end ($\theta = 90°$) of the cell, assuming parallel plate electrodes. Also, the induced transmembrane potetial is known to vary cosinusoidally around the circumference of the cell (DeBruin and Krassowska, 1999) provided transmembrane potential is less than about 1 V (that is, below the electroporation potential). As reported in the literature, pore density is maximized at the poles and decreases towards the equator (DeBruin and Krassowska, 1999). Asymmetrical pore density between the two poles is observed, for short unipolar pulses less than approximately 200 μs due to the effect of the membrane rest potential (DeBruin and Krassowska, 1999). The model in this chapter reproduces this effect as shown in Figure 3.9 where a 13 μs unipolar square pulse is applied. As observed with increasing pulse length (DeBruin and Krassowska, 1999), increasing the pulse amplitude also acts to normalize pore density symmetry to some degree. Figure 3.10 shows a similar response when a 1 μs, single bipolar sinusoidal electric field pulse is applied, with an improvement that completely symmetrical pore density is observed. Increasing the field amplitude of the sine wave only acts to symmetrically increase pore density around the cell. The transmembrane potential sign remains the same on both polar regions, since it is only an indication of peak amplitude of a symmetrical bipolar transmembrane potential, and thus has no specific polarity.

Larger field amplitudes than that shown in Figure 3.10 do not substantially alter the maximum magnitude of transmembrane potential but increase the height and width of the pore density profile and increase the fraction of cell membrane with transmembrane potential higher than the critical value for electroporation.

3.5 Conclusion

In this chapter a numerical model based on a piecewise time domain step response method incorporating pore formation dynamics was developed and tested. Results from the numerical model support the conclusion that bipolar

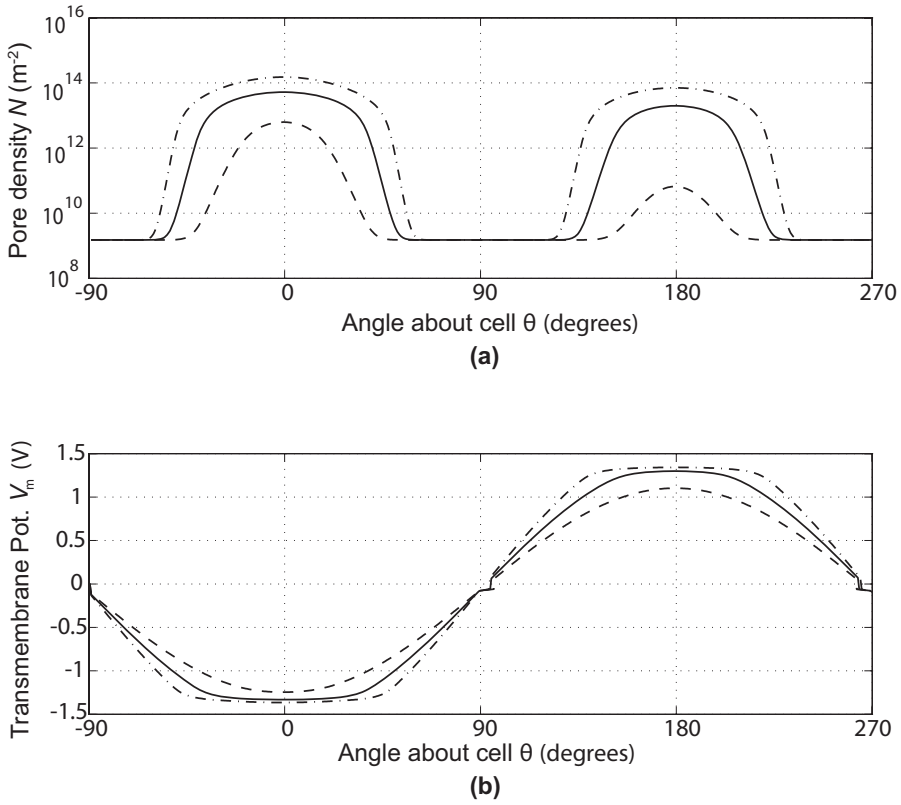

Figure 3.9: Response around the cell with unipolar pulse: (a) Maximum pore density and (b) transmembrane potential around a 15 μm radius spherical cell at the end of a 1 μs, unipolar square pulse for three electric field amplitudes (62 kV/m (dash-dotted line), 52 kV/m (solid line), 42 kV/m (dashed line)).

pulses can be used as an effective alternative to conventional unipolar pulses in the applications of electropermeabilization. Simulations describe the dynamic electro-physical membrane behaviour for a single cell exposed to arbitrary electric fields in the form of transmembrane potential and pore density. With reasonably accurate real system parameters and the assumption that cells can be considered in isolation, the model is a useful tool for prediction of electropermeabilization results. An informed variation of the parameters can then be made to maximize the efficacy of a specific application.

Although this chapter has demonstrated predicting the effect of the type of electric field used on transmembrane potential, pore density and the symmetry between the two poles, there are other significant physical and electrical parameters that can affect electroporation. One very important physical parameter that can be varied for optimal results of electroporation, is the extracellular conductivity. Also, the effect of frequency of applied electric field on electro-

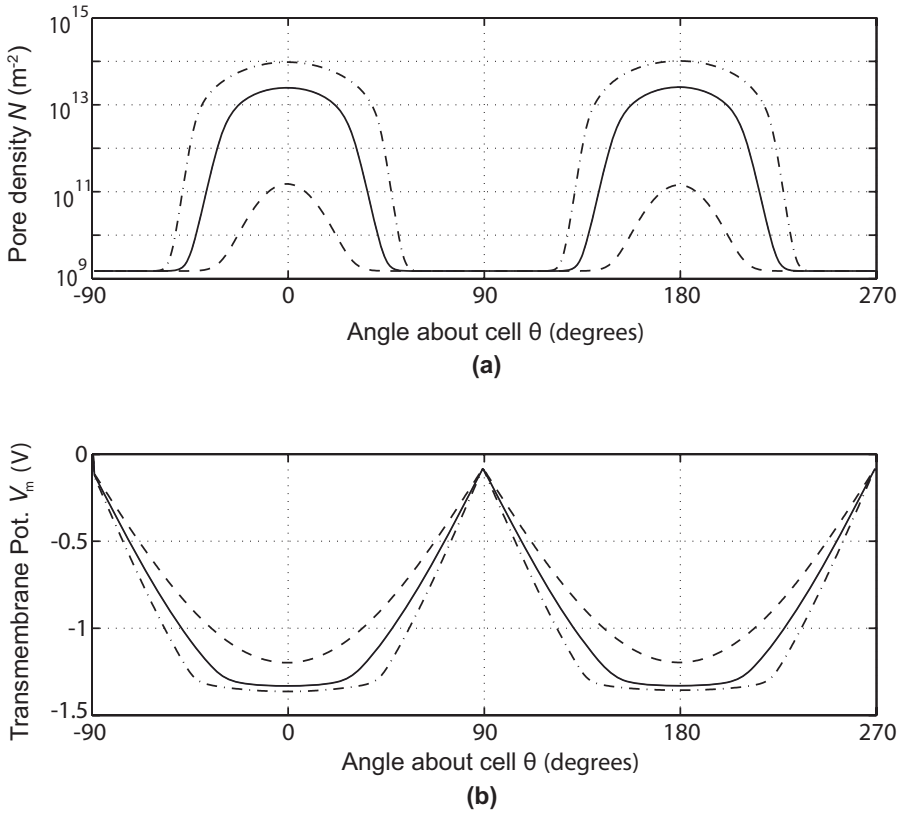

Figure 3.10: Response around the cell with bipolar sinusoidal pulse: (a) Maximum pore density and (b) transmembrane potential around a 15 μm radius spherical cell at the end of a 1 μs, single cycle bipolar sinusoidal pulse for three electric field peak amplitudes (62 kV/m (dash-dotted line), 52 kV/m (solid line), 42 kV/m (dashed line)).

poration needs to be studied. The model presented here needs to be exploited further to simulate more results that can help comment on the effect of extracellular conductivity and applied electric field parameters for suitable use in applications. These simulations are described in the next chapter.

Chapter 4

Effect of Parameters on Electroporation.

In the previous chapter, a numerical model for modelling single cell electroporation under arbitrary applied electric field is presented along with discussion of the preliminary results. This chapter describes more results obtained from the numerical model of the previous chapter for a single cell exposed to an arbitrary waveform electric field pulse. The simulation results presented in this chapter are concentrated on how the efficiency of electroporation related applications can be significantly improved by appropriately adjusting the parameters of the applied electric field and the extracellular conductivity. Emphasis is given on the normalization of the degree of electroporation for two cell sizes of 7.5 μm and 15 μm radius.

Many biological applications require large molecules to be introduced into the cellular cytoplasm without compromising cell function. Electroporation is an effective method to obtain this. However, a large variety of parameters can influence the efficacy of electroporation. Parameters of primary importance are the conductivity of the cell interior, membrane and surrounding medium, the amplitude, duration and waveform of applied electric field pulses, and the radius/geometry of target cells. If the parameters are not appropriately optimized, then it is possible that at one extreme, electroporation may not occur at all, or at the other extreme, cells may reach an unstable condition where the induced membrane pores continue to expand, compromising membrane integrity leading to lysis (loss of cell viability). In addition, the efficiency of electroporation depends on many other physical and chemical properties of the

extracellular medium such as ionic strength and composition (Rols and Teissié, 1989; Djuzenova *et al.*, 1996; Pucihar *et al.*, 2001), osmotic pressure (Rols and Teissié, 1989; Golzio *et al.*, 1998), and temperature (Rols *et al.*, 1994) before and after electroporation.

Conventional electroporation methods typically use unipolar electric field pulses that are either rectangular or exponential decay in form. Such methods have serious shortcomings. It is well known that unipolar pulses typically lead to asymmetrical pore formation which is not optimal for most electroporation applications (DeBruin and Krassowska, 1999; Tekle *et al.*, 1990; Teissié and Rols, 1993; Mehrle *et al.*, 1985; Gabriel and Teissié, 1997). Conventional unipolar pulses introduce a significant cellular radius/geometry dependency on the level of electroporation which, also is not optimal for applications that include heterogeneous populations of target cell radii/geometries. Finally, use of bipolar pulses has been found to reduce electrolytic contamination that occurs due to release of metal ions from electrodes and dissociation of medium constituents during electroporation, thus reducing the detrimental effects of electroporation on the cells (Kotnik *et al.*, 2001a).

The most recent publication by Chen *et al.* (2008) reports experimental results on efficiency of cell membrane electroporation using alternating fields of frequencies 20 kHz -160kHz. Their study confirms that efficient electroporation may be achieved using ac fields and raises the possibility of a wider range of clinical and laboratory applications using ac field with appropriate parameters and avoiding use of invasive needle electrodes.

To help predict the choice of primary electrically-based parameters for optimal electroporation, there is need for a model which can simulate electroporation taking into consideration the non-linear dynamic dependence of the pore density on several applied electric field and cellular dielectric parameters simultaneously. This chapter presents such simulations and relevant discussions.

4.1 Important Parameters affecting Electropermeabilization

4.1.1 Effect of extracellular conductivity

Few studies exist about the effect of extracellular conductivity σ_{ex} on electropermeabilization. A number of empirical studies have been reported about the effect of different ranges of extracellular conductivity σ_{ex} on permeabilization of various cells (Pucihar *et al.*, 2001). One series of studies has shown that the threshold value for permeabilization of Chinese hamster ovary cells is independent of the ionic strength of the pulsing medium (Rols and Teissié, 1989). The actual conductivities of the pulsing medium were not given. Another study indicated that the percentage of permeabilized green algae cells (*Chlamydomonasreinhardtii*) decreases if extracellular conductivity decreases (the range of conductivities was from 5.6×10^{-3} to 3.5×10^{-2} S/m) (Golzio *et al.*, 1998). Another investigation showed that decreasing the extracellular conductivity results in lower viability of the cells, however the range of conductivity tested was quite narrow (8×10^{-2} to 3.7×10^{-1} S/m) (Djuzenova *et al.*, 1996). Research from a separate group confirmed the theoretical predictions that the membrane relaxation time constant decreases with increasing extracellular conductivity, although their studies were performed on artificial lipid bilayers, and only in a range of very low conductivities (up to 5×10^{-3} S/m) (Lojewska *et al.*, 1989).

Another investigation of a broader range of conductivities between 1.1×10^{-3} to 1.61 S/m reported that medium conductivity influences the survival of the cells, while no detectable effect was observed on electropermeabilization of the cells (Pucihar *et al.*, 2001). While all above mentioned experiments use unipolar electric fields, another study using bipolar electric field reports increased electropermeabilization efficiency due to reduced electrolytic contamination (Kotnik *et al.*, 2001a). The actual extracellular conductivities used for the bipolar pulse experiments are not mentioned. The electrolytic contamination was reported as being higher for higher levels of extracellular concentration when using unipolar pulses. Another study which uses a single square pulse, unipolar square wave and bipolar square wave for DNA transfection of cells, reports increased number of transformants with DNA concentration and highest transfection efficiency with a bipolar pulse followed by a unipolar pulse (Tekle

et al., 1991).

4.1.2 Effect of applied electric field frequency

Owing to the variable nature of biological growth dynamics, all electroporation applications treat cells that have some range of cell size. Although this range may only be in the order of a few percent, some applications may have ranges exceeding 200 percent (Foster and Schwan, 1996). As such, whatever the application, there may be a substantial benefit of being able to normalize the degree of electropermeabilization (pore density) with respect to cell radius/size. It has been shown through passive modelling of bipolar electric field induced transmembrane potential V_m, that as the frequency of a similar amplitude applied electric field is increased, transmembrane potential reduces and becomes less dependent on cell radius (Grosse and Schwan, 1992). However, whether this effect translates to dynamic modelling of electroporation, is not established. This is presented in section 4.3.2.

4.2 Modelling Methodology

The numerical model recently developed (Talele and Gaynor, 2007) and presented in Chapter 3, that predicts the development of transmembrane potential V_m, and pore density N, once the various parameters of the cell system and applied electric field are chosen, is used in this chapter. We investigate what combination of fundamental parameter values could provide optimal electroporation in a range of possible applications. It was shown in Chapter 3, Figure 3.9 and 3.10, that short unipolar electric fields were not conducive to optimal symmetrical electroporation dynamics. As such, only bipolar electric field pulses (square and sinusoidal wave) are investigated here. A single cell is exposed to a variety of bipolar electric field strengths and waveforms for a range of extracellular conductivity at two different frequencies and two different cell radii to simulate pore density.

For *in vitro* applications, water-based media is generally used which has a fairly constant permittivity, and *in vivo* applications usually have a bulk tissue permittivity not that dissimilar to water (Foster and Schwan, 1996). Therefore, although the model is able to vary this parameter, effects of variation in external permittivity are not considered important thus not presented.

Although there is some variation in the conductivity and permittivity amongst the cell membrane and cell cytoplasm of various cells, it is usually not substantial (Foster and Schwan, 1996). Thus, although the model is capable of varying these parameters, the effects of such variation are not presented in this study.

4.3 Simulation Results and Discussion

4.3.1 Effect of extracellular conductivity on permeabilization

To cover the range of most electroporation applications (*in vitro* and *in vivo*) the electropermeabilization model developed and presented in Chapter 3 was used to compare the pore density N, when a single spherical cell is exposed to a variety of bipolar peak field strengths and waveforms, for a range of extracellular conductivity from 1×10^{-2} to 4 S/m. Figure 4.1 shows the variation in terminal N (pore density at the end of the pulse duration) with respect to extracellular conductivity σ_{ex}, and the induced transmembrane potential V_m for four different waveforms of applied electric field pulse (two-cycles of bipolar sine, square, rectangular, and triangle), with a frequency of 100 kHz. Figure 4.2 shows similar plots for the four different waveforms of applied electric field pulse for the same conditions as Figure 4.1, but with a frequency of 1 MHz.

As observed in Figures 4.1(c) and 4.2(c) there is a clear variation in terminal pore density with change in extracellular conductivity for the different waveforms. This indicates that electropermeabilization is substantially affected by extracellular conductivity, and the combination of the waveform and peak amplitude of the applied field. The square wave electric field appears to provide the maximum pore density for a given extracellular conductivity. Comparison of Figure 4.1(b) and Figure 4.2(b) clearly illustrates the increasing of pore density dependency on the time the electric field induces a transmembrane potential above the threshold required for electroporation (±1 V).

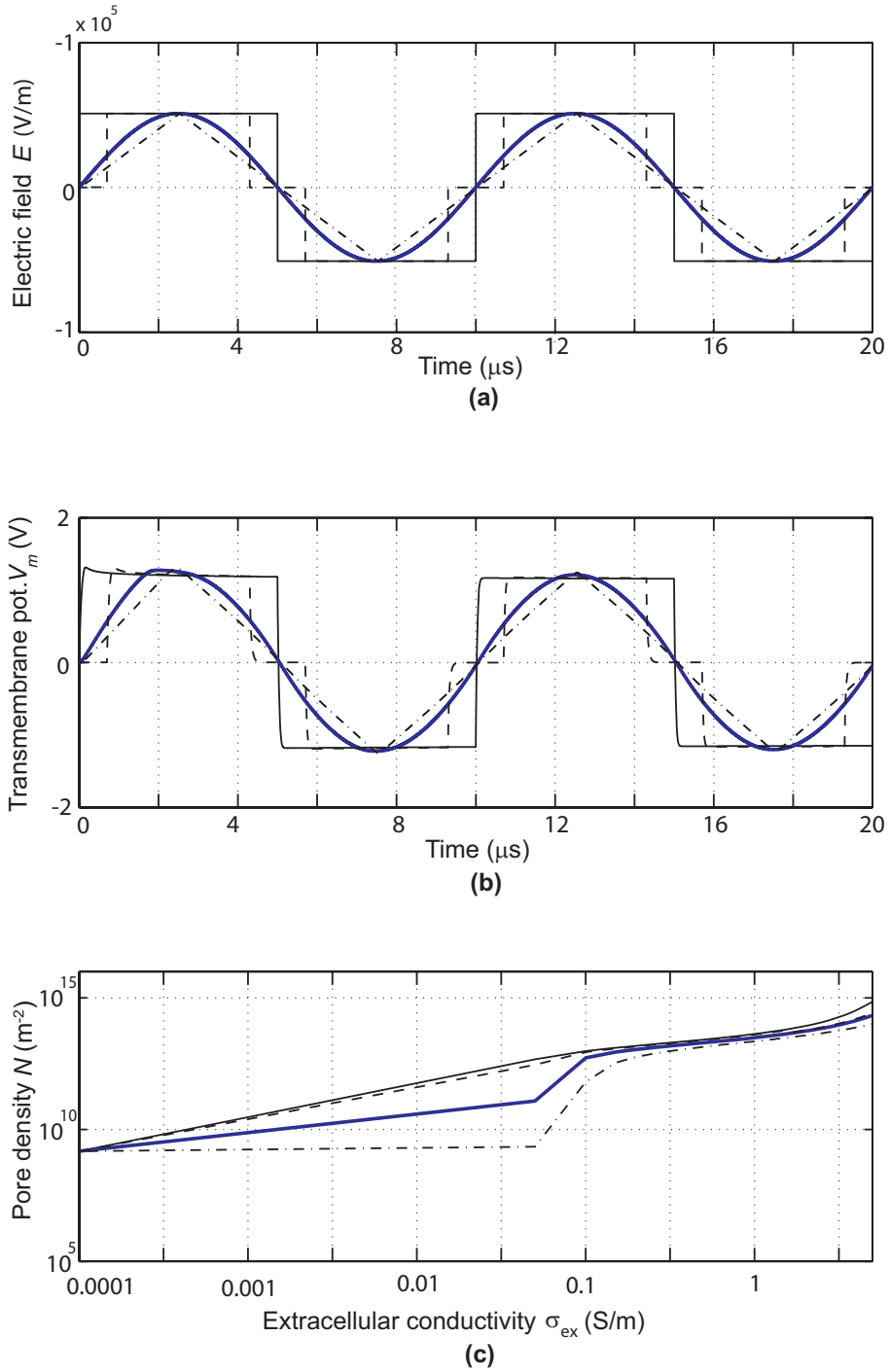

Figure 4.1: Response to 100 kHz electric fields at varying σ_{ex}. (a) Two-cycle sine wave (solid bold), square wave (solid), rectangular wave (dashed), and triangle wave (dash-dotted) electric field pulses applied to a 15 μm radius cell. The amplitude of all four waveforms is 51 kV/m peak, with a frequency of 100 kHz. (b) Induced transmembrane potential for the corresponding applied electric field pulse, with $\sigma_{\text{ex}} = 1.2$ S/m. (c) Terminal pore density as a function of σ_{ex} for each of the applied field pulses.

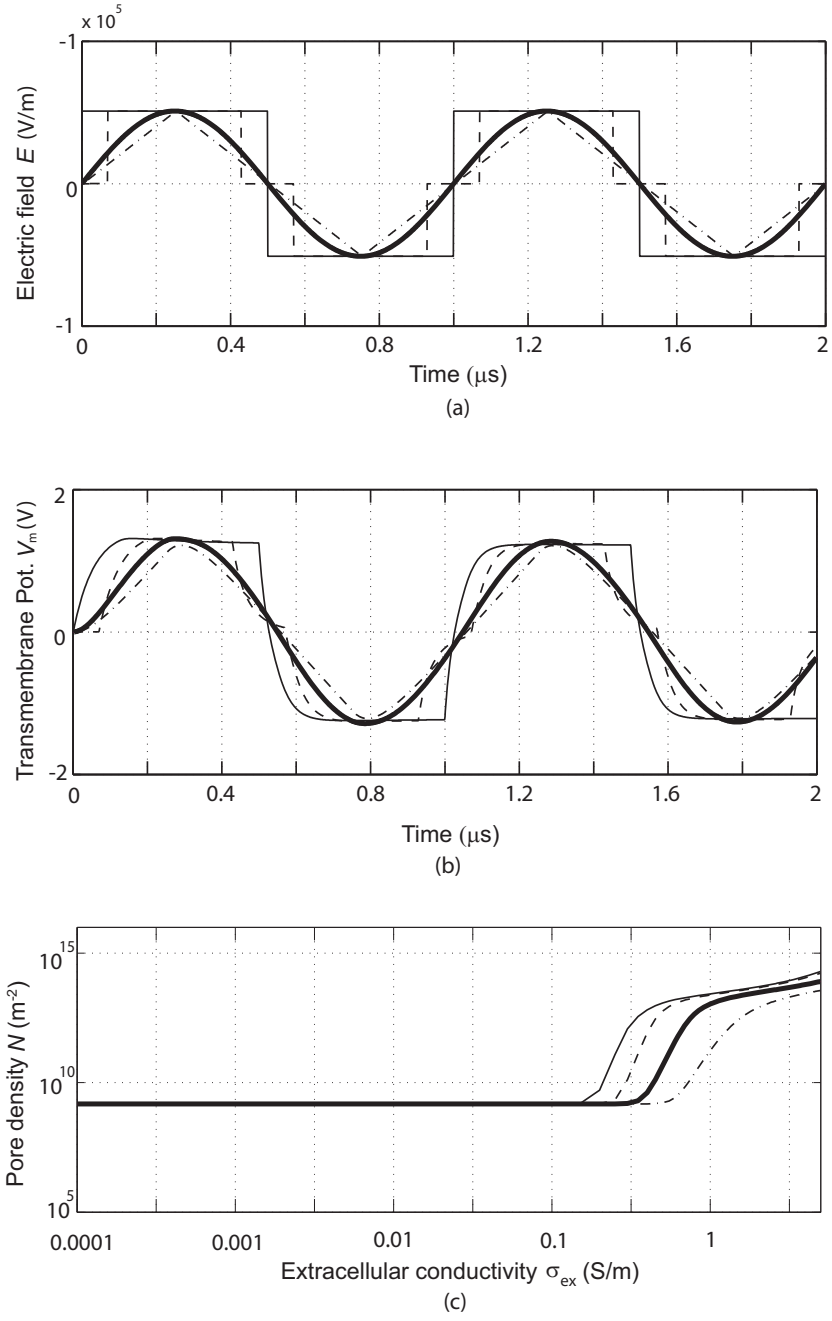

Figure 4.2: Response to 1 MHz electric fields at varying σ_{ex}. (a) Two-cycle sine wave (solid bold), square wave (solid), rectangular wave (dashed), and triangle wave (dash-dotted) electric field pulses applied to a 15 μm radius cell. The amplitude of all four waveforms is 51 kV/m peak, with a frequency of 1 MHz. (b) Induced transmembrane potential for the corresponding applied electric field pulse, with $\sigma_{\text{ex}} = 1.2$ S/m. (c) Terminal pore density as a function of σ_{ex} for each of the applied field pulses.

4.3.2 Frequency dependence of electropermeabilization in a heterogeneous population of cell radii/sizes.

To determine effect of electric field frequency on electropermeabilization in a heterogeneous population of cell radii/sizes to dynamic electroporation modelling, two higher frequency electric field pulses of 100 kHz and 1 MHz were used for electropermeabilization. Two substantially (yet realistically) different cell radii of 7.5 μm, and 15 μm were considered.

Figure 4.3 shows pore density for 7.5 μm and 15 μm radius cells exposed to a two-cycle sine wave electric field pulse of 100 kHz and 1 MHz. The peak amplitude of the electric field, E_p was set to provide an average terminal pore density (for the two cell radii) of approximately 3×10^{13} pores/m^2 (presented by Hibino *et al.* (1991) as being within a good range of permeabilization), at a extracellular conductivity of 0.2 S/m. It is evident from Figure 4.3 that the 1 MHz electric field pulse reduces the relative difference in pore density between the two cell sizes. However, a significantly higher peak amplitude of electric field is required to create the same level of average pore density, when a sine-wave electric field is applied.

Figure 4.4 shows a similar result for a square wave electric field pulse of 100 kHz and 1 MHz. Although the required square wave electric field amplitude is less than the equivalent frequency sine wave, the relative difference in pore density between the two cell sizes is greater than the sine wave result for the same average pore density at extracellular conductivity of 0.2 S/m. Further, considering the results from Figure 4.4, it is apparent that the relative difference of pore density between the two cell sizes is consistently lower for the 1 MHz sine wave electric field compared to the square wave electric field, even though the square wave electric field amplitude is always lower for an equivalent pore density.

4.3.3 Simultaneous effect of extracellular conductivity and applied field amplitude and frequency

It can be very complex and time consuming task to select the most appropriate parameters for an electroporation application through individual trials. The numerical model developed is used here to generate predictions of pore density developed for the two chosen cell radii and frequencies, when exposed to a range

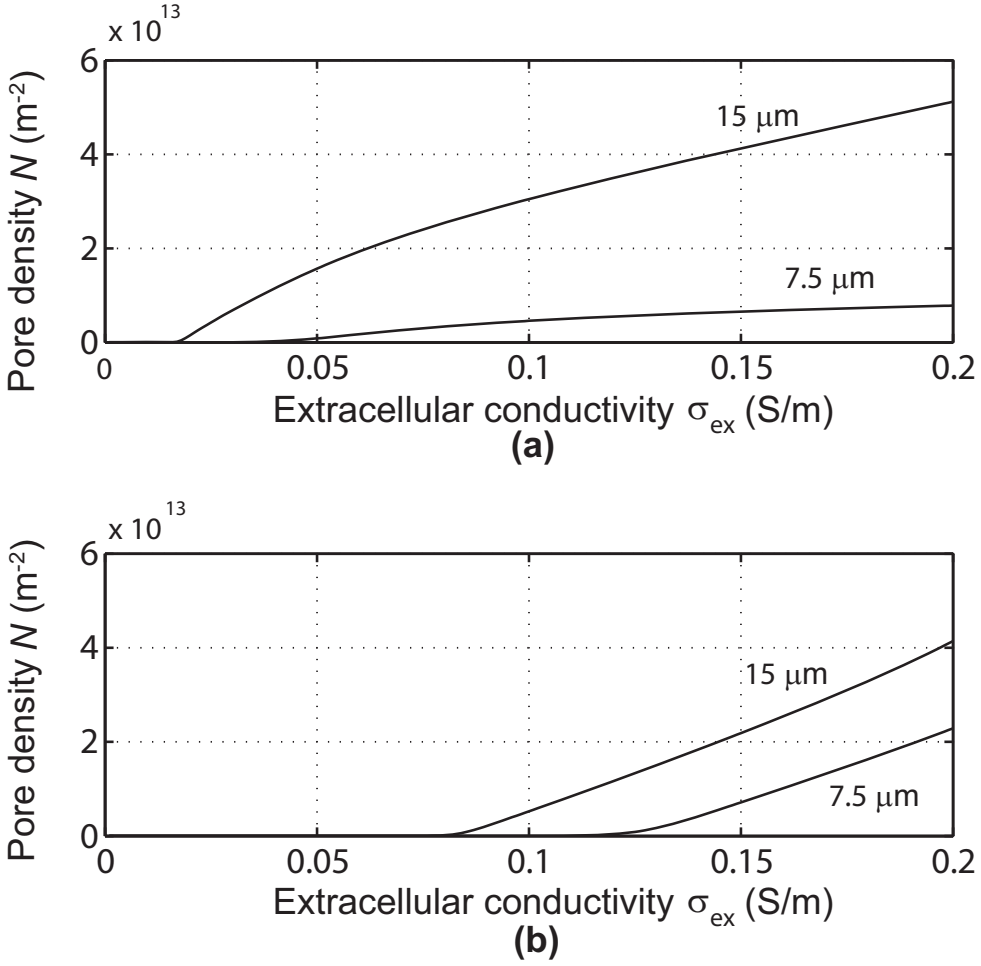

Figure 4.3: Response to 100 kHz and 1 MHz sine wave electric field for varying extracellular conductivity. Pore density versus extracellular conductivity for 7.5 μm and 15 μm radius cells exposed to two-cycles of a sine wave electric field of (a) $E_p = 90$ kV/m, and $f = 100$ kHz, and (b) $E_p = 147$ kV/m, and $f = 1$ MHz.

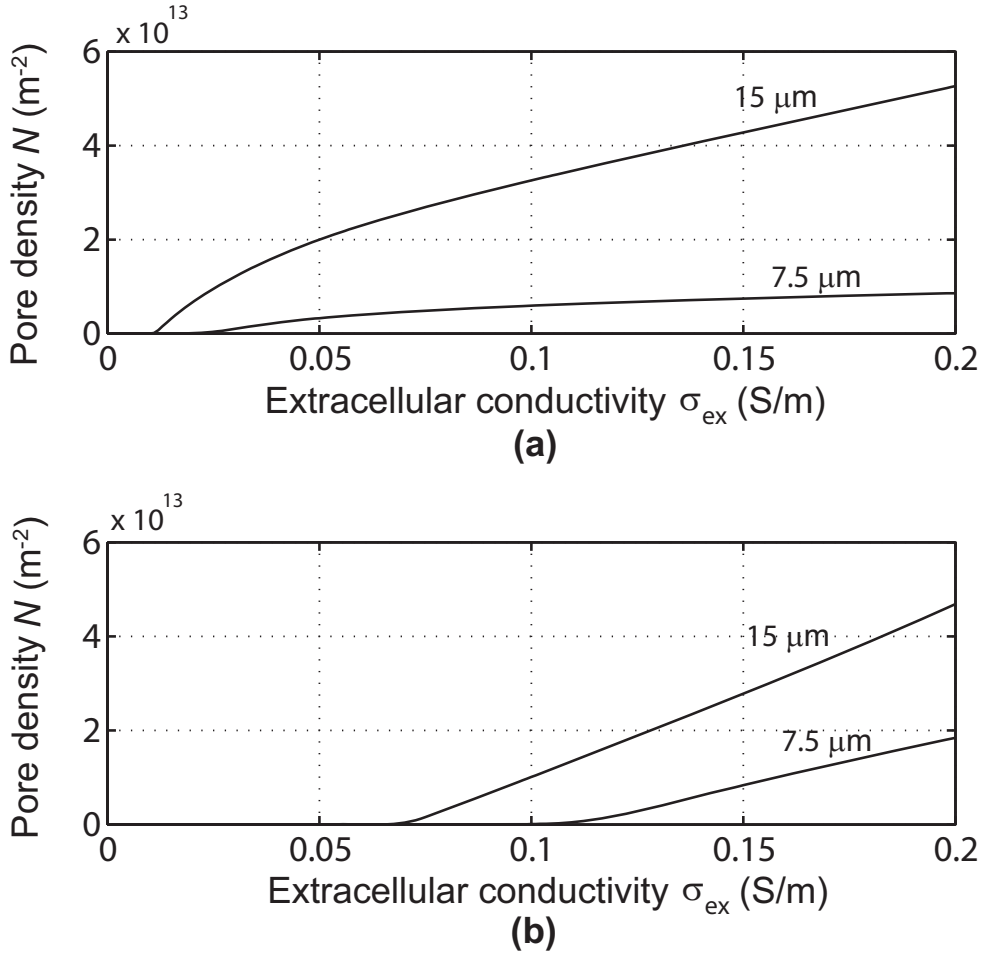

Figure 4.4: Response to 100 kHz and 1 MHz square wave field for varying extracellular conductivity. Pore density versus extracellular conductivity for 7.5 μm and 15 μm radius cells exposed to two-cycles of a square wave electric field of (a) $E_p = 86$ kV/m, and $f = 100$ kHz, and (b) $E_p = 112$ kV/m, and $f = 1$ MHz

of values of extracellular conductivity and applied electric field amplitude.

Figure 4.5 shows the effect of extracellular conductivity and electric field amplitude on the pore density. Extracellular conductivity values range from 0.01 S/m to 4.0 S/m, and peak electric field amplitude, E_p for a two-cycle 100 kHz sine wave ranges from 0 to 120 kV/m. In order to determine the pore density trend, two electric field frequencies (100 kHz and 1 MHz), two electric field waveforms (sine and square wave), and two cell radii, (7.5 μm and 15 μm) were used.

Similarly, Figure 4.6, Figure 4.7 and Figure 4.8 show how pore density varies with both extracellular conductivity and peak electric field amplitude, E_p for a two-cycle 1 MHz sine wave, two-cycle 100 kHz square wave, and a two-cycle 1 MHz square wave electric field respectively.

It is apparent from the diverging nature of the two contours of $N = 3\times10^{13}$ pores/m^2 (given by Hibino *et al.* (1991) as within a good range of electropermeabilization) in Figure 4.5(b), Figure 4.6(b), Figure 4.7(b) and Figure 4.8(b), that to minimize the relative difference in pore density between the large and small cells, extracellular conductivity should be kept as small as possible while E_p is chosen to fall mid-way between the constant pore density limits defined by the 7.5 μm and 15 μm cells for that extracellular conductivity. Electropermeabilization of both cell sizes begins at a lower amplitude for the square wave electric field amplitude compared to the sine wave. Additionally, pore density diverges more rapidly between the large cell and small cell, at higher extracellular conductivity, for the square wave electric field compared to the sine wave.

Comparing the contour plots, it is apparent that for achieving the highest degree of electroporation normalization for the radii variation considered, choosing a lower extracellular conductivity and/or choosing a higher pulse frequency would be appropriate. Of course the corresponding electric field amplitude required would be larger in both cases. At high extracellular conductivity the effect of practical increase in AC frequency is negligible. The high extracellular conductivity reduces the membrane relaxation time constant (Talele and Gaynor, 2007) and forces pore density to be almost proportional to cell radius. The apparent indication is that cells of substantially various sizes can not be close to uniformly electroporated in a surrounding media of around 1.6 S/m (which is a typical physiological medium conductivity (Pucihar *et al.*, 2001)) using bipolar pulses up to and around 1 MHz in frequency. This finding is

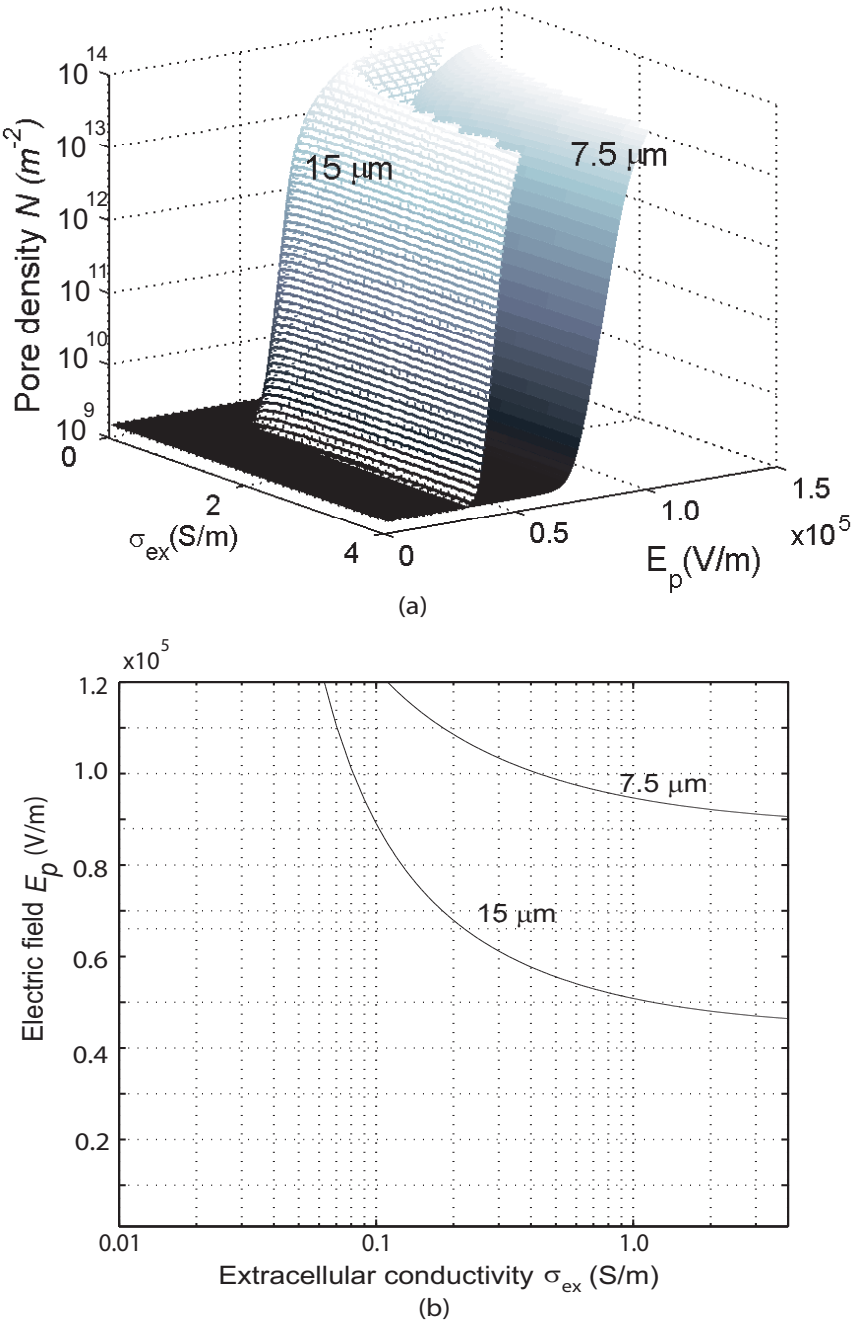

Figure 4.5: Response to 100 kHz sine wave electric field at varying extracellular conductivity and field strength.(a) Pore density variation versus extracellular conductivity and applied field pulse amplitude for a 100 kHz sine wave electric field of two-cycles. Upper surface: cell radius = 15 μm; lower surface: cell radius = 7.5 μm. (b) Contours of the intersection of the two surfaces in (a) at a pore density of $N = 3\times10^{13}$ m^{-2}.

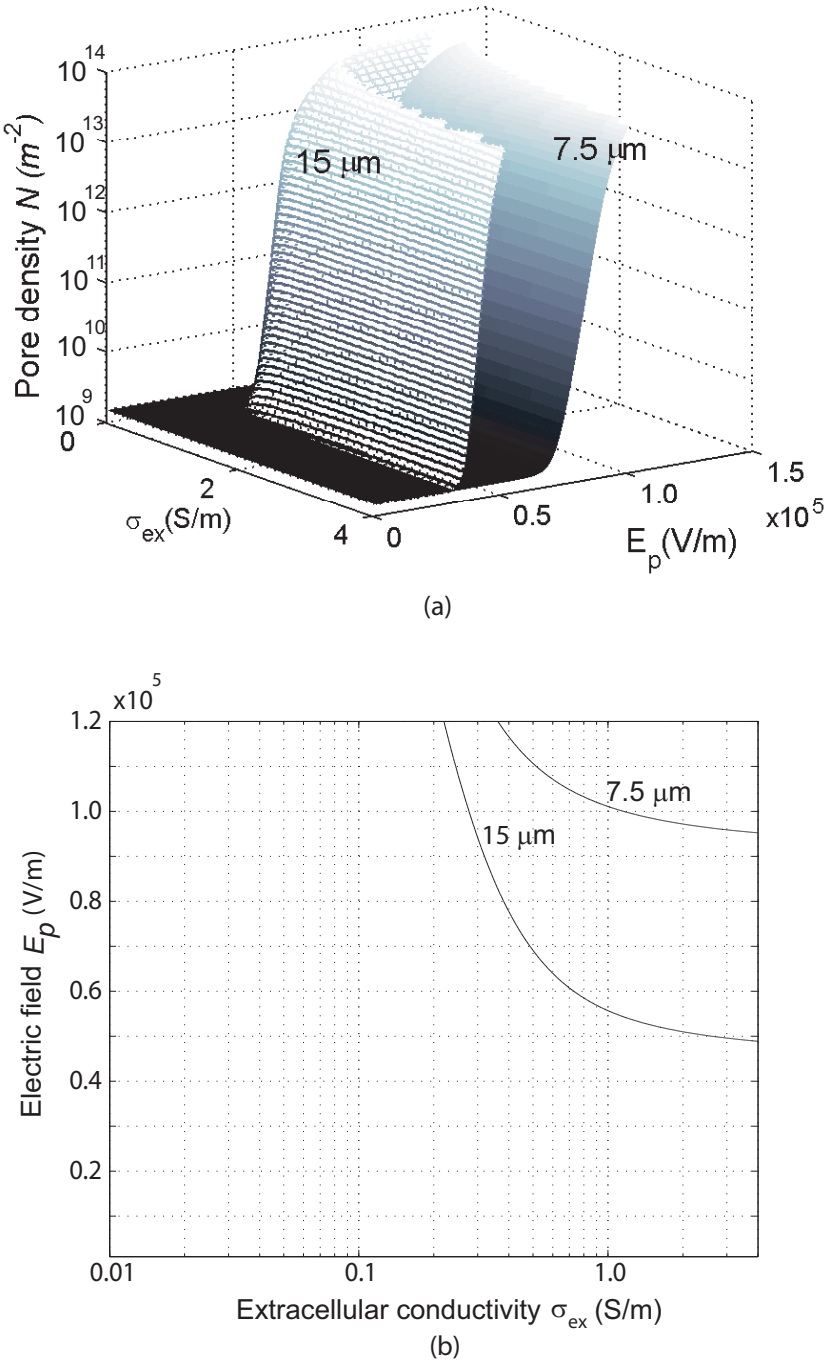

Figure 4.6: Response to 1 MHz sine wave electric field at varying extracellular conductivity and field strength. (a) Pore density variation versus extracellular conductivity and applied field pulse amplitude for a 1 MHz sine wave electric field of two-cycles. Upper surface: cell radius = 15 μm; lower surface: cell radius = 7.5 μm. (b) Contours of the intersection of the two surfaces in (a) at a pore density of $N = 3\times10^{13}$ m^{-2}.

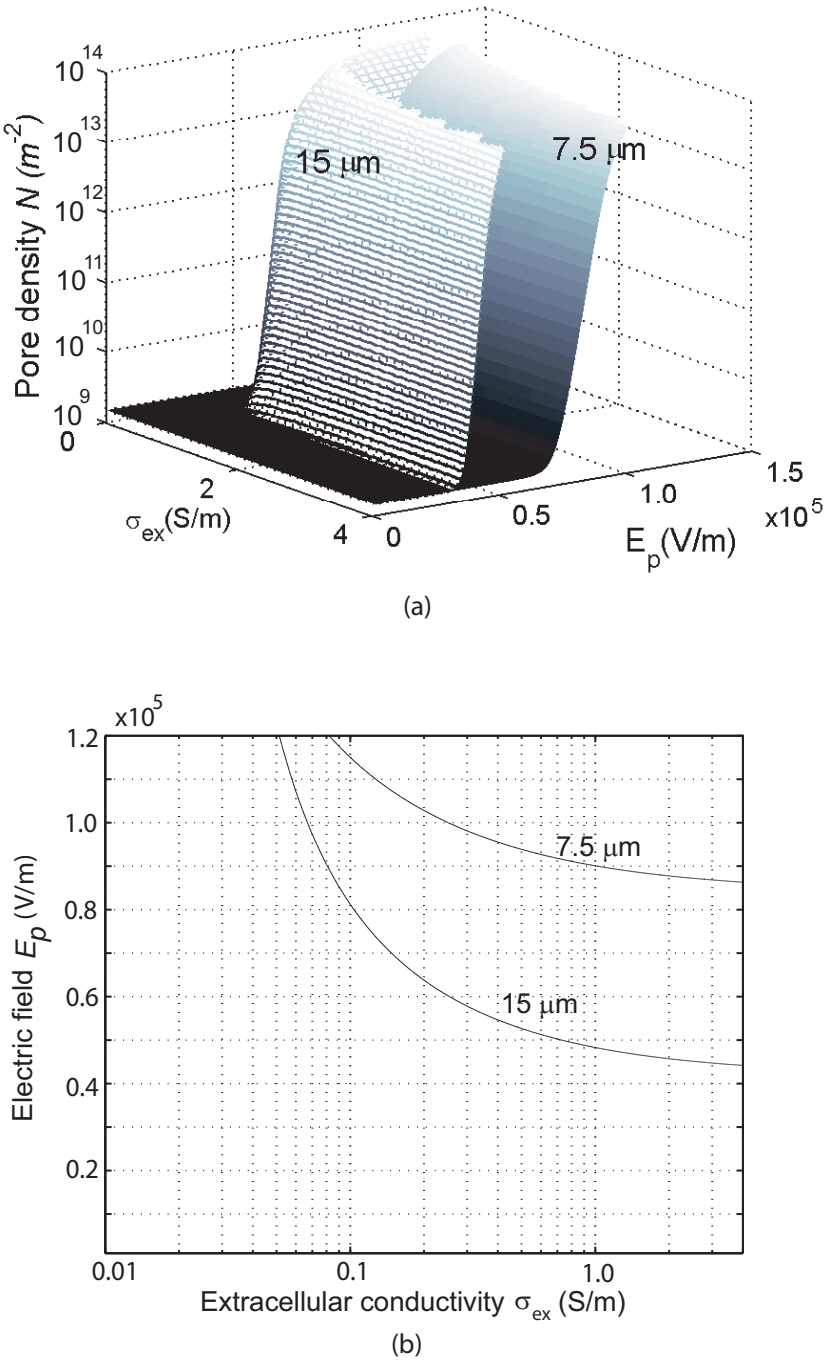

Figure 4.7: Response to 100 kHz square wave electric field at varying extracellular conductivity and field strength. (a) Pore density variation versus extracellular conductivity and applied field pulse amplitude for a 100 kHz square wave electric field of two-cycles. Upper surface: cell radius = 15 μm; lower surface: cell radius = 7.5 μm. (b) Contours of the intersection of the two surfaces in (a) at a pore density of $N = 3\times10^{13}$ m^{-2}.

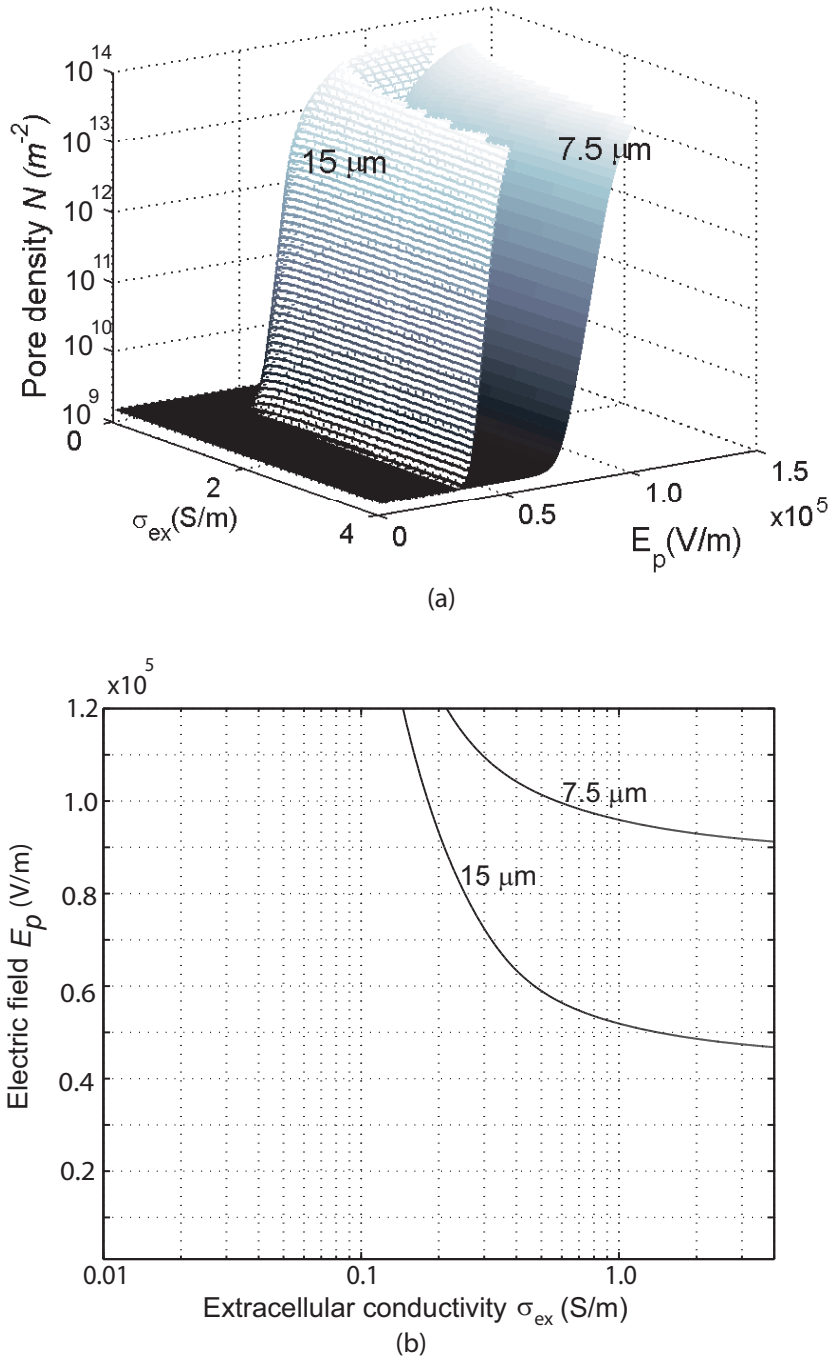

Figure 4.8: Response to 1 MHz square wave electric field at varying extracellular conductivity and field strength. (a) Pore density variation versus extracellular conductivity and applied field pulse amplitude for a 1 MHz square wave electric field of two-cycles. Upper surface: cell radius = 15 μm; lower surface: cell radius = 7.5 μm. (b) Contours of the intersection of the two surfaces in (a) at a pore density of $N = 3\times10^{13}$ m^{-2}.

subject to the assumption that closely neighbouring cells do not create a substantially non-linear electric field gradient that amplifies the electric field at the polar ends of cells, as the model assumes there is a uniform applied electric field. This assumption is supported by Pavlin *et al.* (2002); Qin *et al.* (2005) who show that a lowering of the field strength is observed in multicellular, tissue-like structures. This assumption is valid for suspensions in which the cells represent less than one percent of the total suspension volume (Kotnik, 2003).

4.4 Conclusion

Results from the present study indicate that the efficiency of electroporation related applications can be significantly improved through symmetrical electropermeabilization and normalization of the degree of electroporation, by appropriately adjusting the parameters of the applied bipolar electric field pulse and the conductivity of the external medium.

The results also show that it may be very difficult for cells of substantially different sizes to be close to uniformly electroporated if surrounded by media with a conductivity higher than around 5×10^{-2} S/m for 100 kHz pulses, or 0.2 S/m for 1 MHz pulses. Since typical *in vivo* applications have an external conductivity equal to the physiological conductivity in the region of 1.6 S/m (Pucihar *et al.*, 2001), it is unlikely that normalization of the degree of electroporation can be achieved in these applications.

For achieving as normalized as possible electroporation for the radii/size variation required in a particular application, using a lower extracellular conductivity and/or higher electric field frequency would be preferable. There is, however, a limit to how low the external conductivity and how high the frequency can be made, as the applied electric field amplitude must stay within practical limits. Considering 3×10^{13} pores/m^2 as the required pore density, extracellular conductivity could be as low as 0.08 to 0.37 S/m for a 7.5 μm cell radius and peak electric field of 120 kV/m (depending on the pulse shape and frequency detailed here). For a 15 μm cell radius extracellular conductivity could be as low as $0.05-0.22$ S/m (again depending on the pulse shape and frequency).

It is apparent that the relative difference of pore density between the two cell sizes investigated is consistently lower for the sine wave electric field com-

pared to the square wave electric field, even though the square wave electric field amplitude is always lower for an equivalent pore density.

4.4.1 Limitations of this model

At present the model developed can only predict the electropermeabilization results for spherical cells in a uniform electric field. Including other shapes of cells and a non-linear electric field gradient would require substantial alteration to the model. The pore radius is assumed to remain constant irrespective of other parameters. The effect on pore radius could be a subject of future study. The model only considers the effect of variation of the electrical parameters in electroporation. The effect of other physical and chemical properties of the electropermeabilization system are not simulated. Although the electrical parameters have the greatest effect on electroporation dynamics, the other properties may need to be included at some stage in an ultimate model of electroporation. Such inclusion of additional parameters may improve simulations and provide additional information.

The model described in Chapter 3 and used in this chapter is efficient in handling arbitrary waveshapes as fields, to which the cell is exposed. This model assumes all pores to be of the same size of about 0.76 nm. Model based on this assumption is useful for comparing onset of pore density dependent on various parameters such as cell radius, peak electric field, extracellular and intracellular fluid permittivity and conductivity. Although, this approach gives a fair indication of the extent of electroporation in terms of pore density, the inclusion of radius evolution can give a more realistic picture of the extent of electroporation because pore radius and pore numbers affect the transmembrane potential, which in turn affects the pore density and the pore radii spatially and temporally.

Chapter 5

Modelling Single Cell Electroporation: Inclusion of Pore Radii

The model described in Chapter 3 and used in Chapter 4 is efficient in handling arbitrary waveshapes as fields to which the cell is exposed. This model also assumes all pores to be of the same size of about 0.76 nm. Models based on this assumption are useful for comparing onset of pore density dependent on various parameters such as cell radius, peak electric field, extracellular and intracellular fluid conductivity. Although, this approach gives a fair indication of the extent of electroporation in terms of pore density, the approximation that all pores have the same size, that do not change with time, may not be most appropriate. There is a need to model electroporation so as to reflect the growth or shrinkage of pore radii with time, as well as efficiently handle arbitrary waveshapes of electric fields. The additional information about pore radius evolution can give a more realistic picture of the extent of electroporation, especially if one is to model for longer times or if an application required the existence of larger pores. Pore radius and pore numbers can affect the transmembrane potential, which in turn can affect pore density and radius.

Previous reported models include spatial and temporal aspects of pore radius evolution (Smith *et al.*, 2004; Krassowska and Filev, 2007), however, the electric fields used in these models were limited to unipolar DC pulses.

In this chapter a model is developed for single spherical cell electroporation that simulates spatial and temporal aspects of pore radius as an effect of any

given form of applied electric field (including unipolar and bipolar), and other important electroporation system parameters. In particular, a single spherical cell of 15 μm radius, under the application of a 2 μs DC unipolar pulse and two-cycles of a 1 MHz sinusoidal AC pulse is modelled. The transmembrane potential and pore radius at various polar angular positions about the cell membrane and as a function of time are presented.

Then two cell radii (15 μm and 7.5 μm) are considered, and fractional pore area (FPA) is calculated to compare the extent of electropermeabilization at varying extracellular conductivities and the effect of higher frequency sinusoidal AC pulses. The simulation results are used to compare the extent of electroporation in response to sinusoidal AC (bipolar) electric field pulses of two different frequencies in a range of extracellular conductivity for the two cell radii. The results show that the number of pores and their radii tend to be more normalized when an AC (bipolar) field is used when compared to a DC (unipolar) field. It is also observed that a 1 MHz bipolar sinusoidal applied electric field pulse reduces the relative difference in fractional pore area between the two cell sizes compared to a 100 kHz pulse. However, a significantly higher amplitude is required to create the same level of average fractional pore area.

5.1 Model of a Single Cell

Consider a spherical cell of radius a with intracellular conductivity σ_{in}. The cell is immersed in a medium with conductivity σ_{ex}. This system is exposed to a time-varying electric field $E(t)$. Azimuthal symmetry about the axis of the applied electric field is assumed.

5.1.1 Transmembrane potential

It is assumed that the intracellular and extracellular regions are source free. The homogeneous external electric field of strength $E(t)$ is used as a boundary condition, the potential being fixed at

$$\Phi(3a, \theta) = -3aE(t)\cos\theta, \tag{5.1}$$

on a sphere of radius $3a$ surrounding the cell, where θ is the polar angle. Since there are no sources inside the region, the potential obeys Laplace's equation except at the cell membrane at a radial distance of $(r = a)$ where the potential is discontinuous because of the abrupt change in conductivity and the approximated infinitely thin membrane. Thus internal and external potentials can be defined as,

$$\Phi(r,\theta) = \begin{cases} \Phi_{\text{in}}(r,\theta) & r < a, \\ \Phi_{\text{ex}}(r,\theta) & a < r < 3a. \end{cases} \tag{5.2}$$

The current across the membrane is used to relate the internal and external potentials (DeBruin and Krassowska, 1999), that is,

$$-\hat{\mathbf{r}} \cdot (\sigma_{\text{in}} \nabla \Phi_{\text{in}}(a,\theta)) = -\hat{\mathbf{r}} \cdot (\sigma_{\text{ex}} \nabla \Phi_{\text{ex}}(a,\theta)) = C_m \frac{\partial V_m}{\partial t} + J_m \tag{5.3}$$

where

$$V_m(\theta) = \Phi_{\text{in}}(a,\theta) - \Phi_{\text{ex}}(a,\theta). \tag{5.4}$$

Here $\hat{\mathbf{r}}$ is the unit outward radial vector, C_m is the specific membrane capacitance, V_m is the transmembrane potential and J_m is the current density at the cell membrane due to existing pores.

The current density is made up of three terms as follows,

$$J_m = J_{\text{ion}} + J_{\text{sml}} + J_{\text{lge}}, \tag{5.5}$$

where $J_{\text{ion}} = g_m(V_m - V_{\text{rest}})$ is the ionic current density (DeBruin and Krassowska, 1999), (g_m is the specific membrane conductance, and V_{rest} is the membrane rest potential).

The remaining two current density terms are explained in the following paragraphs. J_{sml}, is the current density through small pores and is given by

$$J_{\text{sml}} = N i_{\text{sml}}(r), \tag{5.6}$$

where N is the pore density of the initial small pores formed and $i_{\text{sml}}(r)$ is the diffusion current through a single pore of radius r (and is true for small pores only). As previously introduced in section 2.4.1, Equation 2.23 for i_{sml} based upon the Nernst-Planck equation models, is used for pore radius below 1 nm.

We repeat Equation 2.23 here for completeness:

$$i_{\text{sml}} = \frac{\pi r^2 \sigma_{\text{ps}} v_m RT}{Fh} \cdot \frac{(e^{v_m} - 1)}{(G_- e^{v_m} - G_+)} \tag{5.7}$$

with

$$G_\pm = \frac{w_0 e^{w_0 \pm n v_m} \pm n v_m}{w_0 \pm n v_m}. \tag{5.8}$$

Equation 5.7 for pore current i_{sml} accounts for the electrical interactions between the ions and the pore wall (DeBruin and Krassowska, 1999).

Now, assume Q larger pores exist, and i_{lge} is the current through the electropores larger than 1 nm. Then, J_{lge} is the total current density through Q larger pores; r_q being the radius of the q^{th} pore. Hence,

$$J_{\text{lge}} = \frac{1}{A} \sum_{q=1}^{Q} i_{\text{lge}}(r_q) \tag{5.9}$$

where A is the corresponding cell surface area. For these larger pores, the current-voltage relationship assumes that the transmembrane potential V_m occurs across the sum of pore resistance R_p and the series input resistance R_{in} (Smith *et al.*, 2004; Newman, 1966), as follows:

$$i_{\text{lge}}(r) = \frac{V_m}{R_p + R_{\text{in}}}, \tag{5.10}$$

where

$$R_p = \frac{h}{\pi \sigma_{\text{ps}} r_q^2}, \tag{5.11}$$

and

$$R_{\text{in}} = \frac{1}{2\sigma_{\text{ps}} r_q}. \tag{5.12}$$

5.1.2 Formation of pores

Initially pores are assumed to be formed with the minimum-energy radius r_m = 0.76 nm, at a rate given by Equation 2.9, repeated here for completeness,

$$\frac{dN}{dt} = \psi e^{(V_m/V_{\text{ep}})^2} \left(1 - \frac{N}{N_{\text{eq}}(V_m)}\right). \tag{5.13}$$

As described in section 2.4, N is the pore density of the initial small pores formed, ψ is the creation rate coefficient and N_{eq} is the equilibrium pore density

Table 5.1: Geometric, electrical and electroporation parameters.

Symbol	Value	Description
a	15.0 (μm)	cell radius
C_m	10^{-2} (Fm^{-2})	specific membrane capacitance[a]
h	5.0 (nm)	membrane thickness[b]
g_m	1.9 (Sm^{-2})	specific membrane conductance[b]
V_{rest}	–80 (mV)	membrane rest potential[b]
σ_{in}	0.3 (S m^{-1})	intracellular conductivity[c]
σ_{ex}	1.2 (Sm^{-1})	extracellular conductivity[d]
r_*	0.51 (nm)	minimum radius of hydrophilic pores[e]
r_m	0.76 (nm)	minimum energy radius at V_m=0[e]
T	295 (K)	absolute room temperature[b]
n	0.15	relative entrance length of pores[b]
b	2.46	pore creation constant[b]
V_{ep}	258 (mV)	characteristic voltage of electroporation[b]
N_0	1.5×10^9 (m^{-2})	initial pore density[b]
w_0	2.65	energy barrier within pore[b]
ψ	1×10^9 (m^{-2}s^{-1})	creation rate coefficient[b]

[a]Values taken from Smith *et al.* (2004).
[b]Values taken from DeBruin and Krassowska (1999).
[c]Values taken from Kotnik *et al.* (1998).
[d]Values taken from Kotnik and Miklavĉiĉ (2000).
[e]Values taken from Glaser *et al.* (1988).

for a voltage V_m given by

$$N_{\text{eq}}(V_m) = N_0 e^{b(V_m/V_{\text{ep}})^2}. \tag{5.14}$$

Here, N_0 is the initial pore density with no applied electric field, V_{ep} is the characteristic voltage of electroporation and b is the pore creation constant equal to $(r_m/r_*)^2$, where r_* is the minimum radius of hydrophilic pores and r_m the minimum-energy radius (Neu and Krassowska, 2003). All parameter values are as given in Table 5.1.

5.1.3 Evolution of pore radii

The pores that are initially created with minimum-energy radius r_m change in size. This change supports minimizing the energy of the entire lipid bilayer (Weaver and Chizmadzhev, 1996). Evolution of the radius of a pore is governed by Equations 5.15–5.16 (Smith *et al.*, 2004). The lipid bilayer energy depends

Table 5.2: Summary of parameters used in simulation for evolution of pore radii.

Symbol	Value	Description
w_{ed}	1.8×10^{-11} (Jm^{-1})	edge energy[a]
ξ_0	1×10^{-6} (Jm^{-2})	tension of the bilayer without pores[b]
ξ'	2×10^{-2} (Jm^{-2})	tension of hydrocarbon-water interface[a]
$F_{\max}$	0.70×10^{-9} (NV^{-2})	max electric force for $V_m = 1$ V[a]
r_h	0.97×10^{-9} (m)	constant[b]
r_t	0.31×10^{-9} (m)	constant[b]
D_f	5×10^{-14} ($\mathrm{m}^{-2}\mathrm{s}^{-1}$)	diffusion coefficient of the pore radius[b]

[a]Values taken from Smith *et al.* (2004).
[b]Values taken from Krassowska and Filev (2007).

on a number of parameters involving the pore radius, electrostatic interaction between the lipid heads, pore edge energy, membrane tension and the electric force acting on the pore. The lipid bilayer energy is given by Equation 2.5, repeated here for completeness,

$$w_m = \sum_{q=1}^{Q} \left[w_{\mathrm{st}} \left(\frac{r_*}{r_q} \right)^4 + 2\pi w_{\mathrm{ed}} r_q - \pi \xi_{\mathrm{eff}}(A_p) r_q^2 + \int_0^{r_q} F_p(r_q, V_m) dr \right]. \quad (5.15)$$

All the terms in this equation are explained in section 2.3.2. The rate of change of pore radii is given by (Smith *et al.*, 2004)

$$\frac{dr_q}{dt} = -\frac{D_f}{kT} \frac{\partial w_m}{\partial r_q}, \qquad q = 1, 2, ..., Q \quad (5.16)$$

where D_f is the diffusion coefficient of the pore radius, k is Boltzman's constant and T is the absolute temperature. All parameter values used in simulation are as given in Table 5.2.

5.2 Numerical Implementation

The model described above is implemented in MATLAB. The following description of model geometry is illustrated in figure 5.1. Azimuthal symmetry about the axis of the applied electric field is assumed. Extracellular space of $2a$ is simulated about the cell. The intra and extracellular space is discretized using spherical co-ordinates, such that $r_i = i\Delta r$ ($i = 1, \ldots, 51$) and $\theta_j = j\Delta\theta$ ($j = 0, \ldots, 24$), thus $\Delta r = 3a/51$ and $\Delta\theta = \pi/24$. Due to azimuthal symmetry,

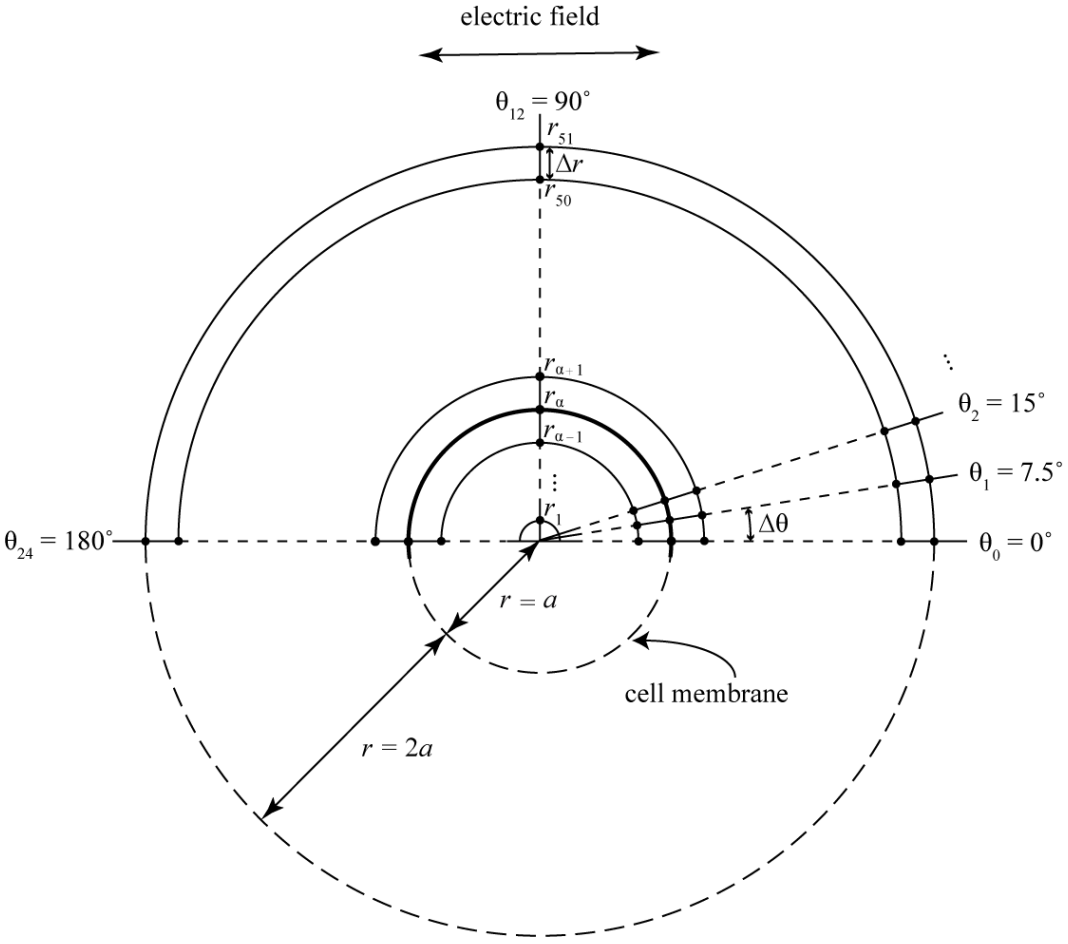

Figure 5.1: Spherical cell model geometry showing the radius and angle discretization used in the numerical model.

discretization in θ results in 25 circular rings on the surface of the cell. Each circular ring is modelled as a single discrete variable. Initially, each circular ring of the cell membrane is assigned a pore density N_0, of 'small pores', each of the pores having identical radius r_m, the minimum energy radius. Each ring also has a transmembrane voltage V_m calculated as given below. The evolution of pore radii is calculated as follows. N_j is the pore density for the j^{th} circular ring on the cell membrane. In accordance with Equations 5.15 and 5.16, the pore radius evolves. An array of radii variables, one element per large pore, keeps track of these larger pore radii. The algorithm computes $\frac{dr_q}{dt}$ for the q^{th} pore at every time-step. If this quantity is positive, small pores expand in size.

If $\frac{dr_q}{dt} > 0$, then for the j^{th} ring of area A_j, an integer number of large pore variables, namely $\text{floor}(N_j A_j)$, are created. The small pore population is decreased by the corresponding number of large pores that are created. To

ensure that each pore is of a distinct value, the large pores are created at random radii normally distributed about the minimum-energy radius, r_m, with an extremely small standard deviation (order of 10^{-20} m, a value small enough and gives consistently repeatable results). An explicit Euler method is used for solving the first order differential equations. A simulation with a time step of 2 ns gives results with good repeatability. For the calculation of transmembrane potential V_m, the potential field $\Phi(r, \theta, t)$ is modelled in and around the cell as follows to calculate Φ_{in} and Φ_{ex}. The finite difference method is used to solve Laplace's equation in a sphere surrounding the cell to give the electric potential. When discretized on r and θ as described above, the Laplace's equation becomes a large set of linear (algebraic) equations relating the values of Φ at the discrete points. The external electric field is used as a boundary condition at $r = 3a$. Current across the membrane is used as a boundary condition at the cell membrane. Laplace's equation written in spherical coordinates with the assumption of azimuthal symmetry can be reduced to,

$$\frac{\partial^2\Phi}{\partial r^2} + \frac{2}{r}\frac{\partial\Phi}{\partial r} + \frac{1}{r^2}\frac{\partial^2\Phi}{\partial\theta^2} + \frac{\cot\theta}{r^2}\frac{\partial\Phi}{\partial\theta} = 0. \tag{5.17}$$

For points on the boundary of this region, at $r = 3a$, Φ is made equal to the value set by the boundary condition. For interior points not on the membrane, the derivatives are approximated by finite differences of the cell, which gives the system of linear equations,

$$\frac{\partial\Phi(r_i,\theta_j)}{\partial r} \approx \frac{\Phi(r_{i+1},\theta_j) - \Phi(r_{i-1},\theta_j)}{2\Delta r} \tag{5.18}$$

$$\frac{\partial^2\Phi(r_i,\theta_j)}{\partial r^2} \approx \frac{\Phi(r_{i+1},\theta_j) - 2\Phi(r_i,\theta_j) + \Phi(r_{i-1},\theta_j)}{\Delta r^2} \tag{5.19}$$

$$\frac{\partial\Phi(r_i,\theta_j)}{\partial\theta} \approx \frac{\Phi(r_i,\theta_{j+1}) - \Phi(r_i,\theta_{j-1})}{2\Delta\theta} \tag{5.20}$$

$$\frac{\partial^2\Phi(r_i,\theta_j)}{\partial\theta^2} \approx \frac{\Phi(r_i,\theta_{j+1}) - 2\Phi(r_i,\theta_j) + \Phi(r_i,\theta_{j-1})}{\Delta\theta^2}. \tag{5.21}$$

Substituting the discrete derivatives above into Laplace's equation (Equa-

tion 5.17) and simplifying gives,

$$\begin{aligned}-2\left[\Delta r^2 + r_i^2\Delta\theta^2\right]\Phi(r_i,\theta_j) + r_i\Delta\theta^2\left[r_i - \Delta r\right]\Phi(r_{i-1},\theta_j)\\ + r_i\Delta\theta^2\left[r_i + \Delta r\right]\Phi(r_{i+1},\theta_j) + \Delta r^2\left[1 - \tfrac{1}{2}\cot(\theta_j)\Delta\theta\right]\Phi(r_i,\theta_{j-1})\\ + \Delta r^2\left[1 + \tfrac{1}{2}\cot(\theta_j)\Delta\theta\right]\Phi(r_i,\theta_{j+1}) = 0. \quad (5.22)\end{aligned}$$

In order to include the boundary condition involving the current at the cell membrane, the radial derivatives of Φ_{in} and Φ_{ex} must be estimated. Assume α is the index such that $r_\alpha = a$ (that is, the radial index that gives the point on the cell membrane, see Figure 5.1). Consider $\frac{\partial}{\partial r}\Phi_{\text{in}}(r,\theta_j)$ which is approximated at $r = a - \frac{1}{2}\Delta r$ and $r = a - \frac{3}{2}\Delta r$ by

$$\left.\frac{\partial\Phi_{\text{in}}}{\partial r}\right|_{(a-\frac{\Delta r}{2},\theta_j)} \approx \frac{\Phi_{\text{in}}(r_\alpha,\theta_j) - \Phi_{\text{in}}(r_{\alpha-1},\theta_j)}{\Delta r} \quad (5.23)$$

$$\text{and} \qquad \left.\frac{\partial\Phi_{\text{in}}}{\partial r}\right|_{(a-\frac{3\Delta r}{2},\theta_j)} \approx \frac{\Phi_{\text{in}}(r_{\alpha-1},\theta_j) - \Phi_{\text{in}}(r_{\alpha-2},\theta_j)}{\Delta r} \quad (5.24)$$

respectively. We can estimate $\frac{\partial}{\partial r}\Phi_{\text{in}}(a,\theta_j)$ by linearly extrapolating from these two points out to the membrane itself, so that

$$\begin{aligned}\left.\frac{\partial\Phi_{\text{in}}}{\partial r}\right|_{(a,\theta_j)} &\approx \left.\frac{\partial\Phi_{\text{in}}}{\partial r}\right|_{(a-\frac{\Delta r}{2},\theta_j)} + \frac{1}{2}\left(\left.\frac{\partial\Phi_{\text{in}}}{\partial r}\right|_{(a-\frac{\Delta r}{2},\theta_j)} - \left.\frac{\partial\Phi_{\text{in}}}{\partial r}\right|_{(a-\frac{3\Delta r}{2},\theta_j)}\right)\\ &\approx \frac{3\Phi_{\text{in}}(r_\alpha,\theta_j) - 4\Phi_{\text{in}}(r_{\alpha-1},\theta_j) + \Phi_{\text{in}}(r_{\alpha-2},\theta_j)}{2\Delta r}. \quad (5.25)\end{aligned}$$

Similarly $\frac{\partial}{\partial r}\Phi_{\text{ex}}(a,\theta)$ is computed at the membrane to give,

$$\left.\frac{\partial\Phi_{\text{ex}}}{\partial r}\right|_{(a,\theta_j)} \approx \frac{-3\Phi_{\text{ex}}(r_\alpha,\theta_j) + 4\Phi_{\text{ex}}(r_{\alpha+1},\theta_j) - \Phi_{\text{ex}}(r_{\alpha+2},\theta_j)}{2\Delta r}. \quad (5.26)$$

All these finite difference equations along with the boundary conditions are expressed as a system of linear equations. They are solved at each time step, using the LU-decomposition method to give the solution of the Laplace equation. The value of transmembrane potential V_m is calculated as $V_m = \Phi_{\text{in}} - \Phi_{\text{ex}}$ at the membrane for each θ_j.

Depending on the parameter values a high number of pores may be formed. The total simulation time depends on the number of large pores created by the applied electric pulse. Strong pulses may create many pores, thus requiring

long simulation times. To speed up computation in the event of such large numbers of pores forming (i.e. $> 10^4$), pores are 'created in groups' of identical pore radius. A single radius variable describes the radius of all pores in a group, thus reducing the number of radius variables required. The size of this group is selected as required, based on the total number of pores and number of variables the computer can handle.

To confirm the accuracy of this model, the model results for the transmembrane potential V_m were initially compared with results obtained by calculating the transmembrane potential V_m using analytical solutions given by Holzapfel *et al.* (1982) as presented in section 2.5.7. Solutions to the numerical model and the analytical model were obtained for applied bipolar sinusoidal pulse electric fields (20 kV/m and 40 kV/m at a frequency of 100 kHz) and (40 kV/m,60 kV/m and 80 kV/m at a frequency of 1 MHz), each amplitude is less than that required for onset of electroporation, as the analytical solution does not model the non-linear effects of membrane electroporation. As seen in Figure 5.2 and Figure 5.3, it is found that the steady state model solution follows the analytical solution very closely. For a sinusoidal excitation electric field, applied at time $t = -\infty$, Equation 2.65 applies. The model assumes the field is applied at $t = 0$ so the transient rise in potential is apparent. This confirms that the developed numerical model is a valid numerical calculation technique.

Figure 5.4 shows the transmembrane potential evolution at four differnet angles when the numerical model developed was provided with the same geometric, electrical and electroporation parameters as given by Krassowska and Filev (2007). This model by Krassowska and Filev (2007) includes provision for non-linear electroporation dynamics including pore radius evolution to a unipolar electric field step. The induced transmembrane potential at $\theta = 0$ as shown in Figure 5.4 is very close to that reported by Krassowska and Filev (2007), indicating that the pore dynamics had been correctly calculated in the model presented here.

Induced transmembrane potential and pore radii evolution to a bipolar electric field is not available in literature. The simulation results of this chapter present these.

The model developed in this chapter can thus simulate the electropermeabilization response including pore radii evolution of a spherical cell exposed to any reasonable (practical) electric field varying arbitrarily in amplitude with

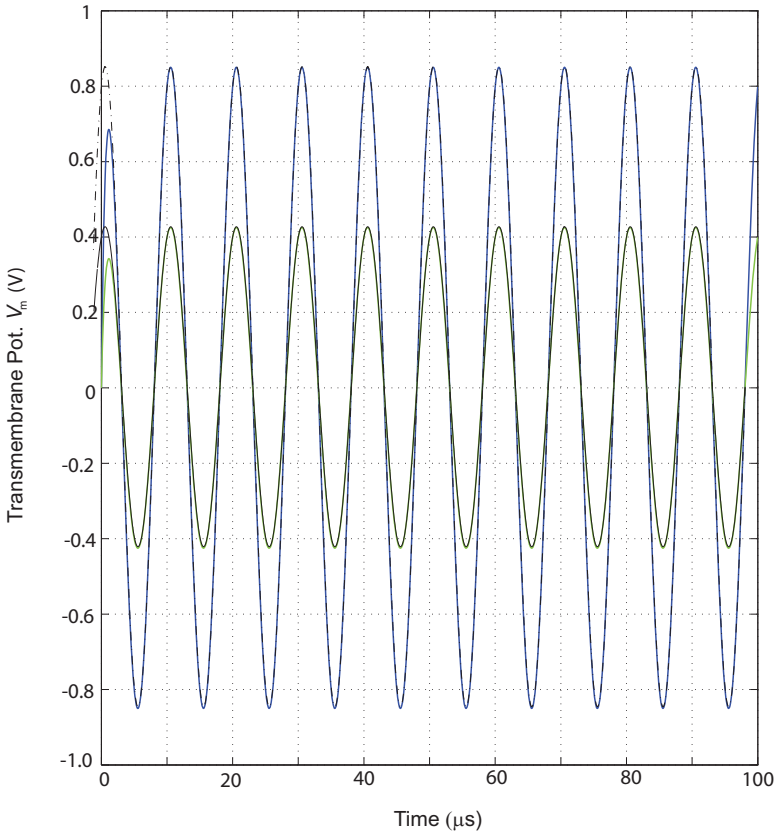

Figure 5.2: Cell response to 100 kHz bipolar sinusoidal pulse: Superposition of the analytical and numerical model solutions for the induced transmembrane potential (a) For peak electric field of 40kV/m: analytical(black dash dot) and numerical model(blue) (b) For peak electric field of 20kV/m: analytical(black solid) and numerical model(green).

time.

5.3 Simulation Results

Details of temporal and spatial evolution of transmembrane potential and pore radius have not been reported in literature as yet. Thus, simulations are carried out for evolution of transmembrane potential and pore radius for two applied electric field pulses (DC and AC) for a single spherical cell. Of particular interest is the cell *charging* time, pore *creation* time and *pore radius evolution* time (Krassowska and Filev, 2007). Cell charging is the time from

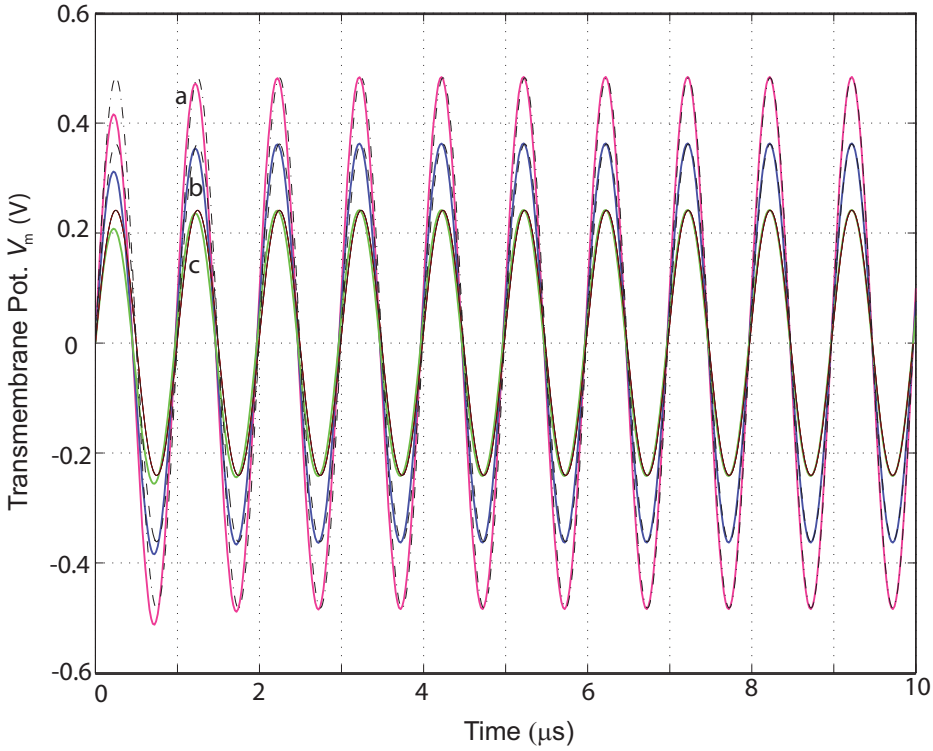

Figure 5.3: Cell response to 1 MHz bipolar sinusoidal pulse: Superposition of the analytical and numerical model solutions for the induced transmembrane potential (a) For peak electric field of 80kV/m: analytical(black dash dot) and numerical model(magenta) (b) For peak electric field of 60kV/m: analytical(black dash) and numerical model(blue) (c) For peak electric field of 40kV/m: analytical(black solid) and numerical model(green).

first application of external electric field to the formation of the first additional pore on the cell membrane. Pore creation phase is time from the first pore to the time of the last pore formed. The remaining time in the simulation is the pore radius evolution time.

5.3.1 Evolution of transmembrane potential, formation of pores, and pore radius evolution

Figures 5.5 to 5.12 show the transmembrane potential and the pore radius evolution around the circumference of a 15 μm radius cell in two individual cases: when a 2 μs, 94.7 kV/m DC electric field pulse is applied, and when a sinusoidal AC (1 MHz), 235 kV/m amplitude electric field pulse is applied for

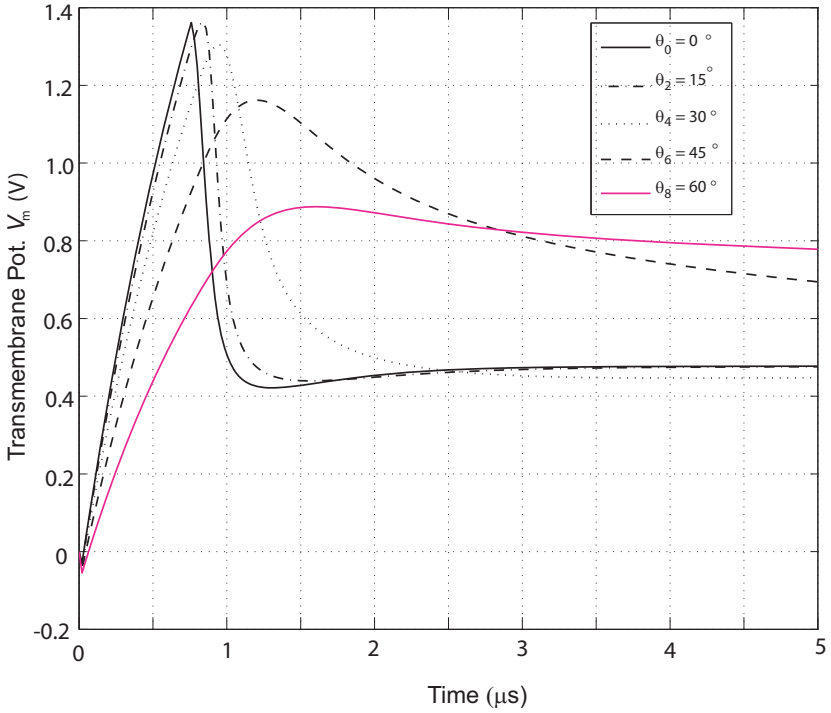

Figure 5.4: Cell response (Transmembrane potential evolution)to a DC pulse: Transmembrane potential evolution at angles 0° to 60° around the cell membrane for a DC applied electric field pulse of 40 kV/m to a cell of 50 μm radius.

the same length of time. The peak amplitude (E_p) of the electric field in each case was set to provide a terminal FPA at the end of 2 μs of approximately 0.015% (presented by Hibino *et al.* (1991) as being within good range of permeabilization). All the other parameters in the model are kept identical for both simulations.

Figures 5.5, 5.6 (DC case), and 5.9, 5.10 (AC case) show the evolution of the transmembrane potential at various positions around the cell. Figures 5.7, 5.8 (DC case) and 5.11, 5.12 (AC case) show the evolution of pores at various positions around the cell. Each black line represents evolution of the first few pores modelled individually since there are only few additional pores formed at the beginning. Each green line represents evolution of a group of pores (groups of 20 pores in these simulations) as many pores begin to be created. The number in the right hand corner of these figures indicate the number of pores eventually formed at the particular polar (θ) position. At the angular positions not shown in these figures ($\theta = 60°$ to $120°$), there are no new pores

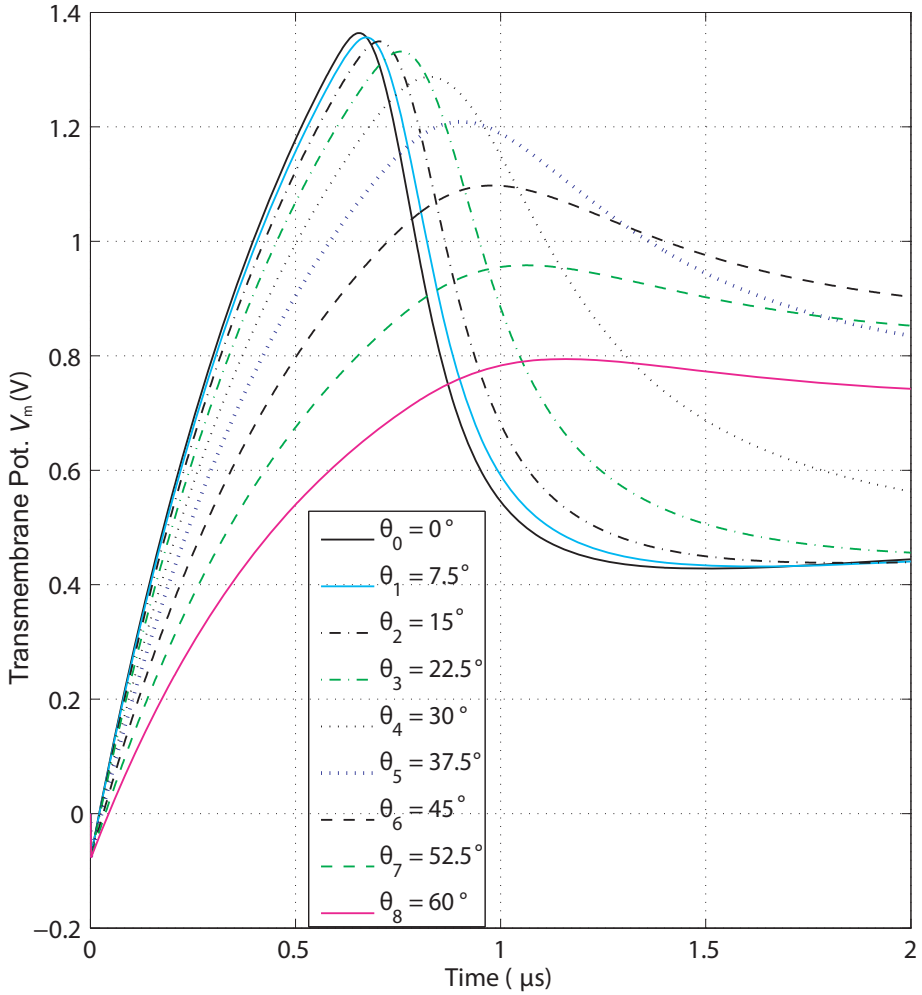

Figure 5.5: Transmembrane potential evolution at angles 0° to 60° around the cell membrane for a DC applied electric field pulse of 94.7 kV/m magnitude.

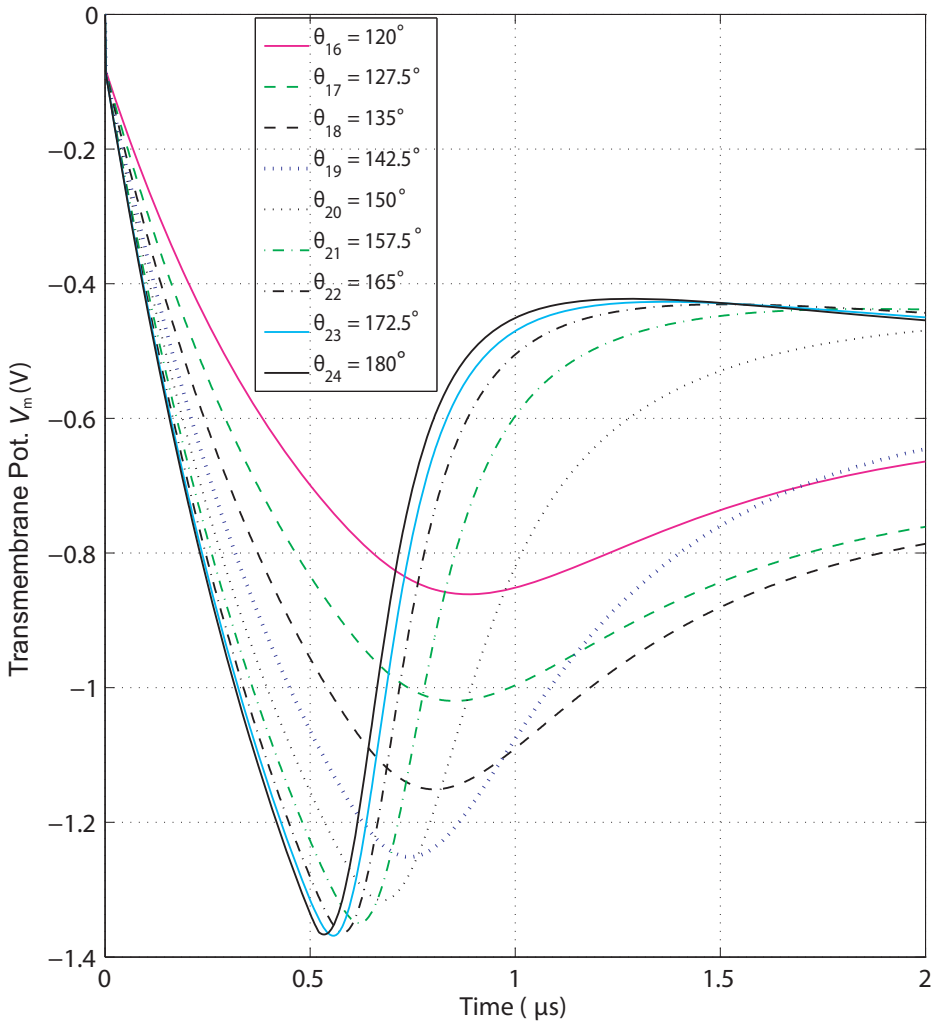

Figure 5.6: Transmembrane potential evolution at angles 120° to 180° around the cell membrane for a DC applied electric field pulse of 94.7 kV/m magnitude.

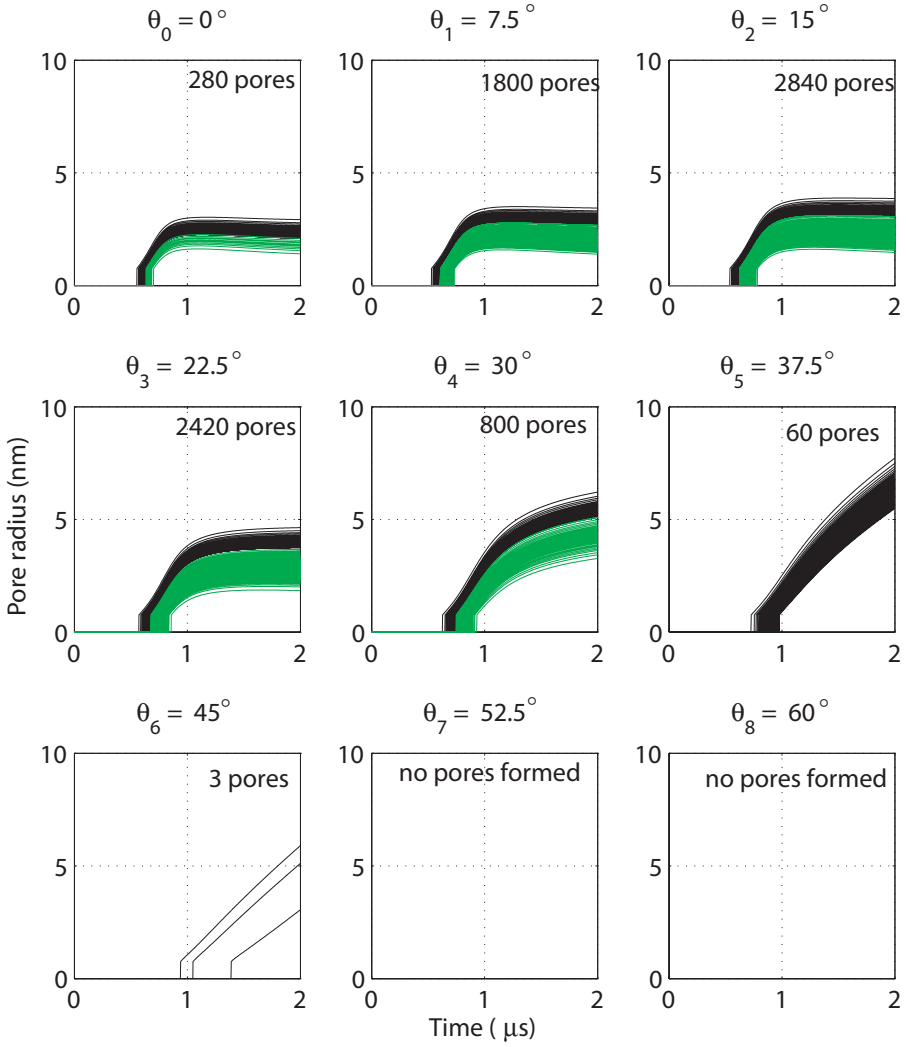

Figure 5.7: Pore radius evolution at angles 0° to 60° around the cell membrane for a DC applied electric field pulse of 94.7 kV/m magnitude. Black lines represent individual pores, green lines represent groups of 20 pores.

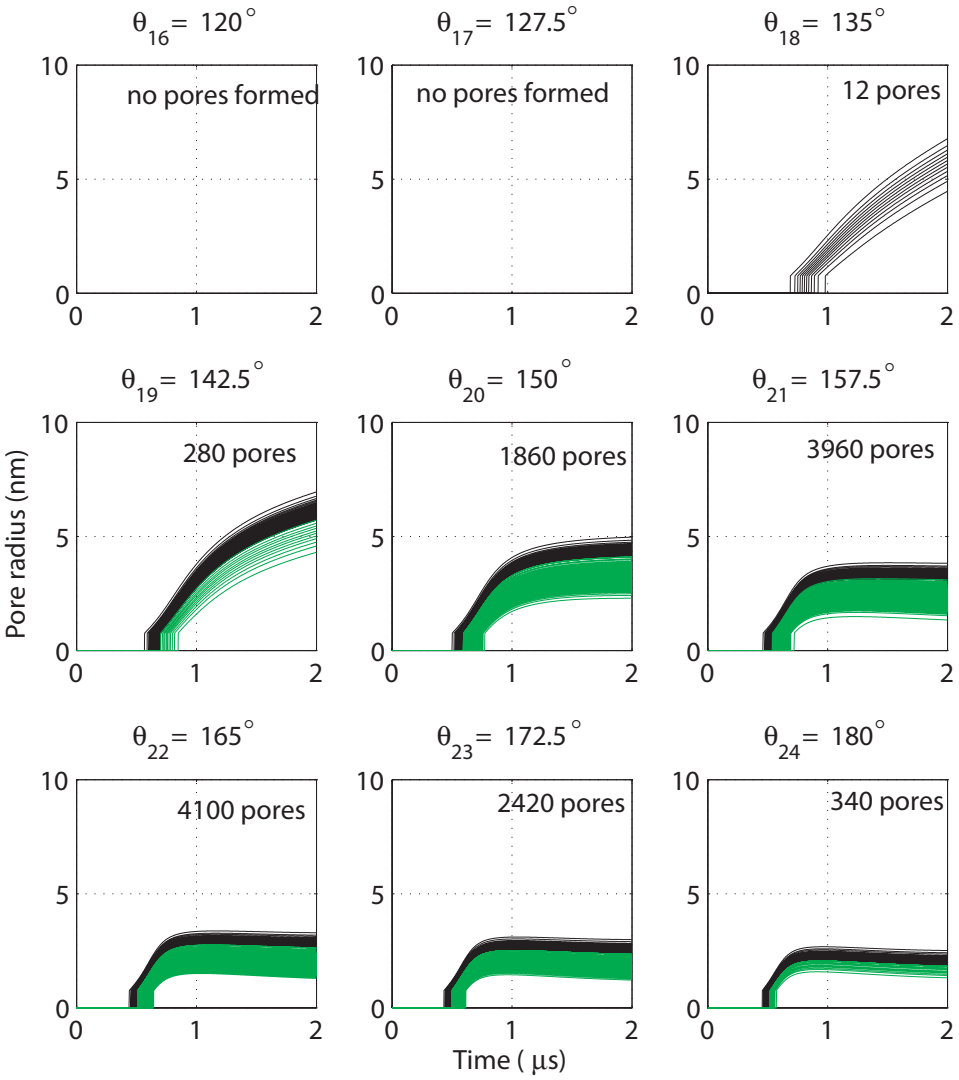

Figure 5.8: Pore radius evolution at angles 120° to 180° around the cell membrane for a DC applied electric field pulse of 94.7 kV/m magnitude. Black lines represent individual pores, green lines represent groups of 20 pores.

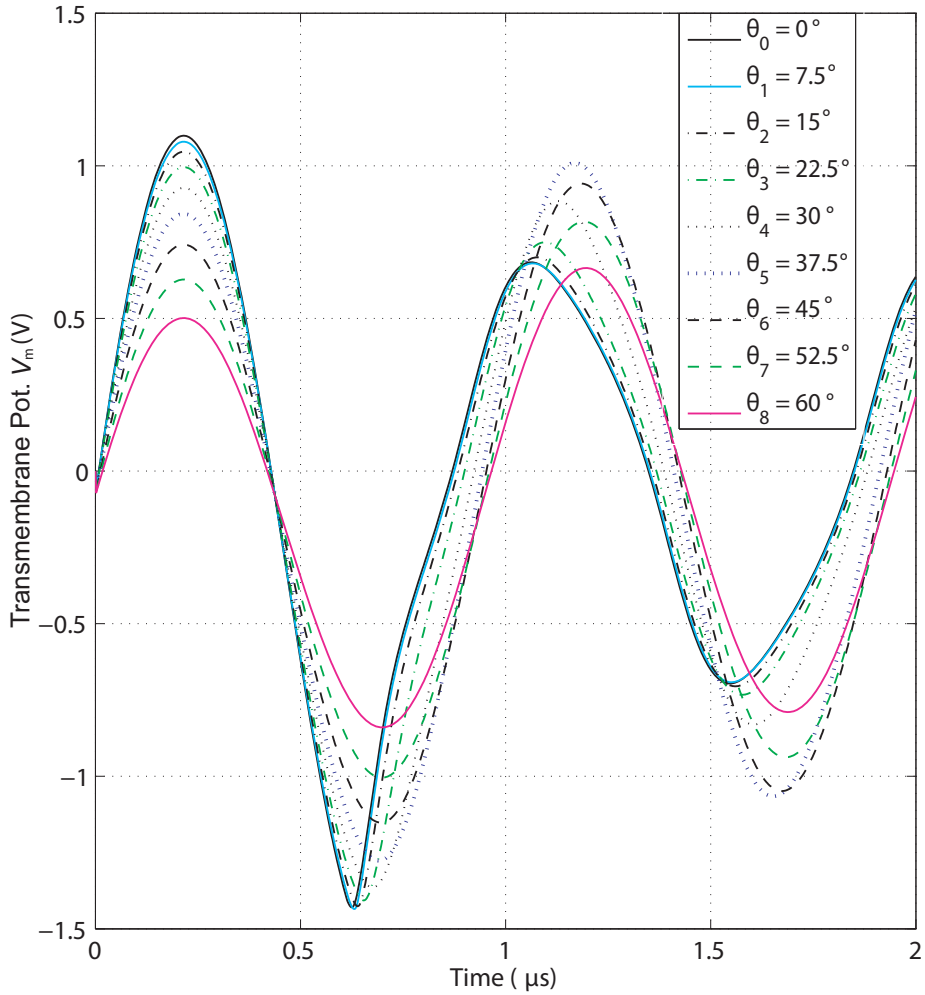

Figure 5.9: Transmembrane potential evolution at angles 0° to 60° around the cell membrane for a two-cycle 1 MHz sinusoidal bipolar applied electric field pulse with 235 kV/m peak amplitude.

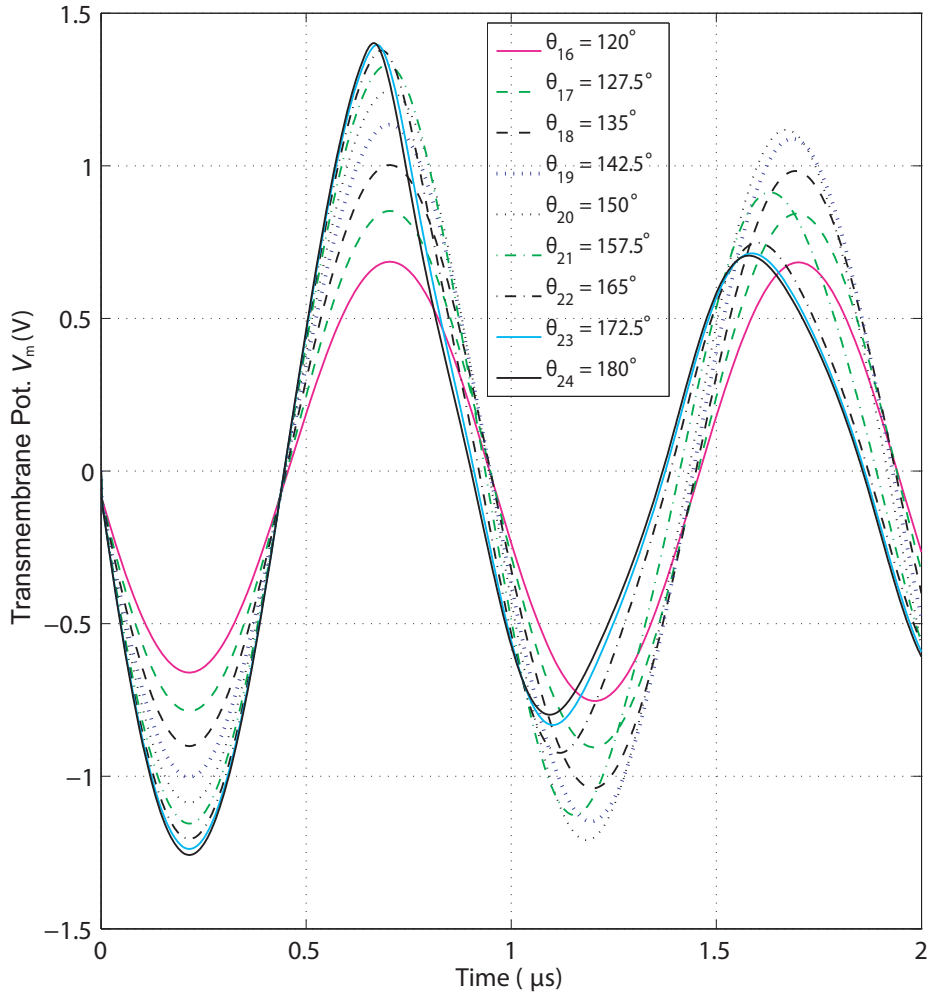

Figure 5.10: Transmembrane potential evolution at angles 120° to 180° around the cell membrane for a two-cycle 1 MHz sinusoidal bipolar applied electric field pulse with 235 kV/m peak amplitude.

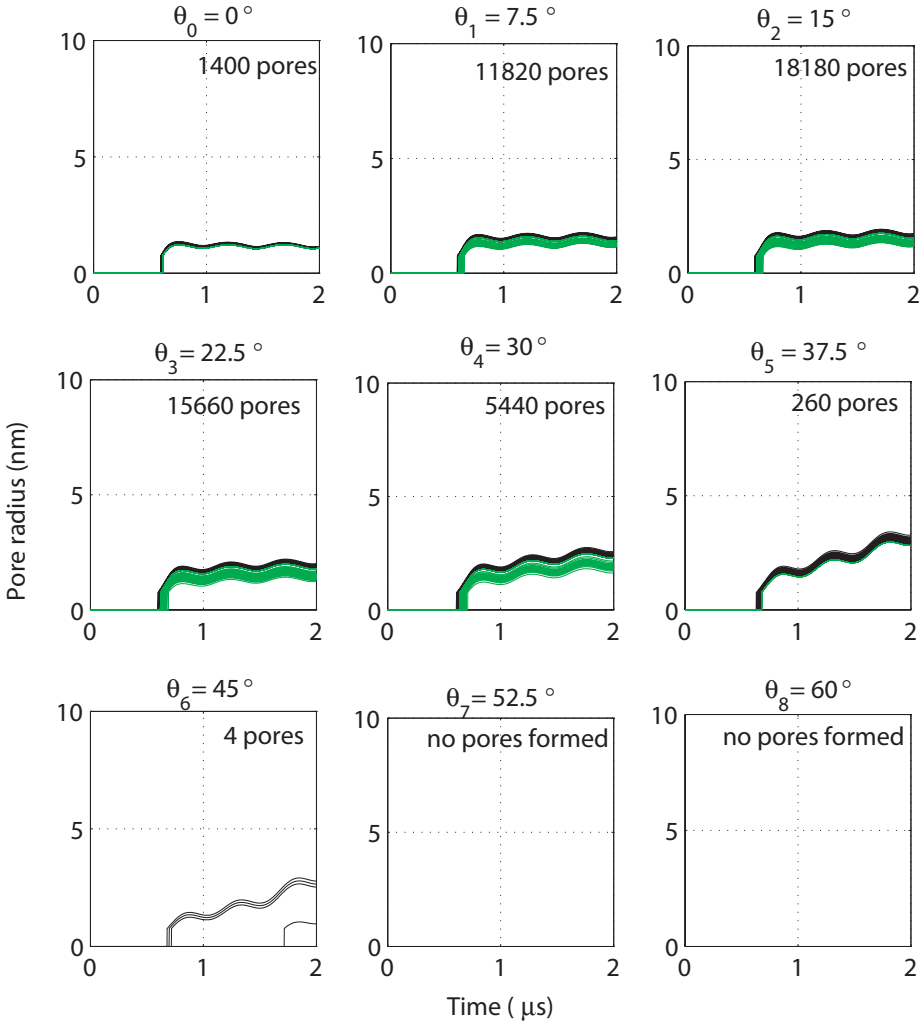

Figure 5.11: Pore radius evolution at angles 0° to 60° around the cell membrane for a two-cycle 1 MHz sinusoidal bipolar applied electric field pulse with 235 kV/m peak amplitude. Black lines represent individual pores, green lines represent groups of 20 pores.

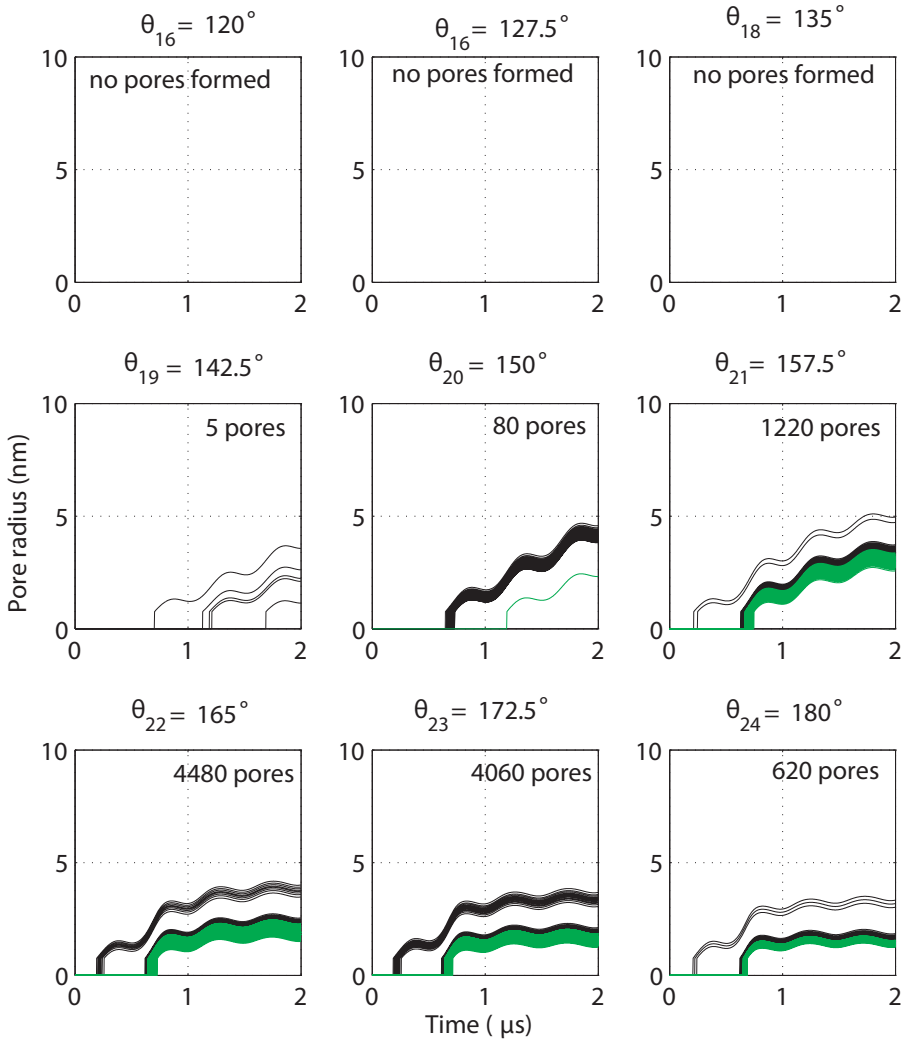

Figure 5.12: Pore radius evolution at polar angles 120° to 180° around the cell membrane for a two-cycle 1 MHz sinusoidal bipolar applied electric field pulse with 235 kV/m peak amplitude. Black lines represent individual pores, green lines represent groups of 20 pores.

created.

In the DC case, the time duration of 2 μs is chosen for the simulation so that the fine temporal features of the relationships between the pore formation, pore radii evolution and transmembrane potential evolution can be seen. As observed in figures 5.7 and 5.8 the first pore is formed on position θ_{24} (at 0.42 μs) and the last pore for this particular pulse protocol is formed at position θ_6 (at 1.3 μs). This constitutes the pore creation phase (0.42 μs–1.3 μs). The initial period when no pores are formed (0–0.42 μs) is the charging of the cell membrane. Once transmembrane potential reaches a magnitude of about 1 V, pores start to form and expand/evolve. These time ranges for charging and pore creation are specific to parameters (such as internal and external conductivities)chosen in this simulation, and will vary with changes in the parameters.

In the case when an AC field is applied, as seen in figures 5.11 and 5.12, additional pores may form at the subsequent peak of transmembrane potential. This happens if the transmembrane potential at the particular position is beyond the threshold value. This increases the pore creation time as compared with DC pulses.

5.3.2 Frequency dependence of electropermeabilization in a heterogeneous population of cell radii/sizes.

Owing to the variable nature of biological growth dynamics, all electroporation applications treat cells of a range of sizes. Although this range may only be in the order of a few percent, some applications may have ranges exceeding 200 percent (Foster and Schwan, 1996). As such, whatever the application, there may be a substantial benefit of being able to normalize the degree of electropermeabilization (considered equivalent to the fractional pore area) with respect to cell radius/size. Earlier passive and dynamic modelling of bipolar electric field induced transmembrane potential, has indicated that as the frequency of a constant amplitude applied electric field is increased, transmembrane potential reduces and becomes less dependent on cell radius (Grosse and Schwan, 1992; Talele and Gaynor, 2007). In order to achieve a transmembrane potential high enough for EP, the electric field amplitude must be increased at higher frequencies. To determine whether this effect translates to dynamic electroporation modelling that includes pore radii variability, two higher frequency

electric field pulses of 100 kHz and 1 MHz were used for electropermeabilization simulation. Two substantially (yet realistically) different cell radii of 15 μm and 7.5 μm were considered.

Figures 5.13 and 5.14 show the fractional pore area for 7.5 μm and 15 μm radius cells exposed to a two-cycle sine wave electric field pulse of 100 kHz and 1 MHz respectively. The peak amplitude of the electric field, E_p was set to provide an average terminal fractional pore area (for the two cell radii) of approximately 0.015% (presented by Hibino *et al.* (1991) as being a good level of permeabilization) at a σ_{ex} of 0.2 S/m. It is seen from figures 5.13 and 5.14 that the relative difference in FPA between the two cell sizes at extracellular conductivity of 0.2 S/m is 1.1 for 100 kHz and 0.6 for 1 MHz. This relative difference increases as σ_{ex} increases to a limit of approximately 1. For a physiological medium with $\sigma_{\text{ex}} = 1.2$ S/m (as found in *in vivo* EP applications), this relative difference is 0.93 for the 1 MHz two-cycle sine wave electric field pulse and 1.0 for the 100 kHz electric field pulse when aiming at a mean fractional pore area of 0.015%.

5.4 Discussion

5.4.1 Evolution of transmembrane potential and pore radius

For a DC pulse protocol, it is seen that during the charging phase, transmembrane potential V_m has a larger magnitude at hyperpolarized pole (position $\theta = 180°$) as compared to the hypopolarized pole (position $\theta = 0°$) due to the negative membrane rest potential of -80 mV. As an effect of this, the poration on the hyperpolarized side occurs earlier than the hypopolarized side, in agreement with reported experimental results in the literature (Hibino *et al.*, 1993). The model also predicts that the DC pulse creates more but smaller pores on the hyperpolarized hemisphere (13406 pores) as against fewer and larger pores on the hypopolarized hemisphere (8282 pores). The effect of higher pore number dominates and is well reflected on the value of fractional pore area as 0.016% against 0.013% for the two hemispheres, at the end of 2 μs. These results are in agreement with experimental results (Hibino *et al.*, 1993) and modelling results (Krassowska and Filev, 2007) in the literature.

The number of pores at a particular position of the cell not only depends

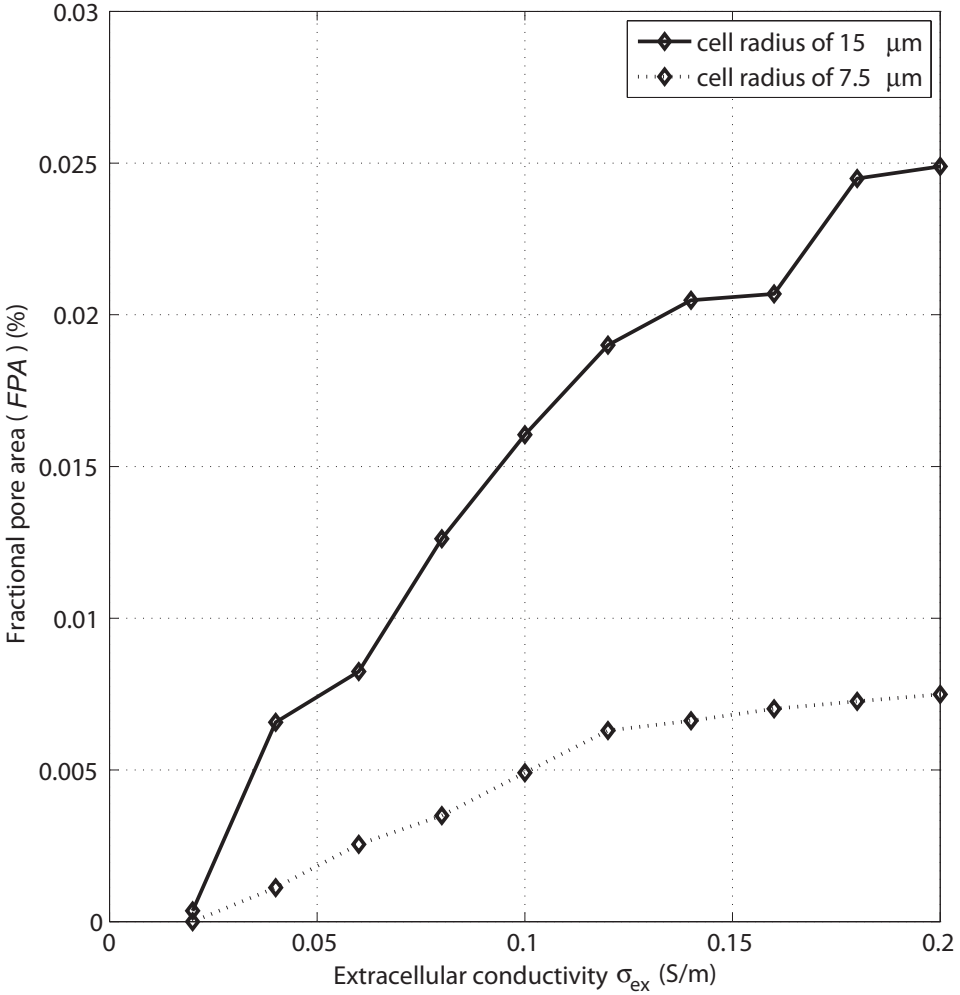

Figure 5.13: Fractional pore area versus extracellular conductivity for 7.5 μm, and 15 μm cell radius exposed to a two-cycle sinusoidal bipolar applied electric field pulse of 130 kV/m peak magnitude at 100 kHz.

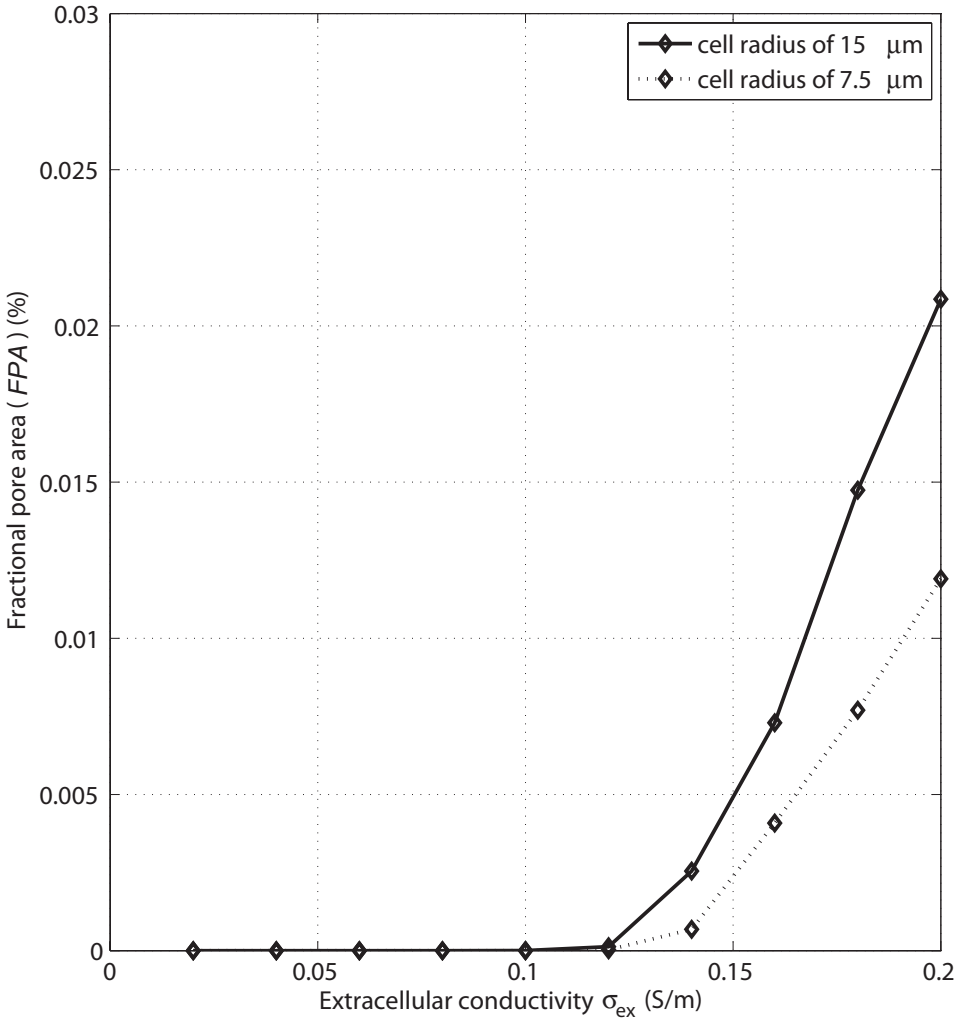

Figure 5.14: Fractional pore area versus extracellular conductivity for 7.5 μm, and 15 μm cell radius exposed to a two-cycle sinusoidal bipolar applied electric field pulse of 350 kV/m peak magnitude at 1 MHz

on the transmembrane potential, but also on the condition of the remaining cell membrane. This may be the plausible explanation of why more pores are formed at $\theta = 7.5°$ and $\theta = 15°$ as well as at $\theta = 172.5°$ and $\theta = 165°$ as compared to position $\theta = 0°$ and $\theta = 180°$ respectively. The pores near to the non-polar regions tend to be larger in agreement with the modelling results of Krassowska and Filev (2007).

5.4.2 Effect of field strength and frequency on pore dynamics

An important aim of this study was to explore the effects of bipolar pulse protocols and its parameters on electroporation. In general the peak transmembrane potential on the cell membrane increases with increasing unipolar field strength up to a maximum value of around 1.43 V. Transmembrane potential does not significantly exceed this limit because the net amount of electroporation (which is measured by the final fractional pore area) depends sensitively on transmembrane potential. The transmembrane potential increases initially by capacitive charging. New pores in the membrane form and expand/evolve due to electroporation and allow current to flow. This prevents further increase of the transmembrane potential.

Fractional pore area is also found to increase with increasing electric field magnitude. This is because additional pores form until their total area allows sufficient current to flow to stop the increase of transmembrane potential. We also note that the radii of the largest pores are smaller for stronger applied fields. The fractional pore area increases in spite of this because, for strong fields, many smaller pores (radii in the range 1–5 nm) are formed.

Similar trends are seen with bipolar (AC) pulse protocols at a fixed frequency. However, to produce a given fractional pore area value, higher bipolar field strengths must be used compared with unipolar (DC) field strengths for the same overall pulse duration. More succinctly then, for a fixed electric field amplitude, fractional pore area decreases with increasing frequency, as does the total number of pores. This is to be expected because electroporation can only occur when the field strength exceeds a certain threshold. For bipolar (AC) fields at higher frequencies, the time intervals during which electroporation can occur are clearly shorter.

For unipolar (DC) electric field pulses, the pores formed in electroporation

have widely distributed radii (around 1–8 nm), with significant contributions to the total fractional pore area from pores with radii in different size-ranges. This is not the case for AC bipolar fields. For example, at 1 MHz, nearly all of the total fractional pore area is contributed by pores with radii 1–3.4 nm. This may be the reason why AC fields are reported to be gentler in experimental research findings on electroporation (Chang and Reese, 1990; Tekle *et al.*, 1991; Chen *et al.*, 2008).

It is evident from figures 5.13 and 5.14 that, considering 0.015% fractional pore area as the desirable fractional pore area, two-cycles of 1 MHz sinusoidal bipolar electric field reduces the relative difference in fractional pore area between the two cell sizes compared to two-cycles of a 100 kHz bipolar electric field. However, a significantly higher amplitude is required to create the same level of average fractional pore area. Lower values of extracellular conductivity are warranted for better normalization of the degree of electroporation (fractional pore area), as higher values of extracellular conductivity increase the relative difference in fractional pore area for cells of different radii/size. Since typical *in vivo* applications have an extracellular conductivity equal to the physiological conductivity in the region of 1.2 S/m (Kotnik *et al.*, 1998), it is unlikely that normalization of the degree of electroporation can be achieved in these applications through utilization of higher frequency AC pulses. Typically, at higher extracellular conductivity, the required magnitude of electric field also reduces.

5.5 Conclusion

The model is capable of simulating transmembrane potential and pore radii formation/evolution when a cell is exposed to any form of electric field. The results show that the pore radii tend to be more normalized when a bipolar sinusoidal AC field pulse is used as compared to a DC field pulse of the same duration. As a result, larger pore radii formation is more likely when a DC unipolar field pulse is used. The results also show that better normalization of the degree of electroporation, measured as fractional pore area FPA, especially at lower values of extracellular conductivity, can be achieved with use of higher frequency (1 MHz) bipolar electric field as compared to 100 kHz. Thus, choice of the electric field parameters (magnitude and frequency) and the extracellular conductivity for optimum electropermeabilization is a trade

off between parameters like the desired pore radii values, and normalization of fractional pore area between the required cell radii/size.

5.5.1 Limitations of the model

The model described in this chapter is capable of simulating transmembrane potential and pore radii formation/evolution when a cell is exposed to any form of electric field, but only for single spherical cell. The model does not consider media permittivity parameter. Including other shapes of cells and the media permittivity would require substantial change to the model. The effect of other physical and chemical properties of electropermeabilization system are not simulated. Although the electrical parameters have the greatest effect on electroporation dynamics, the other properties (temperature changes due to heating of cells, swelling or shrinking of cells, effect of cholesterol or some injected drugs on cell membrane properties etc) may need to be included at some stage in an ultimate model of electroporation. Such inclusion of additional parameters may provide additional information.

Chapter 6

Conclusions

The work of this thesis has developed two models for simulating the dynamic response of electroporation and shown that it is possible and preferential to use bipolar electric field pulses for electroporation applications. The first model assumes all identical small pores and is capable of simulating transmembrane potential and pore density temporally and spatially while the second model is capable of simulating transmembrane potential and pore radii formation/evolution, temporally and spatially when a cell is exposed to any form of electric field. The simulations help define and highlight the advantages of using the bipolar electric field pulses for electroporation.

In Chapter 3 a new method was presented to numerically model electroporation dynamics for a single spherical cell. This numerical model is based on a piecewise time domain step response method incorporating pore formation dynamics. Simulation results from this numerical model support the conclusion that bipolar pulses can be used as an effective alternative to conventional unipolar pulses in the applications of electropermeabilization. Simulations describe the dynamic electro-physical membrane behaviour of a single spherical cell exposed to arbitrary electric fields. With reasonably accurate real system parameters and assumption that the cells can be considered in isolation, the model is a useful tool for prediction of transmembrane potential and pore density when a cell is exposed to any form of electric field. An informed variation of the parameters could then be made to maximize the efficacy for a specific application.

Chapter 3 has demonstrated predicting the effect of the type of electric field used, on transmembrane potential, pore density and the asymmetry between

the two poles, nevertheless there are other significant physical and electrical parameters that can affect electroporation. One very important physical parameter that can be varied for optimal electroporation, is the extracellular conductivity. Also, the effect of frequency of the applied electric field needed to be found out. Thus, more simulations were done and results presented in Chapter 4. These results helped comment on the effect of extracellular conductivity and applied electric field parameters for suitable use in applications.

Chapter 4 presents results that indicate that the efficiency of electroporation related applications can be significantly improved through normalization of the degree of electroporation, by appropriately adjusting the parameters of the applied bipolar electric field pulse and the conductivity of the external medium.

The results also show that it may be very difficult for cells of substantially different sizes to be close to uniformly electroporated if surrounded by media with a conductivity higher than around 5×10^{-2} S/m for 100 kHz pulses, or 0.2 S/m for 1 MHz pulses. Since typical *in vivo* applications have an external conductivity equal to the physiological conductivity in the region of 1.2 S/m, it is unlikely that normalization of the degree of electroporation can be achieved in these applications solely by increasing the bipolar pulse frequency.

It is apparent that the relative difference of pore density between the two cell sizes investigated is consistently lower for the sine wave electric field compared to the square wave electric field, even though the square wave electric field amplitude is always lower for an equivalent pore density.

The size of pores is an important characteristic of pore formation during electroporation, especially when the cell is exposed to an electric field for longer durations. Researchers have attempted to use a variety of electric field strengths or pulse trains for variety of time durations, and found different results. Since the result could depend on a number of parameters involved in the experiment, it becomes extremely difficult to predict the end result of electroporation. To solve this problem, a model that simulates spatial and temporal aspects of pore radius as an effect of any given form of applied electric field (including unipolar or bipolar), and other important electroporation system parameters, is developed and presented in Chapter 5. Once the elctroporation parameters are input to the model, this model is capable of simulating the pore size distribution spatially and temporally. Todate, this has not been addressed in the literature. Thus the thesis adds to better understanding of

electroporation process.

The pore radii tend to be more normalized when a bipolar sinusoidal AC field pulse is used as compared to a unipolar DC field pulse of the same duration. Thus, larger pore radii formation is likelier when a unipolar DC field pulse is used.

Once again, considering 0.015% as the desired fractional pore area, simulations have shown that two-cycles of 1 MHz sinusoidal bipolar electric field reduces the relative difference in fractional pore area between the two cell sizes compared to two-cycles of a 100 kHz bipolar electric field. However, a significantly higher amplitude is required to create the same level of fractional pore area. Lower values of extracellular conductivity (σ_{ex}) are warranted for better normalization of the degree of electroporation (fractional pore area), as higher values of extracellular conductivity increase the relative difference in the fractional pore area for cells of different radii/size. Typically, at higher extracellular conductivity, the required magnitude of electric field also reduces. Since typical *in vivo* applications have an external conductivity equal to the physiological conductivity in the region of 1.2 S/m, it is unlikely that normalization of the degree of electroporation can be achieved in these applications solely through utilization of higher frequency AC pulses. Another way of attempting to control fractional pore area FPA is using a train of pulses. The magnitude, duration and frequency of each of the pulse in the train, as well as the break time between two pulses can be altered suitably to control fractional pore area. It could also be possible that pulse train dynamics could improve normalization of fractional pore area with respect to the required cell radii/size, but this is yet to be confirmed.

6.1 Future Work

Typically, cells exist in a multicellular environment,in which the electric field is affected by the neighbouring cells. It is also known that cells can move when exposed to AC field (via dielectrophoresis) (Schwan, 1989). The organelles inside each cell can also affect electropermeabilization (Schwan, 1989; Beebe and Schoenbach, 2005). There is a mention of surface conductivity around the cell (Zimmermann and Neil, 1996), which could affect electropermeabilization. When cells are placed in low conductivity solution, they swell, and this could alter cell membrane tension, which affects electropermeabilization (Lee *et al.*,

2002). Electric energy may manifest in terms of heat and may affect electroporation (Lee, 1992). All these parameters need to be included in modelling so as to improve prediction of electroporation results. This information would be be useful for physiological experts while applying electroporation thus to help achieve optimum efficiencies in electroporation based applications.

Depending on the application for which the electroporation is being used, there may be a particular necessity of a resultant output, to list a few important ones: pore density, fractional pore area, number of large pores and size of the large pores. These parameters although cannot be practically measured as yet, new nanotechonlogy instrumentation may be useful in the area. Until then these will have to be inferred from the uptake of particular molecules, using fluorescence methods, measuring conductivity of membrane an so on. Based on the invariable physiological and electrical parameters there could be an ideal set of variable parameters to be chosen. The invariable set of physiological parameters could be the cell shape, cell radii, tissue structure, intracellular conductivity, cell shape, membrane thickness and its other properties, dielectric properties of the cell and its dependence of frequency. Accurate knowledge of these parameters and their inclusion in the model will accelerate research in this field. The variable physiological parameter is the extracellular conductivity that seems to affect cell membrane tension and thus the electroporation. Regarding the electrical parameters, physical apparatus must be built that can produce the appropriate pulse shapes, frequency and magnitude, so that biological experiments can be carried out. Commercial apparatus for electroporation from several sources is available, but none offer appropriate bipolar electric field pulses, probably due to the technical challenges in the design. Such apparatus that can deliver high voltage (up to several thousand volts), high frequency (up to several million hertz) bipolar pulse needs to be built.

Ability to predict accurately the transmembrane potential may reveal some other effects of electromagnetic field hazards to living beings (Zimmermann and Neil, 1996).

References

Abidor, I. G., V. B. Arakelyan, L. V. Chernomordik, Y. A. Chizmadzhev, V. F. Pastushenko, and M. R. Tarasevich. Electric breakdown of bilayer membranes: I. The main experimental facts and their qualitative discussion. *Bioelectrochemistry and Bioenergetics*, **6**, pp. 37–52 (1979).

Ausubel, F. M., R. Brent, R. E. Kingston, D. D. Moore, J. Seidman, J. A. Smith, and K. Struhl. *Current Protocols in Molecular Biology*. Wiley, New York (1990).

Barnett, A. and J. C. Weaver. Electroporation: A unified, quantitative theory of reversible electrical breakdown and mechanical rupture in artificial planar bilayer membranes. *Bioelectrochemistry and Bioenergetics*, **25**, pp. 163–182 (1991).

Beebe, S. J. and K. H. Schoenbach. Nanosecond pulsed electric fields: A new stimulus to activate intracellular signaling. *Journal of Biomedicine and Biotechnology*, pp. 297–300 (2005).

Benachir, T. and M. Lafleur. Osmotic and pH transmembrane gradients control the lytic power of melittin. *Biophysical Journal*, **70**, pp. 831–840 (1996).

Bertino, J. R. Transfer of drug resistance genes into hematopoietic stem cells for marrow protection. *The Oncologist*, **13**, pp. 1036–1042 (2008).

Budak-Alpdogan, T., D. Banerjee, and J. R. Bertino. Hematopoietic stem cell gene therapy with drug resistance genes: An update. *Cancer Gene Therapy*, **12**, pp. 849–863 (2005).

Cemaẑar, M., D. Miklavĉiĉ, and G. Serŝa. Intrinsic sensitivity of tumor cells to bleomycin as an indicator of tumor response to electrochemotherapy. *Japanese Journal of Cancer Research*, **89**, pp. 328–333 (1998).

Chang, D. C., B. M. Chassy, J. A. Saunders, and A. E. Sowers, editors. *Guide to Electroporation and Electrofusion*. Academic Press, San Diego, CA (1992a).

Chang, D. C., J. R. Hunt, Q. Zheng, and P. Q. Gao. Electroporation and electrofusion using pulsed radio-frequency electric field. In: *Guide to Electroporation and Electrofusion*, edited by D. C. Chang, B. M. Chassy, J. A. . Saunders, and A. E. Sowers, chapter 19, pp. 303–326. Academic Press, San Diego, CA (1992b).

Chang, D. C. and T. S. Reese. Changes in membrane structure induced by electroporation as revealed by rapid-freezing electron microscopy. *Biophysical Journal*, **58**, pp. 1–12 (1990).

Chen, C., J. A. Evans, M. P. Robinson, S. W. Smye, and P. O"Toole. Measurement of efficiency of cell membrane electroporation using pulsed ac fields. *Physics in Medicine and Biology*, **53**, pp. 4747–4757 (2008).

Chen, W. and R. C. Lee. Electromediated permeabilization of frog skeletal muscle cell membrane: Effect of voltage-gated ion channels. *Bioelectrochemistry and Bioenergetics*, **34**, pp. 157–167 (1994).

Chernomordik, L. V., S. I. Sukharev, I. G. Abidor, and Y. A. Chizmadzhev. Breakdown of lipid bilayer membranesin an electric field. *Biochim Biophys Acta*, **736**, pp. 203–213 (1983).

Chernomordik, L. V., S. I. Sukharev, S. V. Popov, V. F. Pastushenko, A. V. Sokirko, I. G. Abidor, and Y. A. Chizmadzhev. The electrical breakdown of cell and lipid membranes: The similarity of phenomenologies. *Biochim Biophys Acta*, **902**, pp. 360–373 (1987).

Cole, K. S. *Membranes ions and impulses*. University of California Press, Berkeley, CA (1972).

Curtis, H. and N. S. Barnes. *Biology, fourth edition*. Worth Pulishing, New York (1983).

DeBruin, K. A. and W. Krassowska. Modeling electroporation in a single cell. I. Effects of field strength and rest potential. *Biophysical Journal*, **77**, pp. 1213–1224 (1999).

Dev, S. B., D. P. Widera, and G. A. Hofmann. Medical applications of electroporation. *IEEE Transactions on Plasma Science*, **28**, pp. 206–223 (2000).

Dimitrov, D. S. Electroporation and electrofusion of membranes. In: *Handbook of Physics of Biological Systems*, edited by R. Lipowsky and E. Sackmann, volume 1, pp. 854–895. Elsevier (1995).

Djuzenova, C. S., U. Zimmermann, H. Frank, V. L. Sukhorukov, E. Richter, and G. Fuhr. Effect of medium conductivity and composition on the uptake of propidium iodide into electropermeabilized myeloma cells. *Biochim Biophys Acta*, **1284**, pp. 143–152 (1996).

Ellappan, P. and R. Sundararajan. A simulation study of the electrical model of a biological cell. *Journal of Electrostatics*, **63**, pp. 297–307 (2005).

Foster, K. R. and H. P. Schwan. Dielectric properties of tissues. In: *Handbook of biological effects of electromagnetic fields*, edited by C. Polk and E. Postow, chapter 1, pp. 25–97. CRC Press, Boca Raton, Florida, second edition (1996).

Freeman, S. A., M. A. Wang, and J. C. Weaver. Theory of electroporation of planar bilayer membranes: Predictions of the aqueous area, change in capacitance, and pore-pore separation. *Biophysical Journal*, **67**, pp. 42–56 (1994).

Gabriel, B. and J. Teissié. Direct observation in the millisecond time range of fluorescent molecule asymmetrical interaction with the electropermeabilized cell membrane. *Biophysics Journal*, **73**, pp. 2630–2637 (1997).

Garcia, A. L. *Numerical methods for Physics*. Prentice Hall, New Jersey (1994).

Gaynor, P., D. N. Wells, and B. Oback. Couplet alignment and improved electrofusion by dielectrophoresis for a zona-free high-throughput cloned embryo production system. *Medical and Biological Engineering and Computing*, **43**, pp. 150–154 (2005).

Gaynor, P. T. and P. S. Bodger. Electrofusion processes: Theoretical evaluation of high electric field effects on cellular transmembrane potentials. *IEE Proceedings in Science Measurement and Technology*, **142**, pp. 176–182 (1995).

Gehl, J. and L. M. Mir. Determination of optimal parameters for *in vivo* gene transfer by electroporation, using a rapid *in vivo* test for cell permeabilization. *Biochemical and Biophysical Research Communications*, **261**, pp. 377–380 (1999).

Glaser, R. W., S. L. Leikin, L. V. Chernomordik, V. F. Pastushenko, , and A. I. Sokirko. Reversible electrical breakdown of lipid bilayers: Formation and evolution of pores. *Biochim Biophys Acta*, **940**, p. 275287 (1988).

Glass, L. F., N. A. Fenske, M. Jaroszeski, R. Perrott, D. T. Harvey, D. S. Reintgen, and R. Heller. Bleomycin-mediated electrochemotherapy of basal cell carcinoma. *Journal of the American Academy of Dermatology*, **34**, pp. 82–86 (1996).

Golzio, M., M. P. Mora, C. Raynaud, C. Delteil, J. Teissié, and M. P. Rols. Control by osmotic pressure of voltage-induced permeabilization and gene transfer in mammalian cells. *Biophysical Journal*, **74**, pp. 3015–3022 (1998).

Gothelf, A., L. M. Mir, and J. Gehl. Electrochemotherapy: Results of cancer treatment using enhanced delivery of bleomycin by electroporation. *Cancer Treatment Reviews*, pp. 1–17 (2003).

Gowrishankar, T. R. and J. C. Weaver. An approach to electrical modeling of single and multiple cells. *Proceedings of the National Academy of Sciences*, **100**, pp. 3203–3208 (2003).

Graziadei, L., P. Burfeind, and D. Bar-Sagi. Introduction of unlabeled proteins into living cells by electroporation and isolation of viable protein-loaded cells using dextran-fluorescein isothiocyanate as a marker for protein uptake. *Analytical Biochemistry*, **194**, pp. 198–203 (1991).

Griese, T., S. Kakorin, and E. Neumann. Conductometric and electrooptic relaxation spectrometry of lipid vesicle electroporation. *Physical Chemistry Chemical Physics*, **4**, pp. 1217–1227 (2002).

Grimnes, S. and O. G. Martinsen. *Bioimpedance and Bioelectricity basics*. Academic Press, San Diego, NY (2000).

Grosse, C. and H. P. Schwan. Cellular membrane potentials induced by alternating fields. *Biophysical Journal*, **66**, pp. 1632–1642 (1992).

Hibino, M., H. Itoh, and K. J. Kinosita. Time courses of cell electroporation as revealed by submicrosecond imaging of transmembrane potential. *Biophysical Journal*, **64**, pp. 1789–1800 (1993).

Hibino, M., M. Shigemori, H. Itoh, K. Nagayama, and K. Kinosita, Jr. Membrane conductance of an electroporated cell analyzed by submicrosecond imaging of transmembrane potential. *Biophysical Journal*, **59**, pp. 209–220 (1991).

Hofmann, G. and G. Evans. Electronic genetic-physical and biological aspects of cellular electromanipulation. *IEEE Engineering in Medicine and Biology Magazine*, pp. 6–23 (1986).

Holzapfel, C., J. Vienken, and U. Zimmermamm. Rotaion of cells in an electric field. *Journal of Membrane Biology*, **67**, pp. 13–26 (1982).

Israelachvili, J. *Intermolecular and Surface Forces.* Academic Press, London, UK (1992).

Jaroszeski, M. J., R. Gilbert, and R. Heller. *Methods in Molecular Medicine: Electrochemotherapy, Electrogenetherapy, and Transdermal Drug Delivery Electrically Mediated Delivery of Molecules to Cells.* Humana Press, Totowa, New Jersey (2000).

Jones, T. B. *Electromechanics of particles.* Cambridge University Press, New York (1995).

Joshi, R. P., Q. Hu, K. H. Schoenbach, and H. P. Hjalmarson. Improved energy model for membrane electroporation in biological cells subjected to electrical pulses. *Physical Review E*, **65(4)**, pp. 041920–041928 (2002).

Kakorin, S., S. P. Stoylov, and E. Neumann. Electro-optics of membrane electroporation in diphenylhexatriene-doped lipid bilayer vesicles. *Biophysical Chemistry*, **58**, pp. 109–116 (1996).

Kanduŝer, M., M. Fošnaria, M. Ŝentjurc, V. Kralj-Iglič, H. Hägerstrand, A. Iglič, and D. Miklavčič. Effect of surfactant polyoxyethylene glycol $C_{12}E_8$ on electroporation of cell line DC3F. *Colloids and Surfaces A*, **214**, pp. 205–217 (2003).

Kinosita, K. and T. Y. Tsong. Voltage-induced pore formation and hemolysis of human erythrocytes. *Biochim Biophys Acta*, **471**, pp. 227–242 (1977a).

Kinosita, K. and T. Y. Tsong. Formation and resealing of pores of controlled sizes in human erythrocyte membrane. *Nature*, **268**, pp. 438–441 (1977b).

Kinosita, K., Jr., M. Hibino, H. Itoh, M. Shigemori, K. Hirano, Y. Kirinoand, and T. Hayakawa. Events of membrane electroporation visualized on a time scale from microsecond to seconds. In: *Guide to Electroporation and Electrofusion*, edited by D. C. Chang, B. M. Chassy, J. A. . Saunders, and A. E. Sowers, chapter 3, pp. 29–46. Academic Press, San Diego, CA (1992).

Kotnik, T. Biological cells in electric fields. In: *Proceedings of the Electroporation based Technologies and Treatments*, edited by P. Kramar and D. Miklavĉiĉ, pp. 7–12. Bioelectrochemical society IGEA, Ljubljana, Slovenia (2003).

Kotnik, T. and D. Miklavĉiĉ. Theoretical evaluation of the distributed power dissipation in biological cells exposed to electric fields. *Bioelectromagnetics*, **21**, pp. 385–394 (2000).

Kotnik, T., D. Miklavĉiĉ, and L. M. Mir. Cell membrane electropermeabilization by symmetrical bipolar rectangular pulses, Part II. reduced electrolytic contamination. *Bioelectrochemistry*, **54**, pp. 91–95 (2001a).

Kotnik, T., D. Miklavĉiĉ, and T. Slivnik. Time course of transmembrane voltage induced by time-varying electric fields: a method for theoretical analysis and its application. *Bioelectrochemistry and Bioenergetics*, **45**, pp. 3–16 (1998).

Kotnik, T., L. M. Mir, K. Flisar, M. Puc, and D. Miklavĉiĉ. Cell membrane electropermeabilization by symmetrical bipolar rectangular pulses, Part I. increased efficiency of permeabilization. *Bioelectrochemistry*, **54**, pp. 83–90 (2001b).

Kotnik, T., G. Pucihar, M. Rebersek, L. M. Mir, and D. Miklavĉiĉ. Role of pulse shape in cell membrane electropermeabilization. *Biochim Biophys Acta*, **1614**, pp. 193–200 (2003).

Kranjc, S., M. Cemažar, A. Grosel, M. Sentjurc, and G. Serša. Radiosensitising effect of electrochemotherapy with bleomycin in LPB sarcoma cells and tumors in mice. *BMC Cancer* (2005).

Krassowska, W. and P. D. Filev. Modeling electroporation in a single cell. *Biophysical Journal*, **92**, pp. 404–417 (2007).

Lebar, A. M. and D. Miklavčič. Cell electropermeabilization to small molecules *in vitro*: Control by pulse parameters. *Radiology and Oncology*, **35**, pp. 193–202. (2001).

Lee, M. J., S. S. Cho, H. S. Jang, Y. S. Lim, J. R. You, J. Park, H. Suh, J. Kim, J. S. Park, and D. K. Kim. Optimal salt concentration of vehicle for plasmid DNA enhances gene transfer mediated by electroporation. *Experimental and Molecular Medicine*, **34**, pp. 265–272 (2002).

Lee, R. C. The pathophysiology and clinical management. In: *Electrical Trauma: The Pathophysiology, Manifestations and Clinical Management*, edited by R. C. Lee, E. G. Cravalho, and J. F. Burke, chapter 3, pp. 33–40. Cambridge University Press, Cambridge (1992).

Liang, H., W. J. Purucker, D. A. Stenger, R. T. Kubiniec, and S. W. Hui. Uptake of fluorescense-labeled dextrans by 10T 1/2 fibroblasts following permeation by rectangular and exponential-decay electric field pulses. *Biotechniques*, **6**, pp. 550–558 (1988).

Lojewska, Z., D. Franks, B. Ehrenberg, and M. Loew. Analysis of the effect of medium and membrane conductance on the amplitude and kinetics of membrane potentials induced by externally applied electric fields. *Biophysical Journal*, **56**, pp. 121–128 (1989).

Mehrle, W., U. Zimmermann, and R. Hampp. Evidence for asymmetrical uptake of fluorescent dyes through electro-permeabilized membranes of avena mesophyll protoplasts. *Federation of European Biochemical Societies*, **185**, pp. 89–94 (1985).

Miklavčič, D. and T. Kotnik. Electroporation for electrochemotherapy and gene therapy. In: *Bioelectromagnetic Medicine*, edited by M. S. Markov, chapter 40, pp. 637–656. Marcel Dekker, New York (2004).

Mir, L. M. Therapeutic perspectives of *in vivo* cell electropermeabilization. *Bioelectrochemistry*, **53**, pp. 1–10 (2000).

Mir, L. M., S. Orlowski, J. Belehradek, and C. Paoletti. Electrochemotherapy potentiation of antitumour effect of bleomycin by local electric pulses. *European Journal of cancer*, **27**, pp. 68–72 (1991).

Mir, L. M., S. Orlowski, J. J. Belehradek, J. Teissié, M. Rols, G. Serŝa, D. Miklavĉiĉ, R. Gilbert, and R. Heller. Biomedical applications of electric pulses with special emphasis on antitumor electrochemotherapy. *Bioelectrochemistry and Bioenergetics*, **38**, pp. 203–207 (1995).

Moser, D., D. Zarka, C. Hedman, and T. Kallar. Plasmid and chromosomal dna recovery by electroextraction of cyanobacteria. *FEMS Microbiology Letters*, **128**, pp. 307–313 (1995).

Mouneimne, Y., P. F. Tosi, R. Barhoumi, and C. Nicolau. Electroinsertion: An electrical method for protein implantation into cell membranes. In: *Guide to Electroporation and Electrofusion*, edited by D. C. Chang, B. M. Chassy, J. A. Saunders, and A. E. Sowers, chapter 20, pp. 327–346. Academic Press, San Diego, CA (1992).

Mouneimne, Y., P. F. Tosi, Y. Gazitt, and C. Nicolau. Electro-insertion of xeno-glycophorin into the red blood cell membrane. *Biochemical and Biophysical Research Communications*, **159**, pp. 34–40 (1989).

Muramatsu, T., A. Nakamura, and H. M. Park. *in vivo* electroporation: A powerful and convinient means of non viral gene transfer to tissues of living animals (Review). *International Journal of Molecular Medicine*, **1**, pp. 55–62 (1998).

Neu, J. C. and W. Krassowska. Asymptotic model of electroporation. *Physical Review E*, **59**, pp. 3471–3482 (1999).

Neu, J. C. and W. Krassowska. Modeling postshock evolution of large electropores. *Physical Review E*, **67**, pp. 1–12 (2003).

Neumann, E. The relaxation hysteresis of membrane electroporation. In: *Electroporation and Electrofusion in Cell Biology*, edited by E. Neumann, A. E. Sowers, and C. A. Jordan, chapter 4, pp. 61–82. Plenum Press, New York (1989).

Neumann, E., G. Gerisch, and K. Opatz. Cell fusion induced by high electric impulses applied to dictyostelium. *Naturwissenschaften*, **67**, pp. 414–415 (1980).

Neumann, E. and S. Kakorin. Digression on membrane electroporation for drug and gene delivery. *Technology in Cancer Research and Treatment*, **1**, pp. 329–339 (2002).

Neumann, E., S. Kakorin, and K. Toensing. Membrane electroporation and electro-mechanical deformation of vesicles and cells. *Faraday Discuss*, pp. 111–125 (1998).

Neumann, E. and K. Rosenheck. Permeability changes induced by electric impulses in vesicular membranes. *Journal of Membrane Biology*, **10**, pp. 279–290 (1972).

Neumann, E., M. Schaefer-Ridder, Y. Wang, and P. H. Hofschneider. Gene transfer into mouse lyoma cells by electroporation in high electric fields. *European Molecular Biology Organization Journal*, **1**, pp. 841–845 (1982).

Neumann, E., A. E. Sowers, , and C. A. Jordan, editors. *Electroporation and Electrofusion in Cell Biology*. Plenum Press, New York (1989).

Newman, J. Resistance for flow of current to a disk. *Journal of The Electrochemical Society*, **113**, pp. 501–502 (1966).

O'Neil, R. J. and L. Tung. Cell-attached patch clamp study of the electropermeabilization of amphibian cardiac cells. *Biophysical Journal*, **59**, pp. 1028–1039 (1991).

Orentas, R., D. Schauer, Q. Bin, and B. D. Johnson. Electrofusion of a weakly immunogenic neuroblastoma with dendritic cells produces a tumor vaccine. *Cellular Immunology*, **213**, pp. 4–13 (2001).

Pastushenko, V. F. and Y. A. Chizmadzhev. Stabilization of conducting pores in BLM by electric current. *General Physiology and Biophysics*, **1**, pp. 43–52 (1982).

Pastushenko, V. F., Y. A. Chizmadzhev, and V. B. Arakelyan. Electric breakdown of bilayer lipid membranes.II. Calculation of the membrane lifetime in

the steady-state diffusion approximations. *Bioelectrochemistry and Bioenergetics*, **6**, pp. 53–62 (1979).

Pavlin, P., N. Pavŝelj, and D. Miklavĉiĉ. Dependence of induced transmembrane potential on cell density, arrangement, and cell position inside a cell system. *IEEE Transactions on Biomedical Engineering*, **49**, pp. 605–612 (2002).

Pohl, H. A. *Dielectrophoresis, the Behavior of Matter in Non-uniform Electric Fields*. Cambridge University Press, Cambridge (1978).

Potter, H. Electroporation in biology: Methods, applications and instrumentation. *Analytical Biochemistry*, **174**, pp. 361–373 (1988).

Powell, K. T., A. W. Morgenthaler, and J. C. Weaver. Tissue electroporation: Observation of reversible electrical breakdown in viable frog skin. *Biophysical Journal*, **56**, pp. 1163–1171 (1989).

Prausnitz, M. R., V. G. Bose, R. Langer, and J. C. Weaver. Electroporation of mammalian skin: A mechanism to enhance transdermal drug delivery. *Proceedings of the National Academy of Sciences*, **90**, pp. 10504–10508 (1993).

Prausnitz, M. R., U. Pliquett, R. Langer, and J. C. Weaver. Rapid temporal control of transdermal drug delivery by electroporation. *Pharmacological Research*, **11**, pp. 1834–1837 (1994).

Pucihar, G., T. Kotnik, M. Kanduser, and D. Miklavĉiĉ. The influence of medium conductivity on electropermeabilization and survival of cells *in vitro*. *Bioelectrochemistry*, **54**, pp. 107–115 (2001).

Qin, Y., S. Lai, Y. Jiang, T. Yang, and J. Wang. Transmembrane voltage induced on a cell membrane in suspensions exposed to an alternating field: A theoretical analysis. *Bioelectrochemistry*, **67**, pp. 57–65 (2005).

Rols, M. P., C. Delteil, G. Serin, and J. Teissié. Temperature effects on electrotransfection of mammalian cells. *Nucleic Acids Research*, **22**, pp. 540–540 (1994).

Rols, M. P. and J. Teissié. Ionic-strength modulation of electrically induced permeabilization and associated fusion of mammalian cells. *European Journal of Biochemistry*, **179**, pp. 109–115 (1989).

Rosenheck, K., P. Lindner, and I. Pecht. Effect of electric fields on light-scattering and fluorescence of chromaffin granules. *Journal of Membrane Biology*, **20**, pp. 1–12 (1975).

Sale, A. J. H. and W. A. Hamilton. Effects of high electric fields on microorganisms: I. Killing of bacteria and yeasts. *Biochim Biophys Acta*, **148**, pp. 781–788 (1967).

Sale, A. J. H. and W. A. Hamilton. Effects of high electric fields on microorganisms:III. Lysis of erythricuytes and protoplasts. *Biochim Biophys Acta*, **163**, pp. 37–43 (1968).

Ŝatkauskas, S., M. F. Bureau, M. Puc, A. Mahfoudi, D. Scherman, D. Miklavĉiĉ, and L. M. Mir. Mechanisms of *in vivo* DNA electrotransfer: Respective contributions of cell electropermeabilization and DNA electrophoresis. *Molecular Therapy*, **5**, pp. 133–140 (2002).

Saulis, G., J. Naktinis, and M. Venslauskas. Kinetics of pore resealing in cell membranes after elrctroporation. *Bioelectrochemistry and Bioenergetics*, **26**, pp. 1–13 (1991).

Saulis, G. and S. Ŝatkauskas. Pore disappearance in a cell after electroporation: Theoretical simulation and comparison with experiments. *Biophysical Journal*, **73**, pp. 1299–1309 (1977).

Saulis, G. and S. Ŝatkauskas. Electroporation of biological membranes. *Veterinarija ir Zootechnika*, **26**, pp. 82–88 (2004a).

Saulis, S. and G. Ŝatkauskas. Electroporation as a tool for biotechnology and medicine with specific emphasize on its application for drug and gene delivery: Review. *Veterinarija ir Zootechnika*, **26**, pp. 74–81 (2004b).

Scheurich, P. and U. Zimmermann. Electrically stimulated fusion of different plant cell protoplasts. *Plant Physiology*, **67**, pp. 849–853 (1981).

Schmidt, E., U. Leinfelder, P. Gessner, D. Zillikens, E. B. Brocker, and U. Zimmermann. CD19+ B lymphocytes are the major source of human antibody-secreting hybridomas generated by electrofusion. *Journal of Immunological Methods*, **255**, pp. 93–102 (2001).

Schwan, H. P. Electrical properties of tissue and cell suspensions. *Advances in Biological and Medical Physics*, **5**, pp. 147–209 (1957).

Schwan, H. P. Dielectrophoresis and rotation of cells. In: *Electroporation and Electrofusion in Cell Biology*, edited by E. Neumann, A. E. Sowers, , and C. A. Jordan, chapter 1, pp. 3–22. Plenum Press, New York (1989).

Schwister, K. and B. Deuticke. Formation and properties of aqueous leaks induced in human erythrocytes by electrical breakdown. *Biochim Biophys Acta*, **816**, pp. 332–348 (1985).

Scott-Taylor, T. H., R. Pettengell, I. Clarke, G. Stuhler, M. C. L. Barthe, P. Walden, and A. G. Dalgleish. Human tumour and dendritic cell hybrids generated by electrofusion: Potential for cancer vaccines. *Biochim Biophys Acta*, **1500**, pp. 265–267 (2000).

Serŝa, G. Electrochemotherapy. In: *Electrochemotherapy, Electrogenetherapy, and Transdermal Drug Delivery : Electrically Mediated Delivery of Molecules to Cells (Methods in Molecular medicine)*, edited by M. J. Jaroszeski, R. Heller, and R. Gilbert, chapter 6, pp. 119–133. Humana Press, Totowa, New Jersey (2000).

Serŝa, G., M. Cemaẑar, and D. Miklavčič. Antitumor effectiveness of electrochemotherapy with cisdiamminedichloroplatinum(II) in mice. *Cancer Research*, **55**, pp. 3450–3455 (1995).

Serŝa, G., S. Novaković, and D. Miklavčič. Potentiation of bleomycin antitumor effectiveness by electrotherapy. *Cancer Letters*, **69**, pp. 81–84 (1993).

Serŝa, G., B. Stabuč, M. Cemaẑar, D. Miklavčič, and Z. Rudolf. Electrochemotherapy with cisplatin: the systemic antitumour effectiveness of cisplatin can be potentiated locally by the application of electric pulses in the treatment of malignant melanoma skin metastases. *Melanoma Research*, **10**, pp. 381–385 (2000).

Sheng, Y., V. Mancino, and B. Birren. Transformation of escherichia coli with large DNA molecules by electroporation. *Nucleic Acids Research*, **23**, pp. 1990–1996 (1995).

Smith, K. C., J. C. Neu, and W. Krassowska. Model of creation and evolution of stable electropores for DNA delivery. *Biophysical Journal*, **86**, pp. 2813–2826 (2004).

Smith, L. and J. Nordstrom. Advances in plasmid gene delivery and expression in skeletal muscle. *Current Opinion in Molecular Therapeutics*, **2**, pp. 150–154 (2000).

Snoj, M., Z. Rudolf, M. Cemaẑar, B. Jancar, and G. Serŝa. Successful sphincter-saving treatment of anorectal malignant melanoma with electrochemotherapy, local excision and adjuvant brachytherapy. *Anti-Cancer Drugs*, **16**, pp. 345–348 (2005).

Swezey, R. and D. Epel. Stable, resealable pores formed in sea urchin eggs by electric discharge (electroporation) permit substrate loading for assay of enzymes *in vivo*. *Cell Regulation*, **1**, pp. 65–74 (1989).

Talele, S. and P. Gaynor. Nonlinear time domain model of electropermeabilization: Response of a single cell to an arbitrary applied electric field. *Journal of Electrostatics*, **65**, pp. 775–784 (2007).

Teissié, J. and M. Rols. An experimental evaluation of the critical potential difference inducing cell membrane electropermeabilization. *Biophysical Journal*, **65**, pp. 409–413 (1993).

Teissié, J. and T. Y. Tsong. Electric field induced transient pores in phospholipid bilayer vesicles. *Biochemistry*, **20**, pp. 1548–1554 (1981).

Tekle, E., R. D. Astumian, and P. B. Chock. Electro-permeabilization of cell membranes: Effect of the resting membrane potential. *Biochemical and Biophysical Research Communications*, **172**, pp. 282–287 (1990).

Tekle, E., R. D. Astumian, and P. B. Chock. Electroporation by using bipolar oscillating electric field: An improved method for DNA transfection of NIH 3T3 cells. *Proceedings of the National Academy of Sciences*, **66**, pp. 4230–4234 (1991).

Tekle, E., R. D. Astumian, W. A. Friauf, and P. B. Chock. Asymmetric pore distribution and loss of membrane lipid in electroporated DOPC vesicles. *Biophysical Journal*, **81**, pp. 960–968 (2001).

Tozon, N., V. Kodre, G. Serŝa, and M. Cemaẑar. Effective treatment of perianal tumors in dogs with electrochemotherapy. *Anticancer Research*, **25**, pp. 839–946 (2005).

Valic, B., M. Pavlin, and D. Miklavĉiĉ. The effect of resting transmembrane voltage on cell electropermeabilization: a numerical analysis. *Bioelectrochemistry*, **63**, pp. 311–315 (2004).

Vanbever, R., N. Lecouturier, and V. Preat. Transdermal delivery of metoprolol by electroporation. *Pharmacological Research*, **11**, pp. 1657–1662 (1994).

Weaver, J. C. Electroporation: a general phenomenon for manipulating cells and tissues. *Journal of Cellular Biochemistry*, **51**, pp. 426–435 (1993).

Weaver, J. C. and A. Barnett. Progress towards a theoretical model for electroporation: Membrane electrical behavior and molecular transport. In: *Guide to Electroporation and Electrofusion*, edited by D. C. Chang, B. M. Chassy, J. A. Saunders, and A. E. Sowers, chapter 7, pp. 91–118. Academic Press, San Diego, CA (1992).

Weaver, J. C. and Y. Chizmadzhev. Theory of electroporation: a review. *Bioelectrochemistry and Bioenergetics*, **41**, pp. 135–160 (1996).

Weaver, J. C. and R. A. Mintzer. Decreased bilayer stability due to transmembrane potentials. *Physics Letters A*, **86A**, pp. 57–59 (1981).

Weaver, J. C. and K. T. Powell. Theory of electroporation. In: *Electroporation and Electrofusion in Cell Biology*, edited by E. Neumann, A. E. Sowers, and C. A. Jordan, chapter 7, pp. 111–126. Plenum Press, New York (1989).

Yumura, S., R. Matsuzaki, and T. Kitanishi-Yumura. Introduction of macromolecules into living dictyostelium cells by electroporation. *Cell Structure and Function*, **20**, pp. 185–190 (1995).

Zimmermann, U. Electric field-mediated fusion and related electrical phenomena. *Biochim Biophys Acta*, **694**, pp. 227–277 (1982).

Zimmermann, U. and G. A. Neil. *Electromanipulation of Cells*. CRC Press, Boca Raton, Florida (1996).

Zimmermann, U., J. Schulz, and G. Pilwat. Transcellular Ion Flow in Escherichia coli B and Electrical Sizing of Bacterias. *Biophysical Journal*, **13(10)**, pp. 1005–1013 (1973).

Zimmermann, U., J. Vienken, and G. Pilwat. Development of drug carrier systems: electric field induced effects in cell membranes. *Journal of Electroanalytical Chemistry*, pp. 553–574 (1980).